CANADIAN THESES ON MICROFICHE

THÈSES CANADIENNES SUR MICROFICHE

National Library of Canada
Collections Development Branch

Canadian Theses on
Microfiche Service

Ottawa, Canada
K1A 0N4

Bibliothèque nationale du Canada
Direction du développement des collections

Service des thèses canadiennes
sur microfiche

NOTICE

The quality of this microfiche is heavily dependent upon the quality of the original thesis submitted for microfilming. Every effort has been made to ensure the highest quality of reproduction possible.

If pages are missing, contact the university which granted the degree.

Some pages may have indistinct print especially if the original pages were typed with a poor typewriter ribbon or if the university sent us an inferior photocopy.

Previously copyrighted materials (journal articles, published tests, etc.) are not filmed.

Reproduction in full or in part of this film is governed by the Canadian Copyright Act, R.S.C. 1970, c. C-30. Please read the authorization forms which accompany this thesis.

AVIS

La qualité de cette microfiche dépend grandement de la qualité de la thèse soumise au microfilmage. Nous avons tout fait pour assurer une qualité supérieure de reproduction.

S'il manque des pages, veuillez communiquer avec l'université qui a conféré le grade.

La qualité d'impression de certaines pages peut laisser à désirer, surtout si les pages originales ont été dactylographiées à l'aide d'un ruban usé ou si l'université nous a fait parvenir une photocopie de qualité inférieure.

Les documents qui font déjà l'objet d'un droit d'auteur (articles de revue, examens publiés, etc.) ne sont pas microfilmés.

La reproduction, même partielle, de ce microfilm est soumise à la Loi canadienne sur le droit d'auteur, SRC 1970, c. C-30. Veuillez prendre connaissance des formules d'autorisation qui accompagnent cette thèse.

THIS DISSERTATION
HAS BEEN MICROFILMED
EXACTLY AS RECEIVED

LA THÈSE A ÉTÉ
MICROFILMÉE TELLE QUE
NOUS L'AVONS REÇUE

Canada

NL 339 (r. 85/09)

National Library of Canada
Bibliothèque nationale du Canada

Ottawa, Canada
K1A 0N4

(143)

TC –

ISBN 0-315-01337-X

CANADIAN THESES ON MICROFICHE SERVICE – SERVICE DES THÈSES CANADIENNES SUR MICROFICHE

PERMISION TO MICROFILM – AUTORISATION DE MICROFILMER

• Please print or type – Écrire en lettres moulées ou dactylographier

AUTHOR – AUTEUR

Full Name of Author – Nom complet de l'auteur

EDDY HO-KUEN CHUI

Date of Birth – Date de naissance	Canadian Citizen – Citoyen canadien
JUNE 12/57	☑ Yes / Oui ☐ No / Non
Country of Birth – Lieu de naissance	**Permanent Address – Résidence fixe**
HONG KONG	10612-51 AVE. EDMONTON, ALBERTA T6H 0K9

THESIS – THÈSE

Title of Thesis – Titre de la thèse

EFFECTS OF EXHAUST CONDITIONS ON EFFLUENT GAS DILUTION AROUND BUILDINGS

Degree for which thesis was presented Grade pour lequel cette thèse fut présentée	Year this degree conferred Année d'obtention de ce grade
M.Sc.	1985
University – Université	**Name of Supervisor – Nom du directeur de thèse**
UNIVERSITY OF ALBERTA	Dr. D. J. WILSON

AUTHORIZATION – AUTORISATION

Permission is hereby granted to the NATIONAL LIBRARY OF CANADA to **microfilm** this thesis and to **lend** or **sell copies of the film.**

The author reserves other publication rights, and neither the thesis nor extensive extracts from it may be printed or otherwise reproduced without the author's written permission.

L'autorisation est, par la présente, accordée à la BIBLIOTHÈQUE NATIONALE DU CANADA de **microfilmer** cette thèse et de **prêter** ou de **vendre des exemplaires du film.**

L'auteur se réserve les autres droits de publication; ni la thèse ni de longs extraits de celle-ci ne doivent être imprimés ou autrement reproduits sans l'autorisation écrite de l'auteur.

ATTACH FORM TO THESIS – VEUILLEZ JOINDRE CE FORMULAIRE À LA THÈSE

Signature	Date
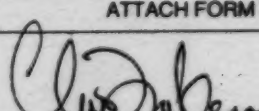	APRIL 18/85

THE UNIVERSITY OF ALBERTA

EFFECTS OF EXHAUST CONDITIONS ON EFFLUENT GAS DILUTION AROUND BUILDINGS

BY

(C)

EDDY H. CHUI

A THESIS

SUBMITTED TO THE FACULTY OF GRADUATE STUDIES AND RESEARCH IN PARTIAL FULFILLMENT OF THE REQUIREMENTS FOR THE DEGREE OF

MASTER OF SCIENCE

DEPARTMENT OF MECHANICAL ENGINEERING

EDMONTON, ALBERTA

SPRING, 1985

THE UNIVERSITY OF ALBERTA

RELEASE FORM

NAME OF AUTHOR: Eddy H. Chui

TITLE OF THESIS: Effects of Exhaust Conditions on Effluent Gas Dilution Around Buildings

DEGREE FOR WHICH THESIS WAS PRESENTED: Master of Science

YEAR THIS DEGREE GRANTED: Spring 1985

Permission is hereby granted to THE UNIVERSITY OF ALBERTA LIBRARY to reproduce single copies of this thesis and to lend or sell such copies for private, scholarly or scientific research purposes only.

The author reserves other publication rights, and neither the thesis nor extensive extracts from it may be printed or otherwise reproduced without the author's written permission.

Signed ...Eddy H. Chui.....

PERMANENT ADDRESS:

10612 - 51 Avenue
Edmonton, Alberta
T6H 0K9

DATED: April 18, 1985

THE UNIVERSITY OF ALBERTA

FACULTY OF GRADUATE STUDIES AND RESEARCH

The undersigned certify that they have read, and recommend to the Faculty of Graduate Studies and Research, for acceptance, a thesis entitled "EFFECTS OF EXHAUST CONDITIONS ON EFFLUENT GAS DILUTION AROUND BUILDINGS"
submitted by EDDY HO-KUEN CHUI in partial fulfillment of the requirements for the degree of Master of Science.

.....

Supervisor

.....

.....

Date ... February 19/85

Abstract

The effects of vertical exhaust velocity and changing wind direction on the dilution of vent gases around buildings were investigated using small scale wind tunnel models. Turbulence measurements verified the effectiveness of the wind tunnel modelling. The wind and turbulence characteristics of a neutrally stable atmospheric boundary layer of a lightly built up urban area were simulated in the model at an overall model scale of about 2000:1. The range of eddy sizes in the model was found to be 300 times smaller than its full scale counterpart due to the Reynolds number mismatch. However, this did not impair the simulation because the equivalent full scale eddies missing in the model were those smaller than 0.2 m which were not expected to participate significantly in the dilution of contaminants over a building roof.

Exhaust from flush, vertically directed roof vents on rectangular building models was studied. It was found that a vertical exhaust jet caused additional dilution near the source at roof level because of plume rise and extra air entrainment during the initial bending over of the exhaust plume. A simple dilution model which assumed an "apparent" initial dilution at the source was developed and compared to experiments. Data correlation established a linear relationship between this initial dilution, D_o, and the momentum flux ratio, M^2, of the exhaust gas to the approach flow. Using this relationship the model provided a reasonable estimation of the minimum dilution on the building roof and could be used as a general design guide. Another model which accounted only for the plume rise caused by vertical momentum was also developed but was shown to be excessively sensitive to the

semi-empirical plume rise formulations and could not be generalized for design purposes.

The influence of changing wind direction on minimum dilution was found to be significant when exhaust momentum was low (M = 0.1). Two to eight times lower dilution levels, depending on building shapes, were observed for wind incidence angles greater than 30°. However, at high exhaust momentum ($M \geq 1.3$), minimum dilution lost its sensitivity to wind direction. As a first approximation to wind angle effect, a simple model was devised to account for the dependence of minimum dilution on wind incidence angle, θ and exhaust momentum, M.

Acknowledgement

I am deeply grateful to Dr. D.J. Wilson who supervised this thesis. His enthusiasm, insightful advice and helpful guidance have made the preparation of this thesis an enjoyable and rewarding experience.

Special appreciation is extended to Dr. M.D. Checkel and Brian Zelt for writing some of the computer programs used in this research project and also to Gary Mandrusiak who helped me a great deal in taking experimental measurements.

I would like to express my gratitude to Barry Bara and Darwin Kiel for their constant support and encouragement, especially to Barry who took time to proof-read this thesis. Also I wish to thank Miss Gail Anderson who did an excellent job in typing this entire thesis in a rather tight schedule.

This thesis was supported by the teaching assistantship of the University of Alberta, scholarships offered by the Province of Alberta and the Natural Sciences and Engineering Research Council of Canada, and grants to Dr. D.J. Wilson from NSERC and Imperial Oil Ltd.

Table of Contents

Chapter		Page
I	Introduction	1
II	Wind Tunnel Modelling	7
	Chapter Overview	7
	2.1 Simulation of an Atmospheric Boundary Layer in a Wind Tunnel	7
	2.1.1 Present Wind Tunnel Model	7
	2.1.2 Reynolds Number Mismatch in Atmospheric Boundary Layer Modelling	9
	2.1.3 Mean Velocity and Turbulence Measurements	10
	2.1.4 Defining the Quality of the Simulated Boundary layer (at the building location but with no building present)	11
	2.1.4a Vertical Profile of Mean Velocity	11
	2.1.4b Turbulence Intensity	13
	2.1.4c Integral Length Scale of Turbulence	14
	2.1.4d Power Spectral Density	15
	2.1.4e Scale Ratio	16
	2.1.4f Comparison With Previous Wind Tunnel Simulation	17
	2.2 Building Models	18
	2.3 Exhaust Gas System Modelling and Concentration Measurements	19
	2.3.1 Sampling Rate	21
	2.3.2 Sampling Time	21
	2.3.3 Calibration of the Tracer Gas System	22
	2.3.4 Repeatability of Concentration Measurements	22
III	Effects of Exhaust Momentum from Building Roof Vents on Effluent Dilution	36

Chapter		Page
Chapter Overview		36
3.1	Initial Dilution Due to Exhaust Momentum	36
3.2	Buoyancy Rise	38
3.3	Exhaust Momentum Factor	39
3.4	Computational Models for Initial Dilution of a Rising Effluent Jet	40
3.4.1	Plume Rise Approach	40
3.4.1a	Gaussian Plume Model	41
3.4.1b	"Triangular" Plume Concentration Profile	42
3.4.1c	Functional Form to Represent Plume Rise	43
3.4.1d	Wind Tunnel Experiments	44
3.4.1e	Discussion of Results and Data Correlations	45
3.4.1f	Plume Rise Dilution Model: Conclusions	48
3.4.2	Accounting for Exhaust Momentum Using Initial Entrainment	49
3.4.2a	Wind Tunnel Data	50
3.4.2b	Experimental Results for Exhaust Momentum Effect on Initial Dilution	52
3.4.2c	Comparison with Previous Dilution Model at Medium and High Momentum	52
3.4.2d	Sensitivity to Building Shapes	53
3.4.2e	Sensitivity to Vent Locations	53
3.4.2f	Comparison with Previous Model at Low Exhaust Momentum	54
3.4.2g	Limitations of the Initial Entrainment Model	54
3.4.2h	Summary Remarks for the Initial Entrainment Model	55

Chapter		Page
IV	Effect of Wind Incidence Angle on Dilution of Effluent at Roof Level	76
	Introduction	76
	4.1 A Theory to Account for Wind Incidence Angle Effect	76
	4.2 Wind Tunnel Tests	78
	4.3 Wind Angle Effect at Low Exhaust Momentum (M = 0.073 to 0.103)	80
	4.3.1 Data Correlation	80
	4.3.2 Sensitivity to Building Shape	82
	4.3.3 Comparison with Other Investigation	83
	4.4 Wind Angle Effect at High Exhaust Momentum (M = 1.28 to 1.76)	84
	4.5 Summary	85
V	Summary, Recommendations and Further Studies	102
	5.1 The Wind Tunnel Model	102
	5.2 Results from Wind Tunnel Studies	103
	5.3 Recommendations for Further Studies	106
References		111
Appendices		
A2	Comparison of the Smallest Eddy Size η in the Model and its Full Scale Equivalent	114
A3-1	Growth of a Plume with Linear Crosswind Concentration Profile	117
A3-2	Entrainment Model for Initial Dilution	120
A3-3	Comparison of Buoyancy Rise and Momentum Rise in the Wind Tunnel Model	123
A4	Additional Experimental Data on the Effect of Wind Incidence Angle on Dilution	129
A5	Additional Experimental Data on the Effect of Building Shape on Dilution	149

List of Tables

Table		Page
2-1	Comparison of Wind Tunnel Simulations with a) Full Scale Measurements and b) Previous Wind Tunnel Measurements (Wilson, 1976)	23
3-1	Conditions for Wind Tunnel Tests	57
4-1	Location of the New Sampling Ports	87
4-2	Conditions for Wind Tunnel Tests	88

List of Figures

Figure		Page
2-1	Schematic of wind tunnel, turbulence generating elements and tracer gas system	24
2-2	Streamlines and exhaust gas dispersion around a building	25
2-3	Flow patterns on a wide flat-roofed building surface, from flow visualization measurements	26
2-4	Vertical profile of mean velocity measured with hot wire anemometer at model building location with no building present	27
2-5	Transition of smooth surface inner wall layer to rough surface outer wall layer in the simulated atmospheric boundary layer	28
2-6	Vertical variation of x-direction turbulent velocity at model building location with no building present	29
2-7	Vertical profile of x-direction integral length scale of turbulence at model building location with no building present	30
2-8	Power spectral densities of along-wind turbulence u' at $z = 1.5$ cm (30 m full scale) and $z = 15$ cm (300 m full scale) of the simulated atmospheric boundary layer at model location with no building present	31
2-9	Building models for wind tunnel concentration measurements with wind direction perpendicular to upwind face ($\theta = 0°$ only)	32
2-10	Building models for wind tunnel concentration measurements at wind incidence angle in the range $0° \leq \theta \leq 45°$	33
2-11	Installation of building model in the wind tunnel	34
2-12	Sampling manifold and building model #2	35
3-1	Effect of exhaust momentum factor M on vertical profiles of exhaust gas dilution for a flush vent located 10.2 cm from the upwind roof edge of a wide (two dimensional step) building	58
3-2	Effect of exhaust momentum factor M on vertical profiles of exhaust gas dilution for a flush vent located 10.2 cm from the upwind roof edge of a wide (two dimensional step) building	59

Figure		Page
3-2a	Plume rise of exhaust gas jets emitted from a flush, vertically directed vent on a two dimensional roof at two different exhaust momentum conditions	60
3-3	Use of $h \alpha S^{1/3}$ power law for plume rise to estimate the effect of plume rise on concentration at roof level. Dashed line represents experimental data and solid lines, theoretical predictions based on linear plume concentration profiles with different values of plume rise constant, B_1	61
3-4	Use of $h \alpha S^{1/3}$ power law for plume rise to estimate the effect of plume rise on concentration at roof level. Dashed line represents experimental data and solid lines, theoretical predictions based on linear plume concentration profiles with different values of plume rise constant, B_1	62
3-5	Use of $h \alpha S^{1/3}$ power law for plume rise to estimate the effect of plume rise on concentration at roof level assuming a virtual origin at downwind distance, S_o in the plume rise formulation equation (3-9) with linear plume concentration profiles	63
3-6	Use of $h \alpha S^{1/3}$ power law for plume rise to estimate the effect of plume rise on concentration at roof level assuming a virtual origin at downwind distance, S_o in the plume rise formulation equation (3-9) with linear plume concentration profiles	64
3-7	Use of $h \alpha S^{1/2}$ power law for plume rise to estimate the effect of plume rise on concentration at roof level. Dashed line represents experimental data and solid lines, theoretical predictions based on linear plume concentration profiles with different values of plume rise constant, B_5	65
3-8	Use of $h \alpha S^{1/2}$ power law for plume rise to estimate the effect of plume rise on concentration at roof level. Dashed line represents experimental data and solid lines, theoretical predictions based on linear plume concentration profiles with different values of plume rise constant, B_5	66
3-9	Effect of vertical exhaust momentum on minimum dilution for $M = 0.768$ and wind angle $\theta = 0°$	67
3-10	Effect of vertical exhaust momentum on minimum dilution for $M = 1.76$ and wind angle $\theta = 0°$	68
3-11	Effect of vertical exhaust momentum on minimum dilution for $M = 1.50$ and wind angle $\theta = 0°$	69
3-12	Effect of vertical exhaust momentum on minimum dilution for $M = 1.50$ and wind angle $\theta = 0°$	70

Figure		Page
3-13	Effect of vertical exhaust momentum on minimum dilution for M = 1.76 and wind angle θ = 0°	71
3-14	Effect of vertical exhaust momentum on minimum dilution for M = 0.103 and wind angle θ = 0°	72
3-15	Dilution from vents located on upwind half of building roof with exhaust momentum M = 0.146	73
3-16	Dilution from vents located on downwind half of building roof with exhaust momentum M = 0.146	74
3-17	Air entrainment into the exhaust gas plume from a flush, vertically directed roof vent	75
4-1	Surface flow patterns on a wide flat-roofed building with wind incidence angle of θ = 0°	89
4-2	Surface flow pattern on a tall flat-roofed building with wind incidence angle of θ = 45°	90
4-3	Effect of wind angle on minimum dilution for a low rise building with low exhaust momentum, M = 0.103 and wind angle θ = 0°	91
4-4	Effect of wind angle on minimum dilution for a low rise building with low exhaust momentum, M = 0.103 and wind angle θ = 15°	92
4-5	Effect of wind angle on minimum dilution for a low rise building with low exhaust momentum, M = 0.103 and wind angle θ = 22.5°	93
4-6	Effect of wind angle on minimum dilution for a low rise building with low exhaust momentum, M = 0.103 and wind angle θ = 30°	94
4-7	Effect of wind angle on minimum dilution for a low rise building with low exhaust momentum, M = 0.103 and wind angle θ = 45°	95
4-8	Effect of wind incidence angle on air entrainment coefficient, α at low exhaust momentum condition, M = 0.1	96
4-9	Effect of wind angle on minimum dilution for a low rise building with high exhaust momentum M = 1.76 and wind angle θ = 0°	97

Figure		Page
4-10	Effect of wind angle on minimum dilution for a low rise building with high exhaust momentum M = 1.76 and wind angle θ = 15°	98
4-11	Effect of wind angle on minimum dilution for a low rise building with high exhaust momentum M = 1.76 and wind angle θ = 30°	99
4-12	Effect of wind angle on minimum dilution for a low rise building with high exhaust momentum M = 1.76 and wind angle θ = 45°	100
4-13	Observed effect of vertical exhaust momentum on air entrainment coefficient. Best fit to all wind angles combined	101
5-1	Effect of building shape on minimum dilution for a median rise building with high exhaust momentum M = 1.65	108
5-2	Effect of building shape on minimum dilution for a low rise building with medium exhaust momentum M = 0.768	109
5-3	Effect of building shape on minimum dilution for a cubical building with low exhaust momentum M = 0.073	110
A4-1	Effect of wind angle on minimum dilution for a low rise building with low exhaust momentum M = 0.103 and wind angle θ = 0°	130
A4-2	Effect of wind angle on minimum dilution for a low rise building with low exhaust momentum M = 0.103 and wind angle θ = 15°	131
A4-3	Effect of wind angle on minimum dilution for a low rise building with low exhaust momentum M = 0.103 and wind angle θ = 22.5°	132
A4-4	Effect of wind angle on minimum dilution for a low rise building with low exhaust momentum M = 0.103 and wind angle θ = 30°	133
A4-5	Effect of wind angle on minimum dilution for a low rise building with low exhaust momentum M = 0.103 and wind angle θ = 45°	134
A4-6	Effect of wind angle on minimum dilution for a medium rise building with low exhaust momentum M = 0.087 and wind angle θ = 0°	135

Figure		Page
A4-7	Effect of wind angle on minimum dilution for a medium rise building with low exhaust momentum M = 0.087 and wind angle θ = 15°	136
A4-8	Effect of wind angle on minimum dilution for a medium rise building with low exhaust momentum M = 0.087 and wind angle θ = 22.5°	137
A4-9	Effect of wind angle on minimum dilution for a medium rise building with low exhaust momentum M = 0.087 and wind angle θ = 30°	138
A4-10	Effect of wind angle on minimum dilution for a medium rise building with low exhaust momentum M = 0.087 and wind angle θ = 45°	139
A4-11	Effect of wind angle on minimum dilution for a cubical building with low exhaust momentum M = 0.073 and wind angle θ = 0°	140
A4-12	Effect of wind angle on minimum dilution for a cubical building with low exhaust momentum M = 0.073 and wind angle θ = 15°	141
A4-13	Effect of wind angle on minimum dilution for a cubical building with low exhaust momentum M = 0.073 and wind angle θ = 22.5°	142
A4-14	Effect of wind angle on minimum dilution for a cubical building with low exhaust momentum M = 0.073 and wind angle θ = 30°	143
A4-15	Effect of wind angle on minimum dilution for a cubical building with low exhaust momentum M = 0.073 and wind angle θ = 45°	144
A4-16	Effect of wind angle on minimum dilution for a medium rise building with high exhaust momentum M = 1.50 and wind angle θ = 0°	145
A4-17	Effect of wind angle on minimum dilution for a medium rise building with high exhaust momentum M = 1.50 and wind angle θ = 45°	146
A4-18	Effect of wind angle on minimum dilution for a medium rise building with high exhaust momentum M = 1.28 and wind angle θ = 0°	147
A4-19	Effect of wind angle on minimum dilution for a medium rise building with high exhaust momentum M = 1.28 and wind angle θ = 45°	148

Figure		Page
A5-1	Effect of building shape on minimum dilution for a low rise building with medium exhaust momentum M = 0.768	150
A5-2	Effect of building shape on minimum dilution for a low rise building with high exhaust momentum M = 1.76	151
A5-3	Effect of building shape on minimum dilution for a low rise building with high exhaust momentum M = 1.76	152
A5-4	Effect of building shape on minimum dilution for a low rise building with high exhaust momentum M = 1.76	153
A5-5	Effect of building shape on minimum dilution for a medium rise building with high exhaust momentum M = 1.50	154
A5-6	Effect of building shape on minimum dilution for a medium rise building with high exhaust momentum M = 1.50	155
A5-7	Effect of building shape on minimum dilution for a low rise building with low exhaust momentum M = 0.103	156
A5-8	Effect of building shape on minimum dilution for a medium rise building with low exhaust momentum M = 0.087	157

Nomenclature

A	projected frontal area of building facing into the wind, cm^2
A_e	effective area of exhaust, cm^2
B_1	plume rise constant (see Eq. 3-7b)
B_2	normalized entrainment coefficient, $B_2 = \alpha/\alpha_o$ (see Eq. (4-1) and (4-4))
B_3	empirical constant (see Eq. (3-13))
B_4	momentum factor in entrainment coefficient (see Eq.(4-4), (4-8))
B_5	plume rise constant (see Eq. (3-8))
C_e	concentration of contaminant in the exhaust gas at the vent exit, kg/cm^3
C_{max}	maximum contaminant concentration on the plume axis, kg/cm^3
C_o	median concentration on the plume axis, kg/cm^3
C_r	roof level contaminant concentration, kg/cm^3
C_t	contaminant concentration at radial distance, t from plume axis, kg/cm^3
C_∞	plume centerline concentration of an unconfined jet, kg/cm^3
d_s	stack inside diameter, cm
D_{min}	minimum dilution for a given wind speed at a fixed distance from the exhaust
D_o	apparent initial dilution at the source
D_{stack}	minimum dilution from stack height
E_u	x-direction power spectral density of turbulence kinetic energy
f	frequency, H_z
F	buoyancy flux parameter (see Eq. (A3-3-2))
F_r	density-related Froude number (see Eq. (3-2))

h	plume rise
h_B	plume rise due to buoyancy
h_f	plume rise at final rise condition
h_M	plume rise due to momentum
H	height of building, cm
ℓ	turbulent length scale
L	length of building, cm
M	exhaust momentum factor (see Eq. (3-3))
Q_e	total exhaust volume flow rate, including air and contaminant cm^3/s
Q_o	initial volume rate of air entrained, cm^3/s
Q_T	total volume flow of contaminated air past a fixed point, cm^3/s
R	radius of exhaust plume, cm
R_o	effective initial plume radius, cm
S	stretched-string distance: the shortest distance measured along building surface between exhaust and intake, cm
S_o	distance from vent centerline to the plume virtual origin, cm (see Eq. (3-9))
t	radial distance measured from plume axis, cm
U	wind speed at the height of the exhaust in the undisturbed flow upwind of the building, cm/s
U_{ref}	wind speed at the reference height (z_{ref} = 15.0 cm) in the undisturbed flow upwind of the building, cm/s
U_{local}	wind speed at the height being considered in the undisturbed flow upwind of the building, cm/s
u'	x-direction turbulent velocity, cm/s

v_a	entrainment velocity of ambient air into the exhaust plume, cm/s
v'	y-direction turbulent velocity, cm/s
W	width of building, cm
W_e	exhaust velocity of a vertical uncapped vent, cm/s
W_v	vertical component of vent gas velocity, cm/s
w'	z-direction turbulent velocity, cm/s
x,y	downwind and crosswind distances from origin at base centerline of building upwind face.
x_1,y_1,z_1	coordinates with reference to flush exhaust vent (see Table 4-1)
z	vertical distance above tunnel surface, cm
z_o	characteristic roughness height, cm
z_{ref}	tunnel reference height, 15.0 cm

Greek Symbols

ρ_a	density of ambient air, kg/cm^3
ρ_e	density of vent gas, kg/cm^3
α	entrainment constant, the ratio of jet or plume entrainment velocity to wind speed
α_o	entrainment constant at wind incidence angle $\theta = 0°$
α_w	entrainment constant of a bending-over jet or plume (see Eq. (3-1))
θ	wind direction incidence angle, measured from a line normal to the upwind wall of the building
σ_y	crosswind plume width (standard deviation), cm
σ_z	vertical plume width (standard deviation), cm
Λ_u	integral length scale of turbulence, cm

T_u	integral time scale of turbulence, sec
η	Kolmogoroff microscale of turbulence, cm

Chapter I

Introduction

Industrial processes, research, medical or even food service facilities sometimes generate toxic gases or undesirable odours that have to be vented into the atmosphere. Unfortunately, these vent gases do not always disappear into the atmosphere. Some of them may be recirculated by wind into nearby buildings through ventilation intakes or open windows and create health hazards. So, a designer of an industrial ventilation system is usually faced with the following fundamental questions:

1) Where should the ventilation intake be located to minimize the contamination from the exhaust vent?
2) How can one evaluate the safety level of an existing ventilation system? If it is not safe, how can it be improved?

To answer these questions, the designer has to be able to estimate the level of contamination for a given exhaust to intake configuration.

One approach to solve this problem is to study the dilution process of vent gases around buildings in a simulated atmospheric boundary layer. Usually a wind tunnel is employed to perform the simulation and the dispersion of tracer gas around model buildings is experimentally measured under controlled conditions. Then, the data can be used to test theoretical dilution models developed from general principles of turbulent mixing. If these models are proven valid by data correlation, they can be readily applied to design.

The pioneering investigation adopting the above approach was done by Halitsky (1962, 1963). Using a uniform, non-turbulent approach

flow, he performed tests on a few general rectangular building models, and a site-specific test of the Clinical Center at the National Institute of Health. Based on his measurements, he proposed the following equations to give the minimum dilution levels (i.e. highest possible contamination level) for a given exhaust-to-intake distance, S:

$$D_{min} = \frac{C_e}{C_{max}} = \left[\left(\frac{U}{W_e}\right)^{0.5} + 0.132\left(\frac{US^2}{Q_e}\right)^{0.5}\right]^2 \qquad (1\text{-}1)$$

$$D_{min} = \frac{C_e}{C_{max}} = \left[5.77\left(\frac{U}{W_e}\right)^{0.5} + 0.182\left(\frac{US^2}{Q_e}\right)^{0.5}\right]^2 \qquad (1\text{-}2)$$

But in discussing his own experimental results, Halitsky (1968) recognized that his data showed an overestimation of concentration level at the building surface by a factor as high as 10. So, his dilution models suffered the limitation of being overly conservative (i.e. underpredicting the minimum dilution level or over-predicting the maximum concentration level).

Wilson (1976,1977) suggested that this overestimation in Halitsky's concentration measurement could probably be caused by the use of a non-turbulent approach flow in his wind tunnel simulation. As a result, the effect on dilution due to turbulent fluctuations in the wind was not accounted for in Halitsky's study. Also, some of Halitsky's measurements were taken on the plume axis above the roof where the concentration should be higher than building surface concentrations. So, in his treatment of the subject, Wilson (1976, 1977) used a carefully simulated turbulent atmospheric boundary layer to study the minimum dilution at the building surface. Flush roof and wall vents with zero stack height were considered for a variety of building shapes. For flush exhaust

vents with negligible exhaust momentum (M = 0.11 to 0.15), the minimum dilution on the building surface could be estimated from the simple relationship

$$D_{min} = 0.11 \left(\frac{US^2}{Q_e}\right) \qquad (1\text{-}3)$$

which implies that D_{min} is conveniently independent of building shape and size, characterized by frontal area, $\sqrt{A}$.

A comprehensive comparison between equation (1-3) and Halitsky's formulations, equations (1-1) and (1-2) by Wilson (1976) revealed that equation (1-3) gave a less conservative but more realistic prediction on D_{min}. Hence, equation (1-3) is now one of the recommended equations in the ASHRAE Handbook - 1981 Fundamentals (pp. 14.6; 14.12 - 14.14).

A full scale study recently done at two large nuclear reactor facilities by Sagendorf et al. (1979, p. 596-602) provides a verification of equation (1-3). According to Meroney's review (1982) of these full scale dilution data, equation (1-3) was found to be able to provide a lower bound to 99% of all measurements.

However equation (1-3) can be applied only at distance far enough downwind where D_{min} is greater than 10 because its approximation of the exhaust as a point source breaks down near the source, predicting unrealistically low D_{min}. Being aware of this limitation, Wilson (1983) used an entrainment velocity model to improve equation (1-3) to the modified form:

$$D_{min} = \left[1 + 0.33 \left(\frac{US^2}{Q_e}\right)^{0.5}\right]^2 \qquad (1\text{-}4)$$

which gives the physically correct value of $D_{min} = 1.0$ at the point of release where $S = 0$. It should be noted that the dilution constant 0.33 was chosen to make equations (1-4) and (1-3) equivalent when S is large. In other words, equation (1-4) is not a completely new model but rather a revised version of equation (1-3) with expanded capability.

The studies of Halitsky and Wilson only consider the case with wind incidence angle, θ, equal to zero, which means that the building frontal face is at 90° to the approach wind. In a recent study by Li and Meroney (1983), gas dispersion around a cubical building with non-zero wind angles was investigated. Their tests were done at negligible exhaust momentum in a simulated atmospheric boundary layer with boundary layer thickness, turbulence intensity and scale and building height all very similar to the one used by Wilson (1976). They found that for a change of wind angle θ from 0° to 45°, the minimum dilution level at the building roof decreased by a factor of 4 to 9. (That is, the roof concentration increased when the wind was not at $\theta = 0°$). They suggested the following correction factor to be applied to equation (1-3) in predicting D_{min}:

$$f(\theta) = \frac{1}{1 + \frac{4}{\pi}\theta} \qquad (1\text{-}5)$$

$$\text{for} \quad 0 \leq \theta \leq \frac{\pi}{4}$$

To summarize, these previous investigations have already established a proven minimum dilution model, equation (1-4) that accounts for the variation on dilution due to wind, U; vent-to-intake distance, S and exhaust flow rate, Q_e. If the wind angle θ is not zero, a correction factor, equation (1-5) can be applied.

However, one essential factor that these studies have not considered explicitly is the effect of exhaust momentum. The existing minimum dilution model equation (1-4) and the observed wind angle effect, equation (1-5) were developed for negligible momentum, which would apply in the case of a capped exhaust vent. Exhaust momentum is an essential factor because it governs plume rise and entrainment and induces significant initial dilution near the source as will be shown later in chapter III. In light of this, the following objectives were set for the present investigation:

1) to determine the effect of exhaust momentum on vent gas dilution;
2) to investigate the influence of wind angle on dilution for varying exhaust momentum;
3) to develop simple minimum dilution models that will account for the effects of exhaust momentum and wind incidence angle.

To achieve these objectives, wind tunnel dilution data over a range of exhaust momentum were required. In a previous study, Wilson and Winkel (1982) collected a large amount of dilution data with significant exhaust momentum when they examined the effects of varying stack heights on contaminant level at the building roof. They investigated 24 building shapes with vertically directed roof vents, over a range of exhaust momentum ratios from M = 0.77 to 1.76 for 5 different stack heights. Their zero-stack-height data formed a baseline case to which data of various stack heights were compared in determining the effect of stack height. From the standpoint of the present study, this baseline data set for zero stack height was also suitable for examining the effects of exhaust momentum. It was used to test preliminary dilution

models and to determine what additional dilution data should be taken. The new dilution data were taken using the same wind tunnel model, equipment, and concentration measurement techniques developed by Wilson (1976,1977).

The major tasks of this investigation included the following:

1) to review the atmospheric boundary layer simulation technique developed by Wilson (1976) by making new turbulence and dilution measurements on the same wind tunnel system to ensure that the data taken in this study were comparable to the data from previous studies by Wilson (1976,82).

2) to construct a two dimensional step to simulate a wide building with a large width to height ratio, W/H and free of the influence of building sides. It was used to probe the behavior of a vertically directed exhaust jet from a flush vent in order to study the physics of bent-over momentum jet rise and initial dilution.

3) to take additional data from four newly constructed building configurations to provide a more extensive data base to properly define the influence of exhaust momentum and wind angle on vent gas dilution.

4) to use the baseline data set from Wilson (1976) and Wilson and Winkel (1982) to develop and test new dilution theories derived to incorporate the effect of exhaust momentum and wind incidence angle.

CHAPTER II

Wind Tunnel Modelling

Chapter Overview

This chapter will describe in detail the three major components of the wind tunnel system used for simulating vent gas dilution. They are:

1) The simulation of an atmospheric boundary layer,
2) Modelling building and exhaust gas, and
3) The concentration measurement system used to check for vent gas dispersion.

Also the limitations of using small scale wind tunnel models will be presented.

2.1 Simulation of an Atmospheric Boundary Layer in a Wind Tunnel

In a study done by Wilson (1976) on the contamination of building air intakes from nearby vents, he noted the importance of simulating the random fluctuations of atmospheric turbulence. His review on Halitsky's test results (1961, 1962) indicated that the absence of such a simulation might result in overestimating concentrations of vent gas near buildings by a factor of 5 to 10. So, the present study sought to account for the effects of atmospheric turbulence on vent gas dispersion by simulating an atmospheric boundary layer in the wind tunnel.

2.1.1 Present Wind Tunnel Model

In the present study, the site chosen for test buildings was to be an isolated region of a lightly built-up urban area with no nearby building influence. So the objectives of this wind tunnel model was to produce a turbulent shear layer that would possess the turbulent

characteristics and wind profile of this type of terrain. To achieve this, the author used a simulation technique that was first conceptualized by Counihan (1973) and further developed by Wilson (1976). This technique has been proven successful in the ASHRAE studies previously done by Wilson (1976, 1977) and it utilized a small, low speed, open circuit wind tunnel plus a system of turbulence generating elements. Their set up is shown schematically in Figure 2-1. Basically the system of turbulence generating elements contained the following:

a) A series of vortex generators 29 cm high. They were there to create horizontal vortices to simulate the full scale large eddies.

b) A barrier, 3.9 cm high, mounted across the width of the tunnel. It acted as a trip to accelerate the development of the boundary layer by inducing vertical momentum into the flow near the surface.

c) A distribution of roughness elements that covered an area of about 82 cm by 30 cm. They were "LEGO" blocks of size 1.5 x 1.5 x 1.0 cm high, evenly distributed to supply additional turbulence generation near the surface. This roughness also helped the developing boundary layer to be more uniform laterally and longitudinally.

As air flowed past these elements, a turbulent shear layer of the desired nature would be generated in the test section of the tunnel. It should be noted that only neutral atmospheric condition was simulated in the present model. Different modelling techniques will be required if stable or unstable conditions are desired. However, stable or unstable conditions usually occur at low wind speeds ($U < 2$ m/s), which enhance

plume rise and reduce the severity of vent gas contamination around buildings. In other words, neutral stability usually prescribes the worst environment for vent gas diffusion and is the appropriate condition to simulate when developing a minimum dilution model.

2.1.2 Reynolds Number Mismatch in Atmospheric Boundary Layer Modelling

Reynolds number by definition represents the ratio of inertial to viscous forces. It can be shown from the nondimensionalized equation of motion that Reynolds number actually governs the contribution of the shear term $(\partial U/\partial z)$ to the dynamics of the flow. Besides, according to Snyder (1972) and Hinze (1975, p. 225), the turbulence structure of a given flow, represented by the ratio of the integral length scale to the Kolmogoroff microscale (Λ_u/η), depends on the Reynolds number in the following manner,

$$\frac{\Lambda_u}{\eta} \alpha R_{e_\Lambda}^{0.75} \qquad (2\text{-}1)$$

For proper simulation, the Reynolds number criterion should be considered. However, for small scale wind tunnel models, large mismatches in Reynolds number often occur simply because of the size reduction of the models. The discrepancy will even be more pronounced if flow speeds in the model are smaller than full scale velocities. In this study, flow speeds in the model are in the same order of magnitude as the full scale ones. So the mismatch is mainly due to the model scale, which is about 2000:1 in this case and the Reynolds number is 2000 times smaller than its full scale equivalent. Using equation 2-1, $(\Lambda_u/\eta)_{model}$ is found to be approximately 300 times less than $(\Lambda_u/\eta)_{full\ scale}$. In other words, the range of eddy sizes is much smaller in the model.

One question that needs to be answered is whether this Reynolds number mismatch leads to an incorrect simulation. To answer that, the turbulence length scales in the simulation were measured so that the effect on turbulence structure due to Reynolds number could be evaluated. Details of these measurements and the results will be presented in the following sections along with the steps that were taken to preserve the dynamic similarity of the flow despite the Reynolds number mismatch.

2.1.3 Mean Velocity and Turbulence Measurements

In order to evaluate the quality of the simulation, turbulence measurements were carried out in the approach flow using a TSI model 1050 constant temperature hot wire anemometry system and a DISA type 55P11 probe.

To simplify the description of flow measurements, x,y and z axes are used to denote the longitudinal, lateral and vertical flow directions respectively. The origin of the coordinates is at the base of test building frontal area which is about 17.6 cm from the last roughness element and equidistant from the sides of the tunnel (see Figure 2-1).

It seemed logical to take measurements at the test building location where vent gases would be emitted. A traverse was performed in the z-direction at the centre of the test building location but with no building present in order to obtain the upwind approach flow profile. During the traverse, the tunnel reference velocity (U_{ref}), i.e. the velocity at z=15 cm, was kept constant at 11.2 m/s. Measurements were taken of U and u' at 15 different z-locations. At each of these locations, the hot wire signal was measured digitally at 6500 samples per

second using a DEC Minc-11 computer equipped with a DT2782D1 analog to digital converter and a hard disk. The digitized hot wire voltage output was then converted to discrete velocity values using the anemometer calibration equation and stored in binary form on floppy disk. A floppy disk was filled with about 506,000 data points at each location. This full disk resulted in an averaging time of about 78 seconds. This averaging time corresponded to the passage of about 15,000 integral scale of turbulence and was sufficient to produce steady values of the spectral density.

2.1.4 Defining the Quality of the Simulated Boundary Layer (at the building location but with no building present)

Table 2-1 summarizes the flow characteristics of the simulated boundary layer. In it a comparison with full scale measurements is also shown. In the following, each of these characteristics will be discussed in detail.

2.1.4a Vertical Profile of Mean Velocity

As wind flows past a building, it creates the flow patterns on the building surface illustrated in Figures 2-2 and 2-3. These streamline patterns depend strongly on the shape of the upwind velocity profile. This complex flow pattern influences the behavior of vent gas dilution. For this investigation to be realistic, the shape of the upwind velocity profile must correspond to that of the atmospheric wind and is one indicator of the quality of the simulation.

Figure 2-4 indicates that the shear layer had a thickness of about 25 cm. For a scale factor of 2000:1 (which will be justified later in

section 2.1.4e) this represents a layer of 500 m thick full scale, which could be divided into three zones:

i) A smooth wall inner layer from tunnel surface to approximately 2 cm (0 to 40 m full scale) which had a roughness height, z_o, of 0.0004 cm (0.8 cm full scale), see Figure 2-5.

ii) From z=2 to 15 cm (40 to 300 m full scale), the layer behaved like a rough wall boundary layer with a roughness height, z_o, of 0.2 cm (4 m full scale), see Figure 2-5.

iii) An outer zone from z=15 to 25 cm (300 to 500 m full scale).

The presence of a smooth inner layer was a direct consequence of the absence of roughness elements in the test section. It was purposely arranged this way to simulate an isolated region in an urban area which is free of localized interactions from nearby buildings.

Since all the building roof heights tested were in region ii, which behaved as a rough wall boundary layer (see Figure 2-4), the thickness of the rough wall regime, 15 cm (300 m full scale), was taken to be the thickness of the simulated urban boundary layer, within a 500 m thick rural boundary layer. A power law representation of the form

$$\left(\frac{U}{U_{ref}}\right) = \left(\frac{z}{z_{ref}}\right)^{0.25} \qquad (2\text{-}2)$$

was chosen to fit the upwind mean velocity profile in Figure 2-4, and this representation predicted the velocity variation with height reasonably well. In the lower half of the inner layer, where $z < 1.0$ cm (20 m full scale), the accuracy error ranged from 3 to 15%. From $z = 1.0$ to 15 cm (20 to 300 m full scale), including the upper half of the smooth wall layer and the entire rough wall layer, the power law was within 2%.

Table 2-1 shows that this power law representation was in good agreement with full scale observations where the power varies from 0.21 to 0.30 depending on the distribution and sizes of urban buildings. The power law function gave poorer agreements in the outer zone, where $z \geq 15$ cm (300 m full scale). However, the deviation was unimportant for none of the building heights interacted with this zone.

2.1.4b Turbulence Intensity

According to the statistical theory of point source dispersion in homogeneous turbulence, turbulence intensity is one of the relevant variables that govern the rate of plume spread. In this investigation, only x direction turbulence intensity (u'/U) was measured although plume growth was actually controlled by the y and z direction turbulence (v'/U and w'/U). However, v'/U and w'/U in the neutrally stable atmosphere are related to u'/U in fixed ratios [see Counihan (1975)]:

$$\frac{v'}{U} \simeq 0.75 \frac{u'}{U} \qquad (2\text{-}3)$$

and

$$\frac{w'}{U} \simeq 0.5 \frac{u'}{U} \qquad (2\text{-}4)$$

So, once u'/U is properly simulated, v'/U and w'/U should also be correct. This assumption was actually verified by Wilson's measurements (1976) taken previously in the same wind tunnel model.

The x-direction turbulence intensity based on local velocities and that based on the reference velocity are both shown in Figure 2-6. Within the lower region of boundary layer, reference velocity intensity, u'/U_{ref} varied between 10 to 15% while u'/U_{local}, 15 to 25%. These measurements were quite consistent with full scale observations [Counihan (1975)], which indicated that urban u'/U_{local} should lie in the range of 20 to 30% (see Table 2-1). In the upper region of the

layer, both u'/U_{local} and u'/U_{ref} decreased steadily with height to below 10%. This was expected because production of turbulence occurred in the shear layer near the surface. A gradual drop in u'/U_{ref} toward the surface was also observed. This was probably due to the transition from the decaying rough wall layer to the smooth inner wall layer in which case a decline in turbulence intensity was a natural consequence. The presence of such a transition was encouraging because it was characteristic of the site that the model was to simulate - an isolated region in an urban area with no nearby building influence.

2.1.4c Integral Length Scale of Turbulence

As discussed in section 2.1.3, Reynolds number mismatch had a significant effect on the turbulence scale ratio, Λ_u/η of the simulated boundary layer. The extent of this effect could be evaluated only if the integral length scale, Λ_u, was known. To estimate Λ_u, the integral time scale, T_u, at varying heights was first determined from the autocorrelation of the x-direction turbulent velocities. Assuming turbulence is convected at the local mean velocity, U, the product of time scale and mean velocity was used to infer the turbulence length scale. It should be noted that an exponential function was used to fit the autocorrelation data in determining T_u. This idea of approximating the autocorrelation as an exponential decay is further discussed in Hinze (1975, p. 66-67).

Figure 2-7 illustrates the variation of the x-direction length scales with height. Roughly speaking, for the first 10% of the boundary layer, the values of length scale increased monotonically, which is typical of a turbulent boundary layer. Then, there was a region with the length scale remaining almost constant at Λ_u = 62 mm. In the upper region where z was larger than 10 cm (200 m full scale) the length scale

declined monotonically. This did not necessarily mean a decrease in eddy sizes but rather might be an indication of turbulence intermittency in this outer region.

As noted in section 2.1.3, $(\Lambda_u/\eta)_{model}$ was about 300 times less than $(\Lambda_u/\eta)_{full\ scale}$ because of Reynolds number mismatch. According to Snyder (1972), it is only the lower end of the eddy sizes that will be cut off in this reduction of Λ_u/η. Letting $(\Lambda_u)_{model}$ be 60 mm, which was the length scale within building heights, the cutoff eddy size in length scale within building heights, the cutoff eddy size in the model was about 0.09 mm which is equivalent to a full scale eddy of 180 mm (see Appendix A2-1 for calculation), whereas the smallest eddy size in the atmospheric boundary layer is of the order 1 mm (Lumley & Panofsky, 1964) and (Appendix A2). The main limitation of the model was its inability to reproduce full scale eddies smaller than 180 mm. However, practically speaking, eddies less than 180 mm are not expected to contribute significantly in the diffusion of a contaminant in the atmosphere. So, although the model did not meet the Reynolds number criterion for similarity, its effectiveness in simulating atmospheric diffusion of contaminants should be unimpaired.

2.1.4d Power Spectral Density

In defining the detailed features of the simulated atmospheric turbulence, both the range of eddy sizes and the distribution of turbulence energy must be considered. To check the turbulence simulation, power spectra, the indicator for the distribution of kinetic energy in eddies, were measured in the simulated layer.

Counihan (1975) in his review on atmospheric boundary layers, cited a number of full scale measurements of x-direction power spectra in

urban areas, and these are listed in Table 2-1. The majority of the data indicates that the atmospheric spectrum had a slope about -5/3 at the high frequency end. Also, this characteristic was found to be invariant with height z according to the experiments of Singer et al. (1967).

Figure 2-8 shows two samples of the spectra obtained in the range of z = 0.3 to 15 cm (6 to 300 m full scale). It was found that the spectra in this range were almost invariant with height. For instance, the two shown in Figure 2-8 both peaked at about 6 Hz indicating that the energy containing eddies at z=1.5 and 15 cm were roughly of the same magnitude. Also both spectra were quite consistent with the -5/3 law in the high frequency end just like their full scale counterparts. However, in each of them, distinguishable "bumps" were noticed at a number of frequencies, particularly at 12 and 25 Hz. They could be possibly the remnants of vortex shedding occurring at the vortex generators upstream.

Major deviations from the ideal spectrum were observed for z > 15 cm where strong evidence of vortex shedding was seen at 12 Hz. Because all building heights were less than 6 cm, so for the purpose of this study, the turbulence in the simulated layer could be regarded as being in good agreement with full scale observations.

2.1.4e Scale Ratio

In comparing the full scale measurements and wind tunnel values of the boundary layer thickness, roughness height and integral length scale, it was found that the model scale varied from 500:1 to about 4000:1 as shown in Table 2-1. The question to consider is whether the choice of model scale will affect vent gas dilution scaling

significantly. The answer depends on how much atmospheric turbulence scale influences plume spread. As demonstrated by Pasquill (1974, p.365-378), plume spreading in the atmosphere could successfully be described by a power function of downwind distance, S. On that basis, Wilson and Winkel (1982) expressed the power relationship as:

$$\sigma_y = \left(\frac{v'}{U}\right)(\beta \Lambda_v)^{1-a_y}(S)^{a_y} \qquad (2\text{-}5)$$

where

σ_y is the plume spread in y direction

$\frac{v'}{U}$ is the y direction turbulence intensity

Λ_v is the Eulerian scale of turbulence

β is the Eulerian-Lagrangian ratio, with a value usually taken as 4.0

According to statistical theories of dilution, a_y must have values between 0.5 and 1.0. In the present study it was seen to vary between 1.0 and 0.75. Then, at most σ_y was proportional to the 0.25 power of Λ_v from equation (2-5), which means that a factor of 2 difference in Λ_v would cause only a 20% change in σ_y in the worst case. Besides, the turbulence responsible for exhaust gas diffusion near a building is mostly generated by the building itself, and the plume spread of a vent gas is only weakly dependent on the atmospheric turbulence scale. The choice of model scale, either 500:1 or 4000:1, is not expected to significantly affect dilution scaling. For the present study, the average model scale was taken as 2000:1, plus or minus a factor of two.

2.1.4f Comparison With Previous Wind Tunnel Simulation

Table 2-1 shows a comparison between the present simulation and measurements reported by Wilson (1976) using the same tunnel and

identical turbulence generating elements but different measurement technique. Wilson's turbulence data were taken using a DISA #55D05 constant temperature anemometer with DISA linearizers. The mean and RMS velocities were obtained utilizing analog devices: an RMS voltmeter complete with external analyser. The results from the two separate simulations were remarkably similar, demonstrating the repeatability of the simulation technique. The only exceptions were a 50% difference in roughness height and a 25% difference in length scale.

2.2 Building Models

Figures 2-9 and 2-10 exhibit all the building shapes used in this investigation. This variety comprises of buildings developed in three different studies; namely:

1) ASHRAE study by Wilson (1976) - Buildings A1, A3 and A4
2) ASHRAE study by Wilson and Winkel (1982) - Buildings 2, 6 to 10, 12 to 15 and 18 to 24
3) The present study - Buildings 31, 43 to 46, and 48 to 62.

They represented low-rise, flat-roofed industrial configurations. All of them were fabricated by cementing together various combinations of aluminum blocks. With the exception of buildings A1, A3 and A4, every building model was furnished with intake locations flush with building surface. The shaded regions shown in Figures 2-9 and 2-10 identified the blocks housing these intake locations. The size of these intakes was 0.1 cm inside-diameter and each block contained 24 to 31 of them. Also there was a number of vent locations on the block for a 0.132 cm inside diameter stack to be inserted. Yet in this study, the stack was always placed at the center of the block, flush with building surface. The unit length on these model buildings was 1.5 cm. Given the present

model having a scale ratio ranging from 500:1 to 4000:1, a building of one unit length in the model represented a height of 7.5 to 60 m full scale.

One notable feature of the building models was their sharp edges which were incorporated to reduce the effect caused by Reynolds number mismatch. According to Golden's experiment (1961), cited by Snyder (1972) in his review on Reynolds number effects, a condition was determined to salvage the dynamic similarity in the model despite Reynolds number mismatch. This condition requires building models to have sharp edges to fix flow separation points and a Reynolds number based on building scale to be greater than 11,000 to minimize viscous effects on dilution. In this investigation, with the Reynolds number kept above 16500 and using only sharp edged buildings, the effect due to Reynolds number mismatch should be negligible.

2.3 Exhaust Gas System Modelling and Concentration Measurements

A tracer gas system, originally developed by Wilson (1976) for previous ASHRAE studies was employed to model the exhaust gas system. Helium was discharged from vents located on buildings to simulate an effluent gas. The rate of emission was controlled by a rotameter flowmeter system as schematically displayed in Figure 2-1. This flowmeter system also allowed the blending of known mixtures of helium and air. The density and helium concentrations of the simulated exhaust gas could be adjusted as desired.

To measure the diffusion of vent gas near buildings, gas samples from each receptor location were aspirated through the helium detector using a vacuum pump. The helium detector was basically a four-arm gas chromatograph cell with two active arms: - one sensing the sample from

the receptor and the other, the reference gas sample taken from tunnel inlet to compensate for possible background build-up of helium inside the tunnel. If the sample from the receptor contained helium, it would result in a bridge imbalance and produce a voltage output proportional to the helium concentration. A mean value of the bridge output was taken by a digital voltmeter and converted to concentration reading by a known calibration constant, 0.46 $\pm$ 0.01 mV/ppth. The fluctuation of the bridge output with time was recorded on a strip chart recorder to facilitate the detection of zero drift in the bridge. The schematic setup of all these equipment is shown in Figure 2-1.

Two techniques were used in aspirating gas samples from receptor locations for analysis:

a) Through intake locations flush with building surface:

All the buildings tested, except the two dimensional step and buildings A1, A3 and A4, were equipped with intake locations flush with building surface described in section 2-2. Each of these locations had a size of 0.1 cm inside diameter and was connected with plastic tubing to a control manifold (see Figure 2-12). Because the helium detector bridge was sensitive to density change caused by pressure drop in the sampling tubes, the tube lengths had to be trimmed at the manifold to maintain a uniform zero signal at all the intake locations.

b) Through concentration probe:

Basically the probe was a bent stainless steel tube with a tip opening of 0.1 cm inside diameter. To aspirate a gas sample it was placed at receptor locations with its inlet facing the direction of flow. This movable probe had the advantage of

measuring not only exhaust gas concentrations on building surface but also at locations away from the surface, ideal for tracing exhaust gas plume trajectory. Its main disadvantage was that it had to be carefully positioned in taking every reading thus making concentration measurements very cumbersome.

These two techniques were compared in a previous ASHRAE study by Wilson (1976). He found that between the two methods there was an average of 10% difference in concentration measurements. So the data measured would at least have a 10% uncertainty level.

2.3.1 Sampling Rate

Sampling rate was controlled by a needle valve and maintained at 90 ml/min throughout the study. That resulted in a suction velocity of 1.9 m/s irrespective of which aspiration technique was used because both had the same inlet diameter of 0.1 cm. The tunnel velocity at building height was typically beween 6.0 to 10 m/s, i.e. three to five times higher than the suction velocity.

2.3.2 Sampling Time

A sampling time of 100 seconds was found to be adequate to provide a stable mean value for concentration measurement. The interesting thing to know is the full scale sampling time that this 100 seconds corresponds to. According to Wilson (1983), this sampling time would be equivalent to a 30 to 60 minute time average full scale. In general, a one hour average value will be adequate to give a realistic estimate of the hazard condition in a particular contamination problem.

2.3.3 Calibration of The Tracer Gas System

Before each set of tests was done, the helium detector bridge was calibrated by blending known mixtures of helium and air using the rotameter flowmeter. Within the range of calibration, 1000 to 9000 ppm, the bridge response usually remained very linear with a maximum deviation of only 2% and a sensitivity of 0.46 mV/ppth. The bridge also possessed a very fine resolution, $\pm$ 0.5 ppm and was accurate to $\pm$ 10 ppm.

2.3.4 Repeatability of Concentration Measurements

The present study utilized the same wind tunnel and tracer gas system as the two previous ASHRAE studies [Wilson (1976,1982)]. The question to ask was whether the results of this investigation would be comparable to the previous ones so that all three could be considered together to draw conclusions. The answer depended on how repeatable the concentration measurements were in this particular wind tunnel system. The author sought to verify it by duplicating two of the tests in the test series by Wilson and Winkel (1982) using buildings 2 and 22. Each test was performed twice. It was found that the maximum concentrations on roof surface were within 10% of the results in the previous tests, an agreement well within the uncertainty limit of concentration measurement.

This concludes the description of the wind tunnel system for the simulation of vent gas dispersion. In the following chapters, data collected from this wind tunnel model will be discussed and used to devise dilution models to account for the effects of exhaust gas momentum and wind incidence angle on exhaust gas dispersion.

TABLE 2-1

Comparison of Wind Tunnel Simulation with

a) Full Scale Measurements
b) Previous Wind Tunnel Measurements (Wilson, 1976)

Parameters	Present Study	Previous Study	Full Scale Measurement	References
MEAN VELOCITY PROFILE	$U\alpha\ Z^{0.25}$	$U\alpha\ Z^{0.23}$	i) $U\alpha(Z)^{0.21}$ for urban terrain	Jones et.al. (1971)
			ii) $U\alpha(Z)^{p}$ p=0.21-0.23, suburban p=0.28-0.30, urban	Counihan (1975)
TURBULENCE INTENSITY				
a) $\frac{\sqrt{(u'^2)}}{U_{REF}}$	0.1 - 0.15	0.1 - 0.15	-	-
b) $\frac{\sqrt{(u'^2)}}{U_{LOCAL}}$	0.15 - 0.25	-	0.2 - 0.3	Counihan (1975)
ONE-DIMEN. POWER SPECTRUM OF TURBULENCE KINETIC ENERGY E_u	$E_u\alpha\ f^{-5/3}$ @ the high frequency end	-	$E_u\alpha\ f^{-5/3}$ @ the high frequency end	Kaimal et.al. (1972) Notess (1957,59) Henry (1959)
BOUNDARY LAYER THICKNESS	15 cm (600 m using 4000:1 scale ratio)	15cm	600 m (average)	Counihan (1975)
ROUGHNESS HEIGHT Z_o	0.2 cm (1 m using 500:1 scale ratio)	0.1 cm	1 m, suburban 2-3 m, urban	Counihan (1975)
INTEGRAL LENGTH SCALE Λ_u	i) increases steadily from 3.5 to 5.8 cm for Z < 2 cm ii) 6.0±0.2cm for 0.2≤Z≤8.5cm	4.5 cm @z=7.5cm	increases with height up to 200-300 m	Counihan (1975)

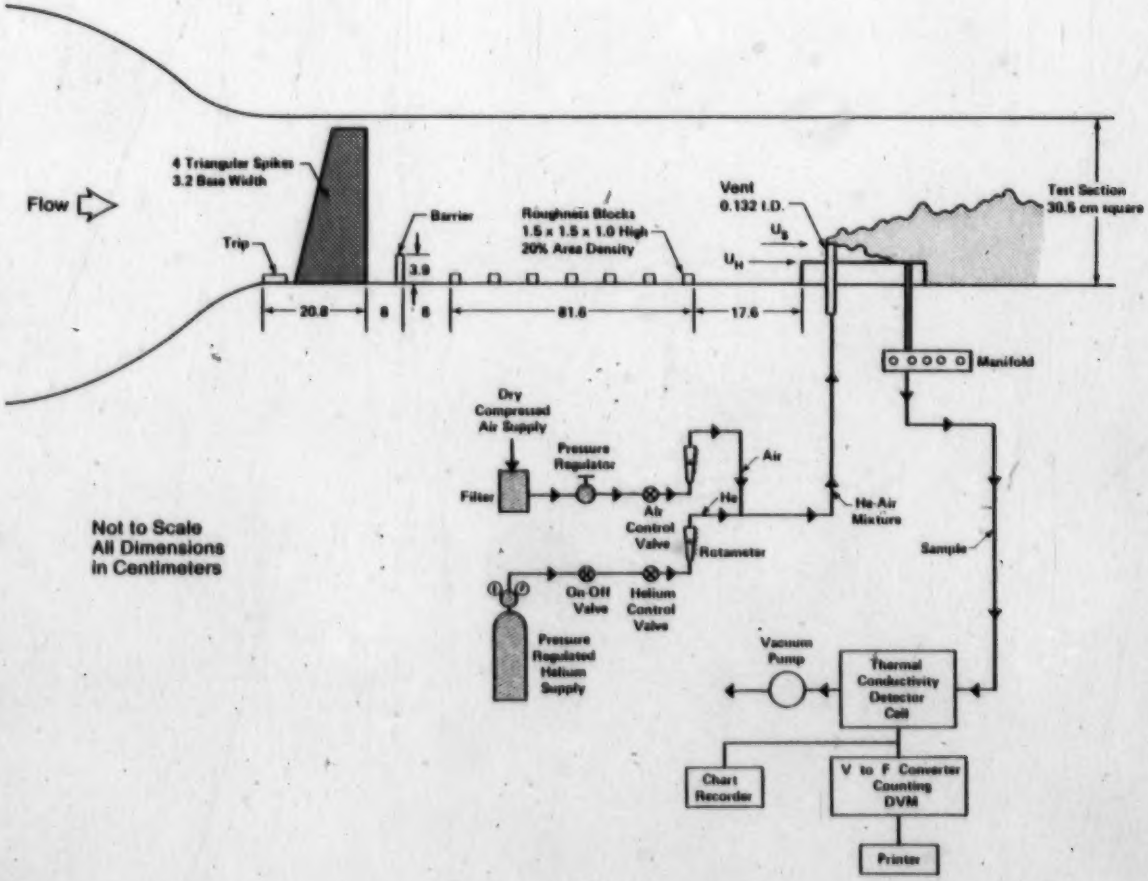

Figure 2-1 Schematic of wind tunnel, turbulence generating elements and tracer gas system

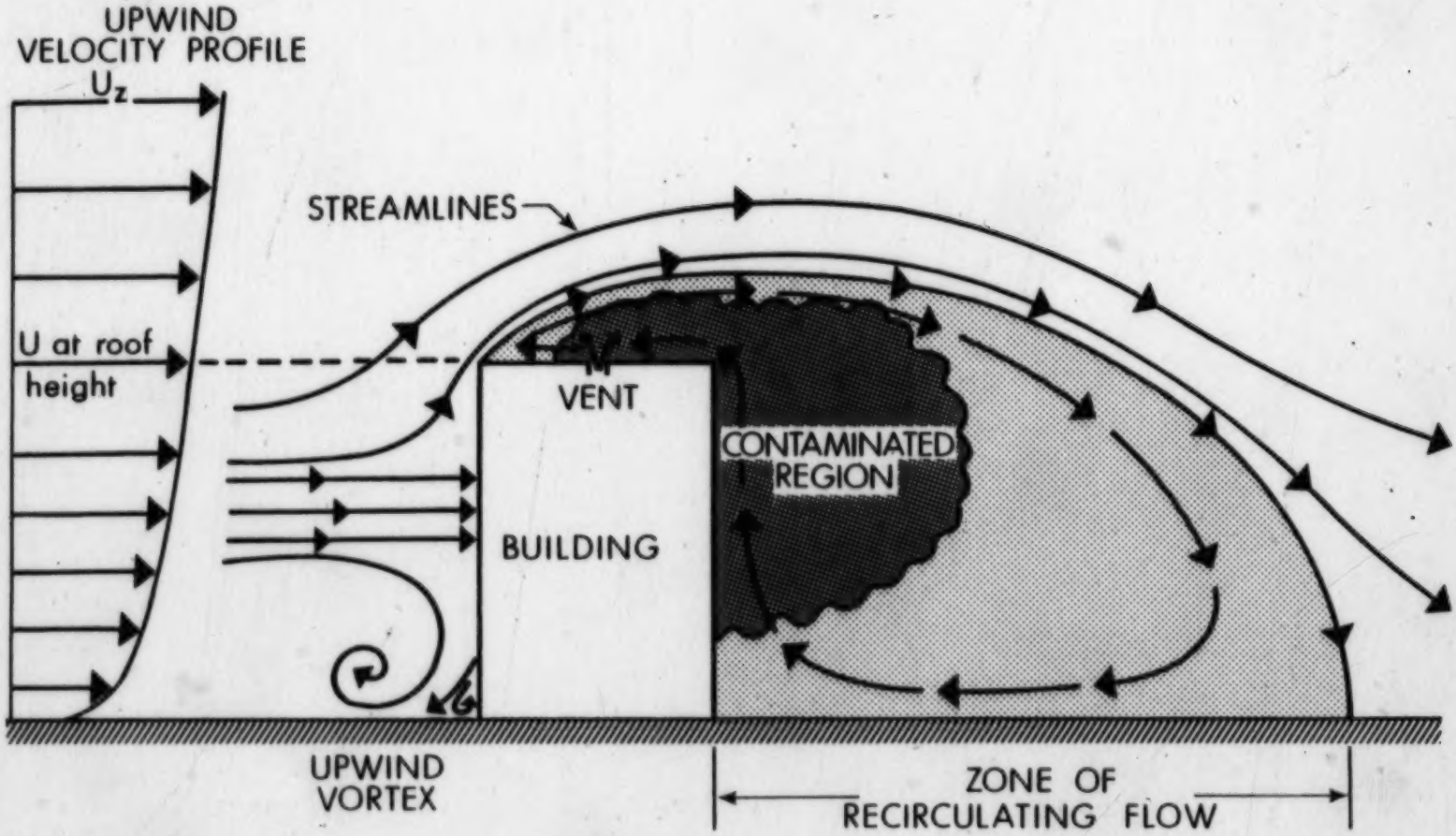

Figure 2-2 Streamlines and exhaust gas dispersion around a building

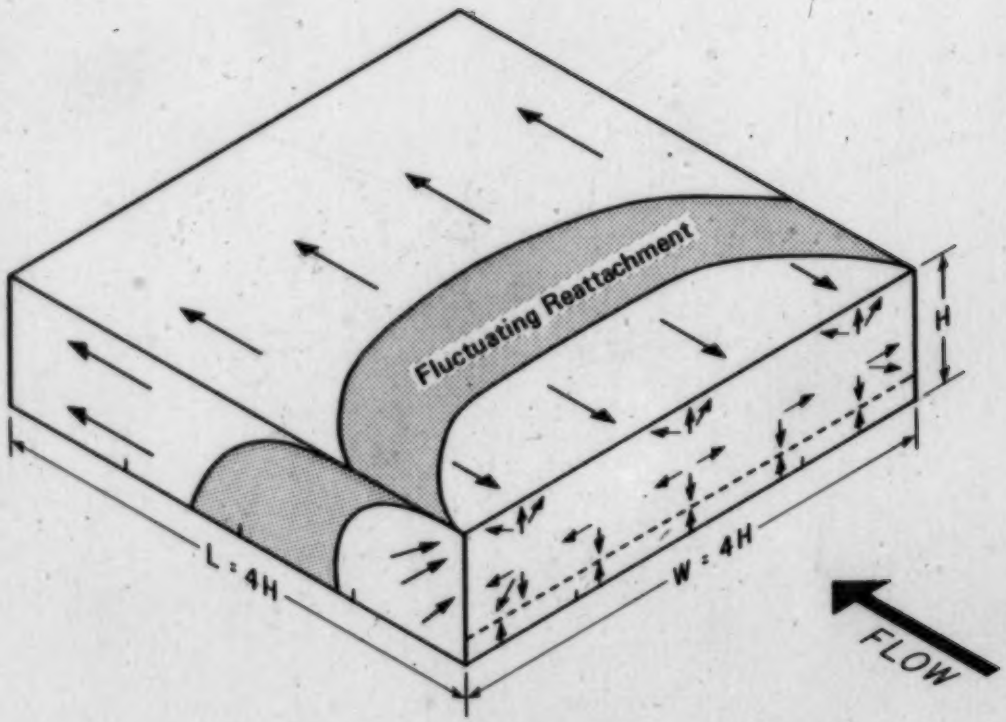

Figure 2-3 Flow patterns on a wide flat-roofed building surface, from flow visualization measurements

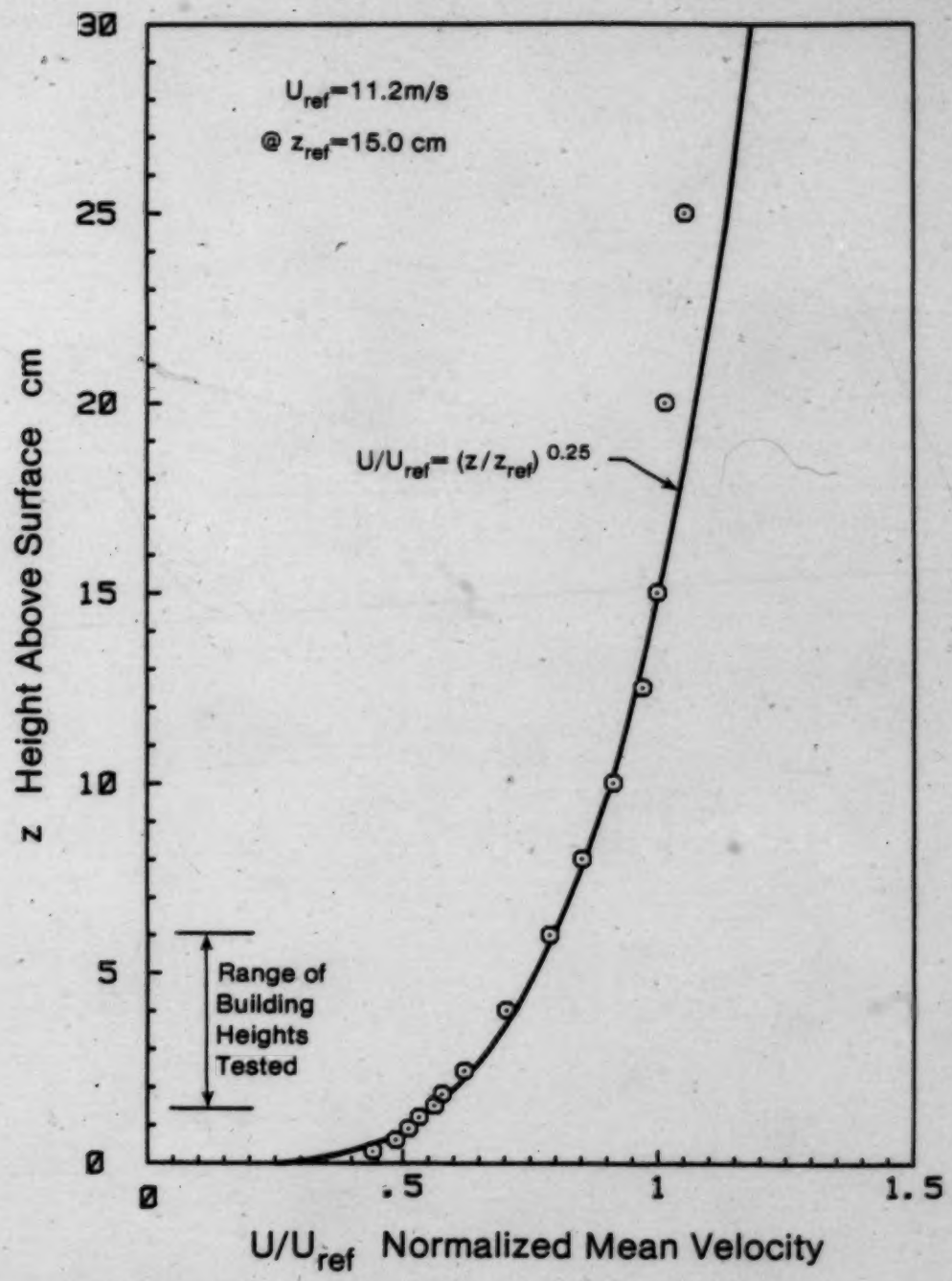

Figure 2-4 Vertical profile of mean velocity measured with hot wire anemometer at model building location with no building present

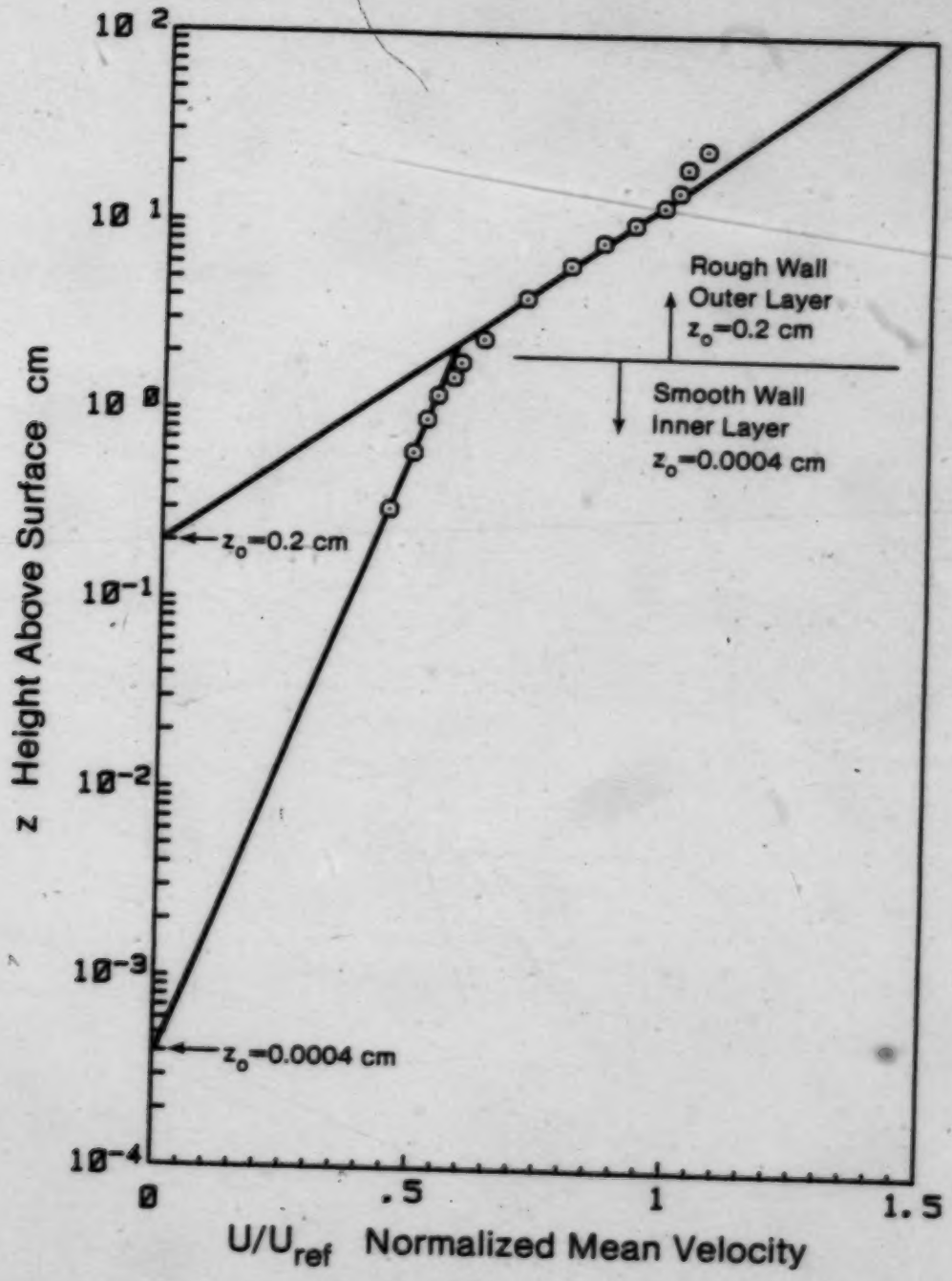

Figure 2-5 Transition of smooth surface inner wall layer to rough surface outer wall layer in the simulated atmospheric boundary layer

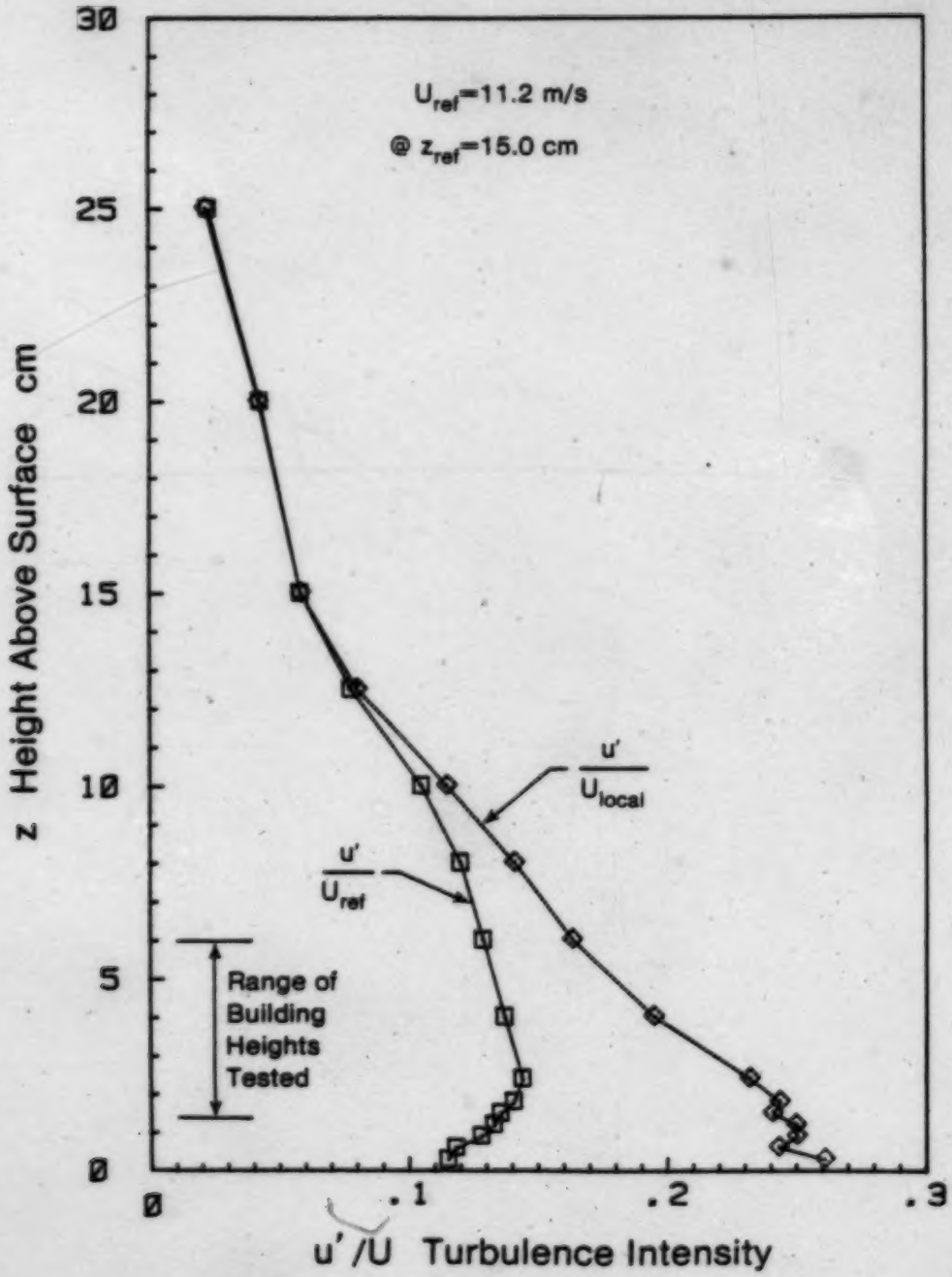

Figure 2-6 Vertical variation of x-direction turbulent velocity at model building location with no building present

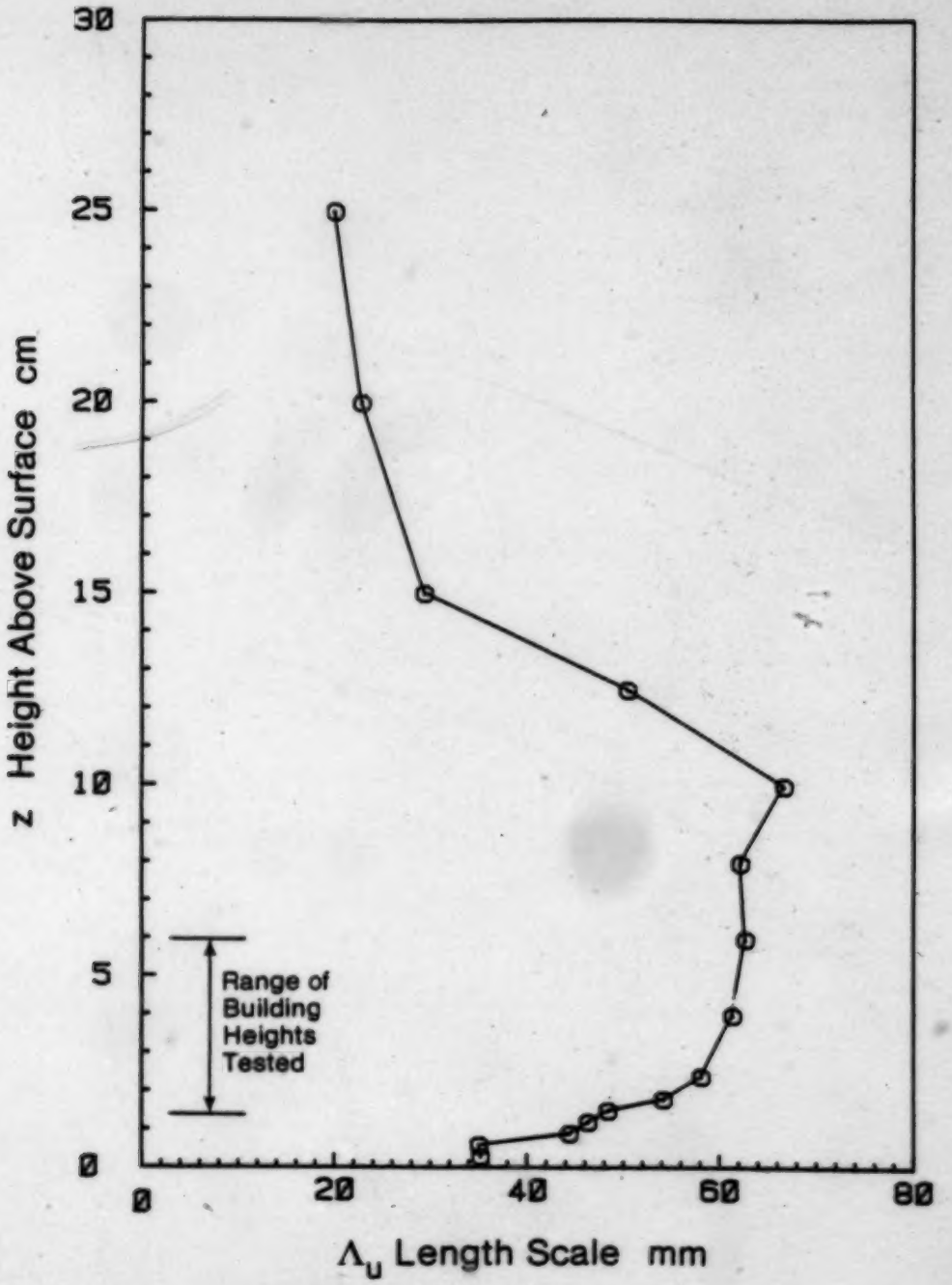

Figure 2-7 Vertical profile of x-direction integral length scale of turbulence at model building location with no building present

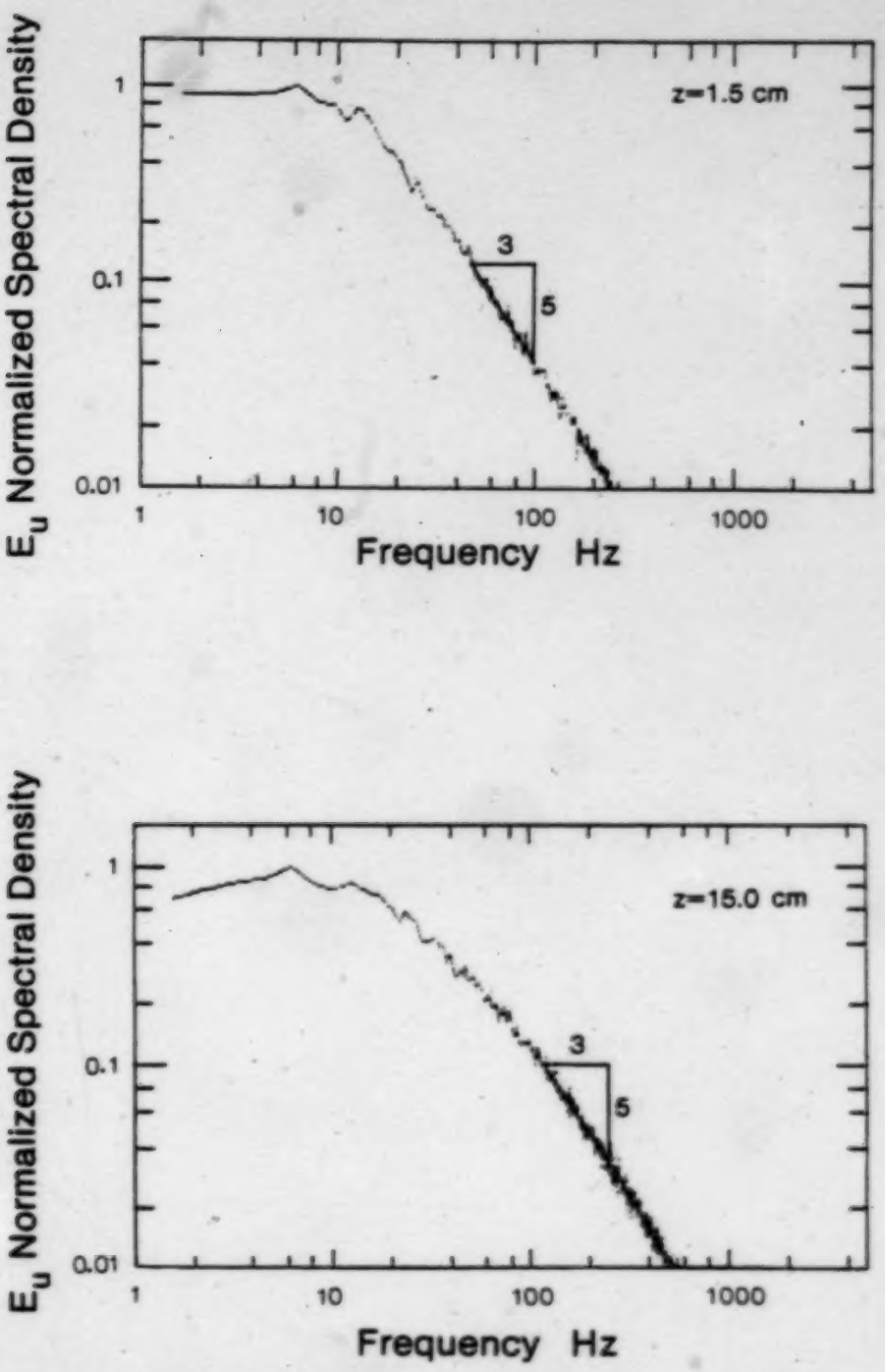

Figure 2-8 Power spectral densities of along-wind turbulence u' at z = 1.5 cm (30 m full scale) and z = 15 cm (300 m full scale) of the simulated atmospheric boundary layer at model location with no building present

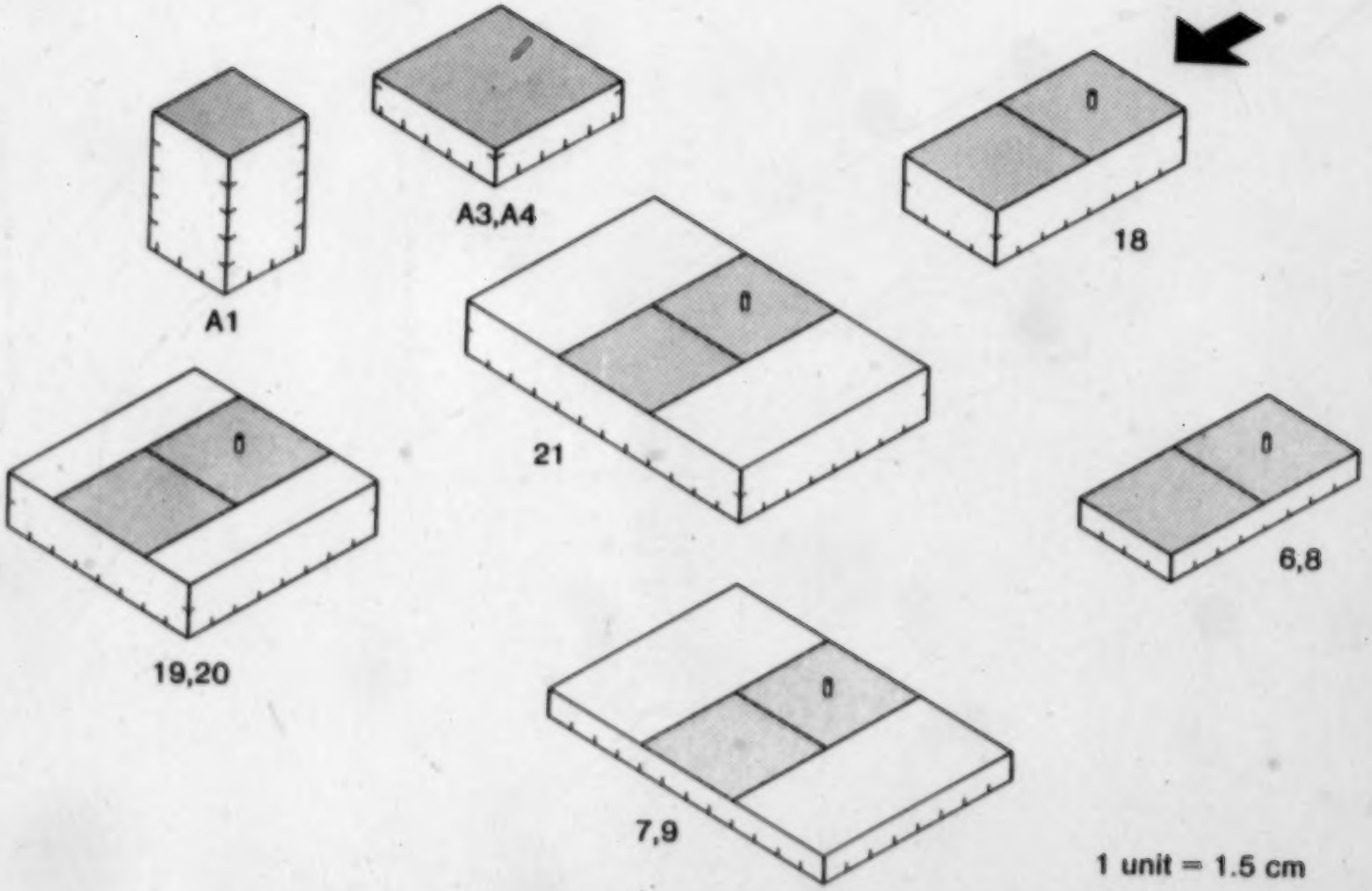

Figure 2-9 Building models for wind tunnel concentration measurements with wind direction perpendicular to upwind face ($\theta = 0°$ only)

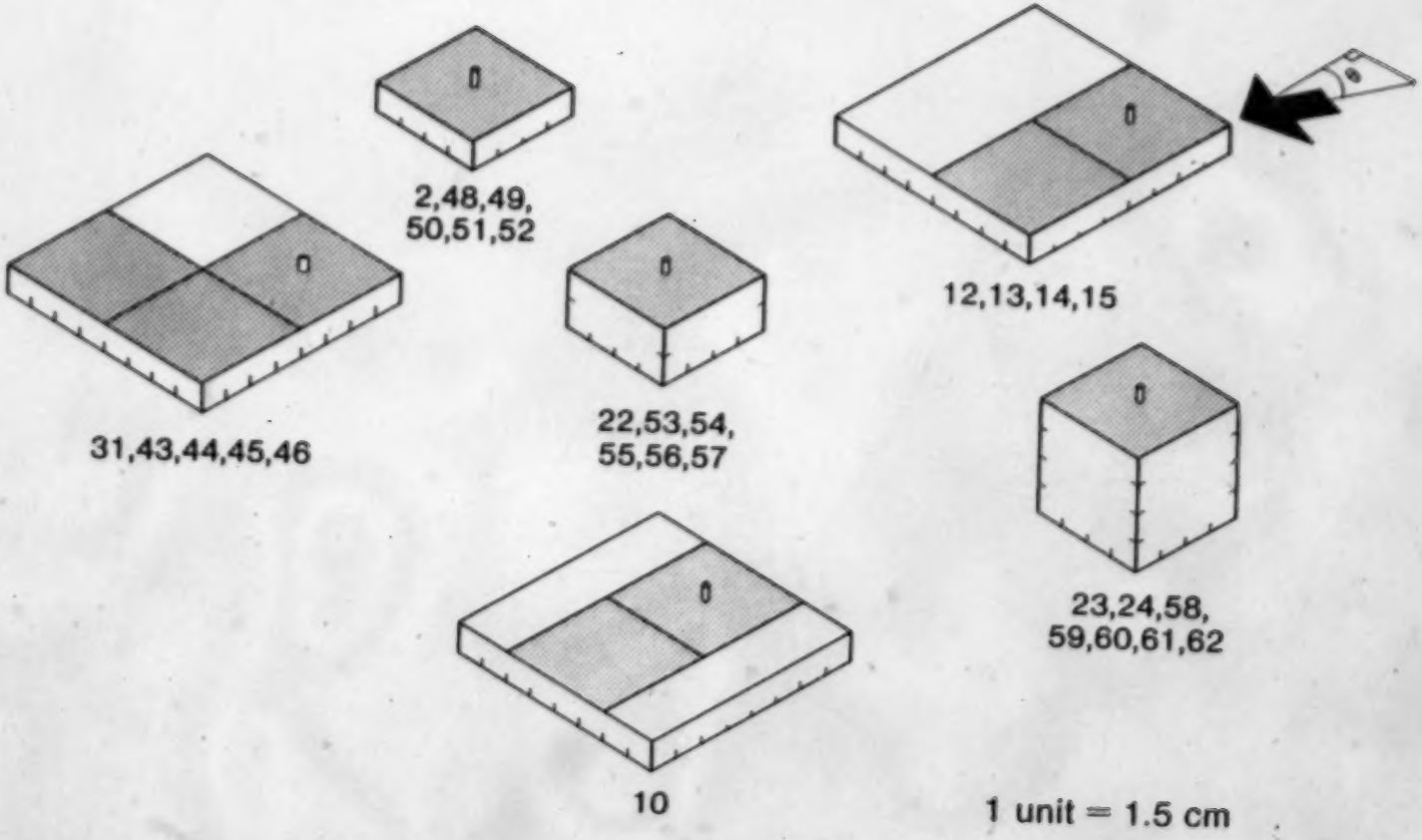

Figure 2-10 Building models for wind tunnel concentration measurements at wind incidence angle in the range $0° \leq \theta \leq 45°$

Figure 2-11 Installation of building model in the wind tunnel

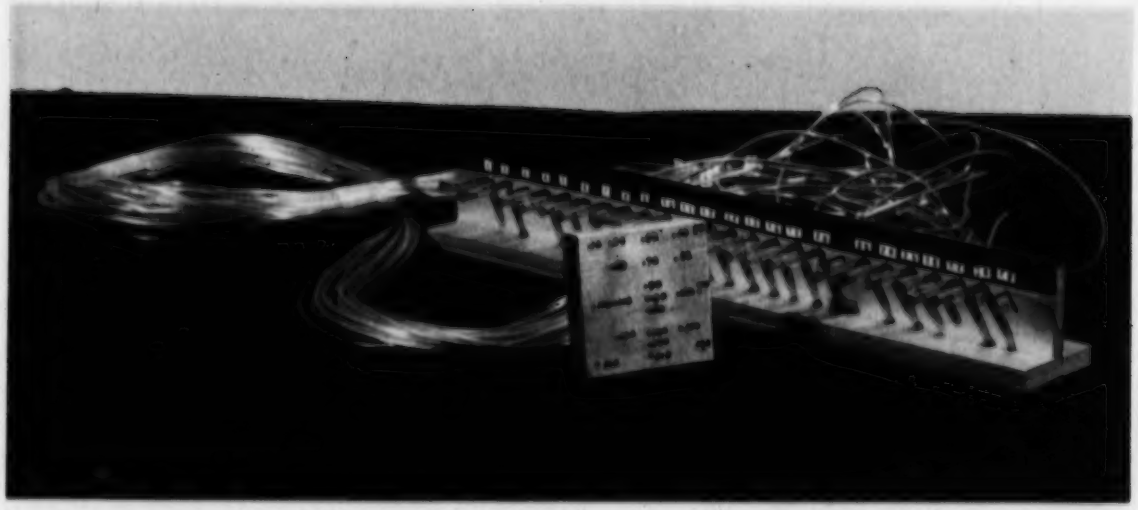

Figure 2-12 Sampling manifold and building model #2

CHAPTER III

Effect of Exhaust Momentum from Building Roof Vents on Effluent Dilution

Chapter Overview:

This chapter will introduce the concept of initial dilution in a rising and bent-over jet of exhaust gas. The two approaches taken to account for this initial dilution, namely

1) The Plume Rise Approach, and

2) the Initial Entrainment Approach

will be discussed. The minimum diluion models developed from these approaches will be presented.

3.1 Initial Dilution due to Exhaust Momentum

When exhaust gas is emitted vertically into the atmosphere through a roof vent, turbulence is generated by the velocity shear between the vent gas and the ambient air. This turbulence causes mixing between the vent gas and the air - a process usually described as entrainment. During this process, air is being entrained into the plume of exhaust gas, thus diluting the vertical velocity of the plume. Furthermore, if wind is blowing in the atmosphere, the entrained air will possess horizontal momentum which will soon cause this vertically directed plume to bend over.

This bending over process and plume rise both increase dilution of the exhaust gas concentration on the building roof. The contribution due to plume rise is obvious for it simply moves the plume centerline further away from the roof. During the initial bending over of the plume, the mean vertical velocity, W_v, becomes perpendicular to the

plume axis and causes mixing over the entire upper region of the plume. So, the entrainment velocity $v_a \simeq W_v$. In the case of a vertical jet, entrainment is mainly due to the turbulent velocities u'and v' induced by W_v and they are a fraction of W_v in magnitude, typically $u' \simeq v' \simeq 0.2\ W_v$ and $v_a \simeq 0.2\ W_v$ too. Hence, a bent-over plume is able to entrain ambient air more efficiently,[see Briggs (1975)], resulting in higher dilution. It has been experimentally confirmed by Briggs (1969, 1975) that the entrainment constant α_w in a bent-over plume has a value of 0.5 - 0.6, about 5 times higher than the α for a free jet or a horizontal plume. By definition the entrainment constant α_w is the proportionality constant between the rate of entrainment of air, v_a and the vertical convection velocity of the plume, W_v.

$$\alpha_w = \frac{v_a}{W_v} \tag{3-1}$$

This relationship was first suggested by Taylor (1945) and is commonly known as the Taylor entrainment assumption. A larger α_w for the bent-over plume means more entrainment of ambient air through the plume surface. More dilution occurs and a lower concentration of exhaust gas at the building roof is expected.

Plume rise and the bending-over process are strongly dependent on the vertical exhaust momentum of the jet. For very high exhaust momentum, vent gas will behave like a free vertical jet. If momentum is very low, the effluent will immediately be swept away by the ambient air, leaving no time for plume rise to develop. So exhaust momentum indirectly controls the amount of dilution incurred in the initial rise of a plume. The objective of this study is to devise a diffusion model to account for this dilution due to exhaust momentum.

3.2 Buoyancy Rise

In the nondimensionalized momentum equation, it can be shown that the buoyancy term is governed by the inverse of the Froude number. The density-related Froude number is defined as:

$$F_r = \frac{U^2}{Hg}\left[\frac{1}{1 - \rho_e/\rho_a}\right] \qquad (3\text{-}2)$$

where U = Wind speed

H = Building height

ρ_e = Density of effluent

ρ_a = Density of ambient air

g = Acceleration due to gravity

Since the tunnel speed U had to be maintained high (about 10 m/s) to eliminate the effects due to Reynolds number mismatch and the building size H was small (6 cm maximum), a model Froude number greater than 200 resulted. Golden (1961) found that buoyancy effects are important only when $F_r \tilde{<} 1.0$, so the helium plume was non-buoyant in the present study and the plume rise considered in this study was solely momentum rise. A quantitative comparison of the relative contributions of buoyancy and exhaust momentum to the total plume rise (see Appendix A3-3) showed that momentum rise was dominant. The extra rise due to buoyancy varied between 0.6 to 11% of the total rise height over the range of exhaust conditions tested in the present study. Buoyancy effects could be assumed to be negligible. This is rather suprising from a common sense point of view because the helium density is about 1/7 of the ambient air density. This would make the results of this study more suitable to industrial ventilation applications because they are more concerned with dilution at short downwind distances where momentum rise usually dominates.

3.3 Exhaust Momentum Factor

Before the effect of exhaust momentum on vent gas dilution can be quantified, a parameter to characterize the exhaust momentum condition is needed. Wilson (1977) suggested the exhaust momentum factor defined as:

$$M = \left(\frac{\rho_e}{\rho_a}\right)^{0.5} \frac{W_e}{U} \qquad (3\text{-}3)$$

where ρ_e = density of effluent

ρ_a = density of ambient air

W_e = exit velocity of effluent

U = approach flow velocity at level of exhaust

By definition, M^2 is the ratio of the momentum fluxes per unit area of the effluent ($\rho_e W_e^2$) and of the approach flow at vent height ($\rho_a U^2$). The square root of their ratio is a normalized velocity ratio that includes momentum effects.

In this study, the stack gas velocity, W_e, was assumed to have a uniform (flat) velocity profile though in reality the profile was parabolic owing to laminar flow in the vent stack on the model. Winkel (1979) attempted to account for this difference in velocity profile by correcting the indicated momentum flux ratio M^2 with a kinetic energy correction factor, defined as the ratio of the integrated mean kinetic energy in the stack gas velocity profile and the kinetic energy of the mean velocity, W_e. However, he found that this kinetic energy factor could not entirely account for the effect of stack gas velocity profile on plume rise and in some cases led to a misrepresentation of the full scale plume rise behavior. Since stack gases in full scale are turbulent, their velocity profiles are relatively flat and probably better

approximated by a uniform profile than a parabolic one. So, exhaust momentum condition is simply characterized by M in equation (3-3) with W_e calculated assuming a flat velocity profile.

3.4 Computational Models for Initial Dilution of a Rising Effluent Jet

Two approaches were employed in this investigation to model the dilution process during the initial rising of an effluent jet:

1) Plume Rise Approach - only plume rise was accounted for. The initial entrainment caused by the bending over process of the plume was ignored.
2) Initial Entrainment Approach - in which an apparent initial entrainment was added at the source to account for the increase in dilution near the vent. Plume rise was ignored and included explicitly as extra entrainment.

Probably the two approaches can be combined to form a more realistic model. However, this will require the entrainment constant α_o to vary thus leading to a model with integral equations which is too complex for most industrial applications.

In the following discussion, the above two models will be presented in detail and for reasons that will become apparent later, the initial entrainment model will be chosen as the recommended one to use.

3.4.1 Plume Rise Approach

In estimating the plume rise effect on exhaust gas concentrations on the roof surface, one has to know the trajectory of the plume and its rate of entrainment. The former identifies how far the plume centerline is away from building roof and the latter determines the amount of dilution occurring in that distance. Hence, the two necessary ingredients in this analysis are:

a) A plume growth model and

b) A functional form to represent plume rise

3.4.1a Gaussian Plume Model

The Gaussian plume model assumes that plume dispersion takes place from its centerline to its outer edges in accordance with a "normal" or "Gaussian" distribution. A discussion of this model can be found in Csanady (1973). Wilson and Winkel (1982) adopted this model to estimate the effect of stack height on contaminant concentration at roof level. From their analysis, the ratio of plume centerline concentration to that at roof height for a flush vent with no stack height is

$$\frac{C_o}{C_r} = \exp\left[\frac{h^2}{2\sigma_z^2}\right] \qquad (3\text{-}4)$$

where "h" is plume rise and "σ_z" is the vertical plume spread. Using the Gaussian plume model, the plume rise effect appears as an exponential which poses a difficulty because the exponential form is very sensitive to the functional form of plume rise. Wilson (1984, private communication) found that any small error in the plume rise formulation will be highly magnified causing unrealistically large errors in the estimation of dilution near the point of release. Thus, the Gaussian plume model is <u>not</u> suitable to account for the initial dilution of a rising effluent plume.

3.4.1b "Triangular" Plume Concentration Profile

This model is termed "triangular" because concentrations are assumed to drop linearly from the plume centerline to its outer edges. This assumption reduces the sensitivity of the model to plume rise formulations compared to the non-linear form of the Gaussian profile.

For plume cross sections close to the source, this linear plume model is just as plausible as the traditional Gaussian equation and basing on the effluent flowrates used in this study, its concentration profile is within $\pm$ 10% of the Gaussian profile from the plume axis to about one standard deviation away.

To examine how this plume model affects vent gas dilution at roof level, the case of a flush roof vent of zero stack height is considered. In Appendix A3-1, the plume growth of a jet that has been bent over and is moving horizontally at the local wind speed, U is determined. It was found that for the mass of exhaust gas through each plume cross section to be conserved, the plume radius, R, of the triangular concentration profile should be

$$R = \left[\frac{3\,Q_e}{\pi\,U}\right]^{0.5} \left[1 + \sqrt{\pi}\,\alpha_o\left(\frac{US^2}{Q_e}\right)^{0.5}\right]$$

or

$$R = \sqrt{3}\left[\left(\frac{Q_e}{\pi U}\right)^{0.5} + \alpha_o S\right] \qquad (3\text{-}5a)$$

Assuming that this bent over jet has a vertical rise h and the roof surface acts as a reflector which redirects any concentration that touches it back to the plume above, the concentrations at plume centerline and roof level can be shown as follows.

If the plume radius is large enough to touch the roof surface i.e. R > h, the concentration at roof level is,

$$C_r = 2\,C_\infty\left(1 - \frac{h}{R}\right) \qquad (3\text{-}5b)$$

where C_∞ is the plume centerline concentration of a plume far from any reflecting surface and $C_\infty\left(1 - \frac{h}{R}\right)$, the amount diffused to as well as the

amount reflected at the roof surface. But if plume radius is small compared to h, i.e. R < h, the plume detaches from the roof level, so

$$C_r = 0 \qquad (3\text{-}5c)$$

For a very large plume radius, part of its reflected portion will reach the plume centerline level if it exceeds two times the rise height of the plume, i.e. R > 2h. An additional amount, $C_\infty(1 - \frac{2h}{R})$ is expected at the plume centerline to give

$$C_o = C_\infty + C_\infty(1 - \frac{2h}{R})$$

which reduces to

$$C_o = 2C_\infty(1 - \frac{h}{R}) \quad \text{for } R > 2h \qquad (3\text{-}5d)$$

However, if R < 2h, none of the reflected amount will reach the plume centerline level and

$$C_o = C_\infty \qquad (3\text{-}5e)$$

Using equations (3-5b) through (3-5e), the plume axis to roof concentrations can be expressed as

$$\frac{C_o}{C_r} = \frac{1}{2(1 - \frac{h}{R})} \quad \text{for } R < 2h \qquad (3\text{-}6a)$$

$$\frac{C_o}{C_r} = 1 \quad \text{for } R \geq 2h \qquad (3\text{-}6b)$$

$$\frac{C_o}{C_r} = \infty \quad \text{for } R \leq h \qquad (3\text{-}6c)$$

3.4.1c Functional Form to Represent Plume Rise

In a review by Wilson (1977) on the prediction of momentum rise he indicated that by dimensional analysis, the momentum rise of a jet in a cross flow has the form

$$\frac{h}{d_s} = B_1 (M)^n \left(\frac{S}{d_s}\right)^m \qquad (3\text{-}7a)$$

where B_1, n and m are constants and (n + m) should be unity, because at large distances from the vent, h is expected to be dependent only on the momentum flux ratio, $(M \cdot d_s)$ and distance, S.

From momentum conservation, Briggs (1969) determined that n = 2/3 and m = 1/3 if the entrainment coefficient, α_o is assumed constant with distance. This leads to the one-third power law representation of plume rise:

$$h = B_1 (M \cdot d_s)^{2/3} S^{1/3} \qquad (3\text{-}7b)$$

If α_o is allowed to vary with distance, n and m may take on other combinations [see Wilson's review (1977)]. Briggs suggested a value of B_1 = 1.44. This study chose to experimentally evaluate B_1. If its value could be established, the effect of exhaust momentum on dilution could be estimated using equations (3-6a) through (3-6c).

3.4.1d Wind Tunnel Experiments

Wind tunnel simulation experiments were carried out to provide data for the evaluation of the constant B_1 in equation (3-7). A two dimensional step of height H = 1.37 and length L = 61 cm, about 45 H, was chosen to represent the flow disturbance caused by a wide building with W >> H. A small step height was used to minimize blockage effect in the tunnel and ample length was provided to measure the plume trajectory above the building roof. An exhaust vent of 0.22 cm inside diameter was located along the x axis, at a distance 7.5 step heights from the upwind edge. This location was positioned beyond the flow separation zone on the building roof to avoid recirculation effects. Also the vent was kept flush with roof so the stack effect on dilution would not have to be considered.

Tests were performed at two exhaust momentum conditions: with M = 0.98 and 2.06. Details of the test condition are summarized in Table 3.1. Concentration profiles were taken at eleven downwind distances from the vent location using the aspiration sampling probe described in Section 2.3, Chapter II. These distances ranged from one to about 200 stack diameters away (4 to 800 m full scale). At each downwind distance, a vertical concentration profile was traced from roof level in steps of 0.5 mm (1 m full scale). Care was taken to ensure that the plume centerline concentration was included in the profile.

3.4.1e Discussion of Results and Data Correlations

Measurement results are shown in Figures 3-1 and 3-2. Each figure shows the change of dilution factor with height at various downwind distances. Dilution factor D is defined as the ratio of the contaminant concentration at source to that at location being considered, C_e/C, so the regions with the lowest dilution identify the plume centerline. Actual rise heights with distance are plotted on Figure 3-2a. The plume at M = 0.98 (see Figure 3-1) rose more slowly than that at M = 2.06 (see Figure 3-2). For instance, at S = 0.4 cm, their rise heights differed by about 2.75 mm (5.5 m full scale). Also the final rise height, h_f at the high momentum case was also 3.0 mm (6 m full scale) higher than that at the lower momentum case. A direct correlation between plume rise and momentum factor M was evident.

Equation (3-7b) was seen to give an acceptable prediction of the overall rise behavior before final rise was achieved. The only disconcerting thing is that the value of B_1 changed with momentum factor, M. However, during the initial stage of rise, the one half power expression

$$h = B_5[M \cdot d_s]^{1/2} S^{1/2} \qquad (3\text{-}8)$$

seemed to provide a better correlation with the actual measurements, with B_5 staying constant with M. The relative merits of equation (3-7b) and (3-8) in predicting plume axis to roof concentrations, C_o/C_r will be discussed in the following sections.

The measured ratios of plume axis to roof concentrations C_o/C_r are plotted on Figures 3-3 and 3-4. The data followed a bell shaped distribution which asymptotically approached the value of unity. During the initial stage of plume rise, the plume axis concentration is high because not much dispersion has occurred so it is substantially higher than the roof level concentration. This condition persists in the first few diameters of travel causing the ratio C_o/C_r to increase. How high the ratio will increase to depends on momentum factor M. The C_o/C_r values at M = 2.06 were 2 to 3 times larger than those at M = 0.98. As plume spread, R, increases with downwind distance S, the plume axis concentration is diluted, reducing its difference with roof level concentration and decreasing C_o/C_r. The effect of plume rise diminishes with downwind distance and eventually disappears where $C_o/C_r = 1$. The higher the exhaust momentum M, the longer it takes for this process to diminish.

The theoretical equation (3-6, a, b, c) is shown in Figures 3-3 and 3-4 and produces the correct, bell-shaped distribution. The various curves represent the different values of B_1 from 1.2 to 1.8 used in the plume rise formulation, equation (3-7b). It is rather disconcerting that they all underestimate the distance to the peak C_o/C_r. Also, the theoretical prediction is seen to be very sensitive to the value chosen for the "constant" B_1. In Figure 3-3, with M = 0.98, the peak Co/Cr

values predicted by $B_1 = 1.8$ and $B_2 = 1.6$ differed by a factor of four. For higher exhaust momentum, M = 2.06 (see Figure 3-4), the peak value of C_o/C_r changed from 27 to infinity when B_1 was increased from 1.2 to 1.3. The best fit value of B_1 was not the same at the two different momentum conditions, with $B_1 = 1.65$ for M = 0.98 and $B_1 = 1.2$ for M = 2.06. In addition, these values were not consistent with the B_1 values (1.02 and 1.26) directly determined from plume rise measurements in Figure 3-2a. Some possible reasons for the model's failure are:

1) The virtual origin of the plume was not at the stack centerline but at some downwind distance, which explains why the model prematurely predicted the occurence of the peak C_o/C_r ratio.
2) The entrainment "constant", α_o, instead of being constant as the model assumed, actually varied with downwind distance, S. Also the assumption of the plume having a linear crosswind concentration profile may have had some error. As a result, "constant" B_1 in equation (3-7b) had to vary to adjust for these errors.

To offset the effect due to a displaced virtual origin, S_o equation (3-7b) was modified as follows:

$$h = B_1 (M \cdot d_s)^{2/3} (S-S_o)^{1/3} \qquad (3\text{-}9)$$

Equation (3-9) is shown in Figures 3-5 and 3-6 using the best value of B_1 in each exhaust momentum condition. By assuming $S_o = 0.2$ to 0.25 cm, the model provided a more realistic prediction of where the peak concentration ratio C_o/C_r occurred and a better estimation of the values

of C_o/C_r in general. Unfortunately, the theoretical values of C_o/C_r were also very sensitive to the value chosen for S_o.

Another attempt was made to improve the theoretical prediction by changing the distance exponent in the plume rise equation from 1/3 to 1/2, using

$$h = B_5 (M \cdot d_s)^{1/2} (S)^{1/2} \qquad (3\text{-}8)$$

instead of equation (3-7b) in equation (3-6a, b, c). This modified theory displays dramatic improvement in Figures 3-7 and 3-8. It correctly showed the location of the peak concentration ratio C_o/C_r without the need for a correction factor for virtual origin. By letting $B_5 = 0.89$ for $M = 2.06$ and $B_5 = 1.08$ for $M = 0.98$, the theoretical prediction followed very closely the measured data (well within a factor of 2). Evidently equation (3-8) is a better plume rise representation than equation (3-7b) probably because the initial stage of rise was better described by a $h \alpha S^{1/2}$ power law than a $h \alpha S^{1/3}$ power law (see Figure 3-2a). However, B_5 in equation (3-8) still failed to be a true constant and the high sensitivity to the value chosen for B_5 persisted in the prediction of C_o/C_r in this modified model, as shown in Figures 3-7 and 3-8.

3.4.1.f Plume Rise-Dilution Model: Conclusions

The "triangular" plume model, though simplistic, provided a theoretical prediction of the plume rise effect which resembled the physical process. Two plume rise equations (3-7b), (3-8) representing $h \alpha S^{1/3}$ and $h \alpha S^{1/2}$ respectively, were tested in this model. Experimental measurements of plume rise showed that the initial rise was better described by $h \alpha S^{1/2}$ while the overall rise followed the one-third power law, $h \alpha S^{1/3}$, see Figure 3-2a. By incorporating a virtual

origin to the one-third power law, or by using the one-half power law, the model provided a reasonable estimation of the concentration ratio C_o/C_r.

Unfortunately, data correlations showed that the plume rise "constants" B_1 and B_5 in equations (3-7b) and (3-8) were in fact variables. B_1 varied from 1.2 to 1.65 and B_5 from 0.89 to 1.08 under different test conditions. Although these variations of B_1 and B_5 do not seem very large, indicating that the basic approach of the model had some physical basis, the concentration prediction was found to be extremely sensitive to the values chosen for the plume rise constants. For instance, in Figure 3-3, a 13% change in B_1 (1.6 to 1.8) could make the peak concentration ratio change by an order of magnitude. It is this extreme sensitivity of the model to the plume rise constants, B_1 and B_5, that makes it inappropriate for quantitative design purposes.

3.4.2 Accounting for Exhaust Momentum Using Initial Entrainment

It has been known that a bent-over jet of vent gas with vertical exhaust momentum has a higher entrainment rate than a horizontal jet, see Briggs (1975). The bending over process coupled with plume rise increases the dilution of vent gas concentration at roof level. The present model assumes that the decrease in roof concentration caused by a combination of plume rise and increased entrainment can be accounted for by introducing an initial entrainment rate, Q_o' at the vent exit as schematically illustrated in Figure 3-17. This concept was first suggested by Wilson, see Wilson and Chui (1985). The total flow rate at the source becomes

$$Q_T = Q_e + Q_o \tag{3-10}$$

The initial dilution near the exhaust can be expressed as

$$D_o = 1 + \frac{Q_o}{Q_e} \tag{3-11}$$

And if the bent-over plume is assumed to have the wind speed U as its convective velocity and an entrainment velocity

$$v_a = \alpha_o U \tag{3-16}$$

the minimum dilution factor on building roof at downwind distance, S is

$$D_{min} = [D_o^{0.5} + (\tfrac{\pi}{2})^{0.5} \alpha_o (\frac{US^2}{Q_e})^{0.5}]^2 \tag{3-12}$$

as derived in Appendix A3-2. To apply equation (3-11), D_o and Q_o must be known. A further assumption was made to relate Q_o to the exhaust momentum M in the following manner

$$\frac{Q_o}{Q_e} = B_3 M^2 \tag{3-13}$$

where B_3 is a proportionality constant. It must be emphasized that this assumption was not based on established physical principles. Instead, it is an attempt to quantify in a simple form the expected dependence of Q_o on M. Since M^2 represents the ratio of the momentum fluxes of vent gas to that of the approach flow, a linear relationship between Q_o and M^2 is quite plausible. Though this dilution model may seem rather simplistic, B_3 will be found to be a true constant by data correlations, and equation (3-12) will prove to be very convenient for industrial ventilation system design.

3.4.2a Wind Tunnel Data

Data collected from three independent wind tunnel simulation

studies were used to determine B_3. The test buildings included were:

1) Buildings A3 and A4 taken from a study by Wilson (1976) on the contamination of building air intakes from nearby vents.
2) Buildings 6 through 21 which were part of the zero stack height baseline data set used by Wilson and Winkel (1982) for their study on stack height effects on building roof concentrations.
3) Building 31 from the present investigation.

The shapes of these buildings are shown in Figures 2-9 and 2-10 of Chapter II. Each of them was tested in the wind tunnel model described in the previous chapter at a set tunnel velocity and exhaust gas flowrate, see Table 3-1. Concentration measurements at intake locations were collected using the techniques discussed in section 2-3. In all cases, flush, vertically directed roof exhaust vents were used.

Dilution measurements are shown in Figures 3-9 through 3-16. Each figure represents the concentration data taken at a single test condition for one building configuration. Different test conditions on the same configuration are shown on separate figures and given different building numbers. The concentration measurements are shown as dilution factor $D = C_e/C_r$.

Typically, there seems to be lot of scatter in the data because the concentrations at intakes do depend not only on how far they are away from the vent but also are governed by their crosswind positions in relation to the plume centerline. For the same distance from vent $S/A^{0.5}$, there can be a variety of dilution factors recorded. The lowest dilution values are those on the plume centerline, and they form a distinguishable lower bound to the data set. These lower bound D values

are the data points that the theoretical minimum dilution model correlates to.

3.4.2b Experimental Results for Exhaust Momentum Effect on Initial Dilution

The data used in the correlation comprise a wide range of exhaust momentum factors M from 0.103 to 1.76. It was found that within this range, the minimum dilution prediction correlated reasonably well with measurements when using an entrainment value of $\alpha_o = 0.2$ in equation (3-12) to give

$$D_{min} = [D_o^{0.5} + 0.25 (\frac{US^2}{Q_e})^{0.5}]^2 \qquad (3\text{-}14)$$

and a $B_3 = 7.0$ in equation (3-13) to express initial dilution as

$$D_o = 1 + 7.0 M^2 \qquad (3\text{-}15)$$

3.4.2c Comparison with Previous Dilution Model at Medium and High Momentum

Equations (3-14) and (3-15) were plotted on Figures 3-9 to 3-16. The minimum dilution equation

$$D_{min} = [1 + 0.33(\frac{US^2}{Q_e})^{0.5}]^2 \qquad (1\text{-}4)$$

from Wilson (1983) was shown for comparison.

In Figure 3-9 showing Building 6 with moderate exhaust momentum M = 0.768, the improvement of the new minimum dilution model represented by equation (3-14) over the old one, equation (1-4) is evident. Near the exhaust vent, the prediction for minimum dilution is improved from a

factor of about 4 uncertainty to a factor of 2. This improvement is even more pronounced at higher exhaust momentum. In Figure 3-10 which shows the same building configuration as the one in Figure 3-9 but with a momentum 2.5 times higher (M = 1.76), equation (3-14) still predicts a minimum dilution within a factor of 2 while equation (1-4) underestimates by a factor as high as 16. This overly conservative prediction of equation (1-4) persists out to $S/A^{0.5} = 1.5$, roughly, 35 vent diameters away from the source vent. Because it was developed at a very low exhaust momentum condition for M = 0.11 to 0.15, Wilson's equation (1-4) fails to account for dilution induced by plume rise and bending over of the exhaust jet.

3.4.2d Sensitivity to Building Shapes

The superiority of equation (3-14) over equation (1-4) is maintained in Figures 3-10 through 3-13 which include a variety of building configurations with aspect ratios of 2, 4, 6 and 8, and high momentum factors M between 1.5 and 1.76. The new dilution model continues to correlate well with experimental data within a factor of 2 consistently. This leads to the important conclusion that equation (3-14) does not seem to be sensitive to building shape and so can be used for general design purposes.

3.4.2e Sensitivity to Vent Locations

Figures 3-15 and 3-16 compare two data sets taken from the same building shape, with the same test condition except having their vents located differently. In one case, the vents were located on the upwind portion of the building roof and the other, the downwind portion. The data in Building A4 seem to portray a slightly smaller minimum dilution

but the discrepancy is well within the uncertainty in data measurement. This is encouraging because minimum dilution does not seem to be very sensitive to vent location, and equation (3-14) does not need any built-in parameter to account for the effect of vent location.

3.4.2f Comparison with Previous Model at Low Exhaust Momentum

The present model is not significantly different from Wilson's (1983) equation (1-4) for low exhaust momentum condition. In Figures 3-14 and 3-15, both equations adequately estimate the minimum dilution level with the present model being slightly more conservative. For building 31 (Figure 3-14) the previous model equation (1-4) is actually superior at distances within about 1 building height, i.e. at $(S/A^{0.5}) < 1$. This result is not suprising because equation (1-4) was devised particularly for this momentum range. The comforting thing to note is that the present model maintains this good performance when the momentum factor is low.

3.4.2g Limitations of the Initial Entrainment Model

It must be emphasized that the initial dilution D_o represented by equation (3-15) is just an apparent one. It is not the true dilution factor at vent exit which will always be $D_o = 1.0$ to be physically correct. The indicated "initial" D_o must occur over some downwind distance from source. For this reason, the model does not apply at distances very close to source. The question is how close is "close"? Pai (1954) in his survey on the dynamics of jets, noted that it would take about 10 diameters of travel for similarity of velocity profiles to be established. The same distance of travel (i.e. 10 diameters) was found to be required for the entrainment coefficient to

reach a constant value in a study on the rate of jet growth by Hill (1972). To extrapolate these observations into our situation, probably it is not unreasonable to recommend the use of equation (3-14) only at distances greater than about 10 stack diameters.

According to Figures 3-9 to 3-13, the model seems to consistently overestimate the minimum dilution factor by 10-15% for $S/A^{0.5} > 1.0$. There can be two possible reasons:

1) The entrainment constant α_0 may have changed when the plume has gone past the initial bending over process and it propagates just like a horizontal plume. It was found that using $\alpha_0 = 0.13$, the typical value for a horizontal plume, the error is reduced to less than 10% for minimum dilution.
2) The plume growth R at this far downwind of the source will no longer be linear with downwind distance, S. Wilson and Winkel (1982) found that roof level concentrations from vent stacks suggest a plume growth $R \propto S^{0.75}$. This idea will be further discussed in Chapter V.

Despite these possible sources of error, the errors are small and do not justify making any modifications to the present model in equations (3-14) and (3-15).

3.4.2h Summary Remarks for the Initial Entrainment Model

The initial entrainment approach to account for the effect of exhaust momentum produced the minimum dilution model in equations (3-14) and (3-15). Extensive correlation with experimental data indicated that the model applies over a range of exhaust momentum factors from $M = 0.103$ to 1.76. It consistently provides a satisfactory estimation

of the lower bound for dilution. Typically the prediction is within a factor of 2, for downwind distances greater than 10 stack diameters and smaller than 3 building heights ($S/A^{0.5} < 3$) regardless of building shapes and vent locations. This demonstrates that B_3 in equation (3-14) is a true constant which lends support to the physical basis of the model although the concept of initial dilution is only a hypothetical one. With the noted capacity of the model, its usefulness is assured in the design of ventilation systems for low rise industrial buildings.

TABLE 3-1

Conditions for Wind Tunnel Tests

BUILDING NUMBER	FLOW PARAMETERS					
	EXHAUST FLOW RATE Q_e		DENSITY RATIO	WIND SPEED AT ROOF HEIGHT	STACK DIAMETER	EXHAUST MOMENTUM FACTOR
	Helium flowrate $(\frac{cm^3}{min})$	Air flowrate $(\frac{cm^3}{min})$	$\frac{\rho_e}{\rho_a}$	U $(\frac{m}{s})$	d_s (cm)	$M=(\frac{\rho_e}{\rho_a})^{0.5}\frac{W_e}{U}$
2 dim. step	3346	0	0.138	5.77	0.216	0.98
2 dim. step	3062	1179	0.378	5.77	0.216	2.06
A1	195	0	0.138	14.4	0.10	0.107
A3	195	0	0.138	10.5	0.10	0.146
A4	195	0	0.138	10.5	0.10	0.146
6	1000	0	0.138	5.89	0.132	0.768
8	1000	385	0.378	5.89	0.132	1.76
12	1000	385	0.378	5.89	0.132	1.76
18	1000	385	0.378	6.91	0.132	1.50
21	1000	385	0.378	6.91	0.132	1.50
31	195	0	0.138	8.56	0.132	0.103

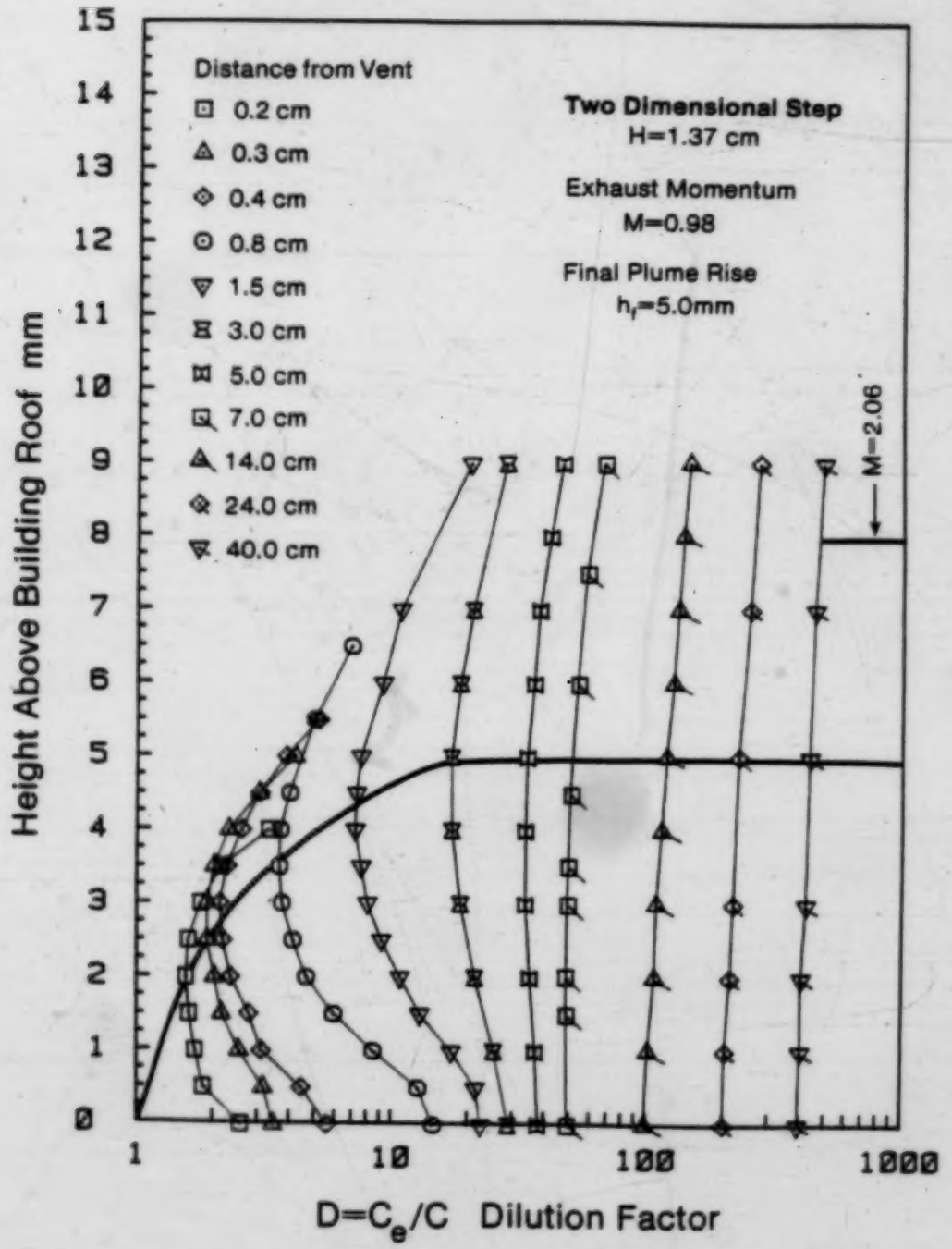

Figure 3-1 Effect of exhaust momentum factor M on vertical profiles of exhaust gas dilution for a flush vent located 10.2 cm from the upwind roof edge of a wide (two dimensional step) building

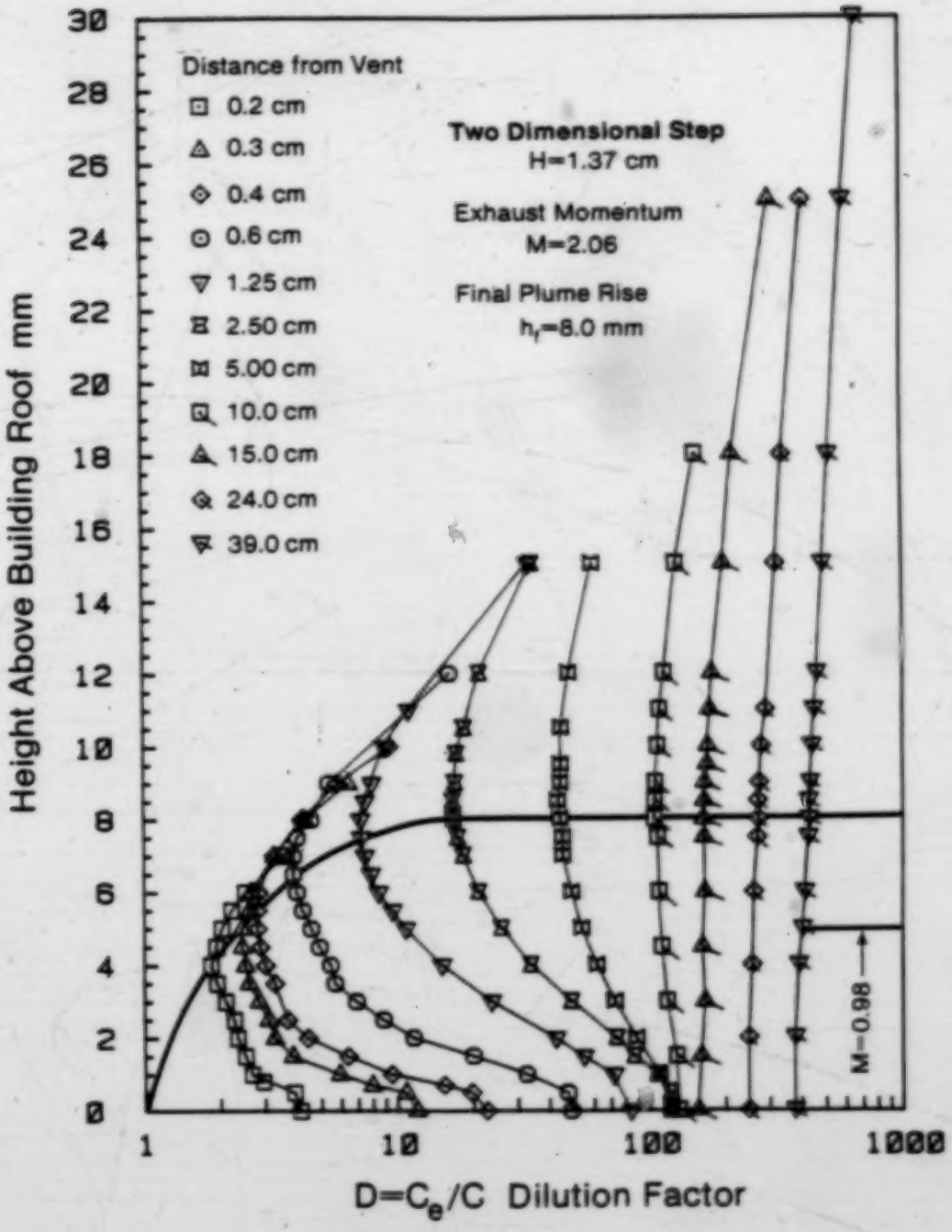

Figure 3-2 Effect of exhaust momentum factor M on vertical profiles of exhaust gas dilution for a flush vent located 10.2 cm from the upwind roof edge of a wide (two dimensional step) building

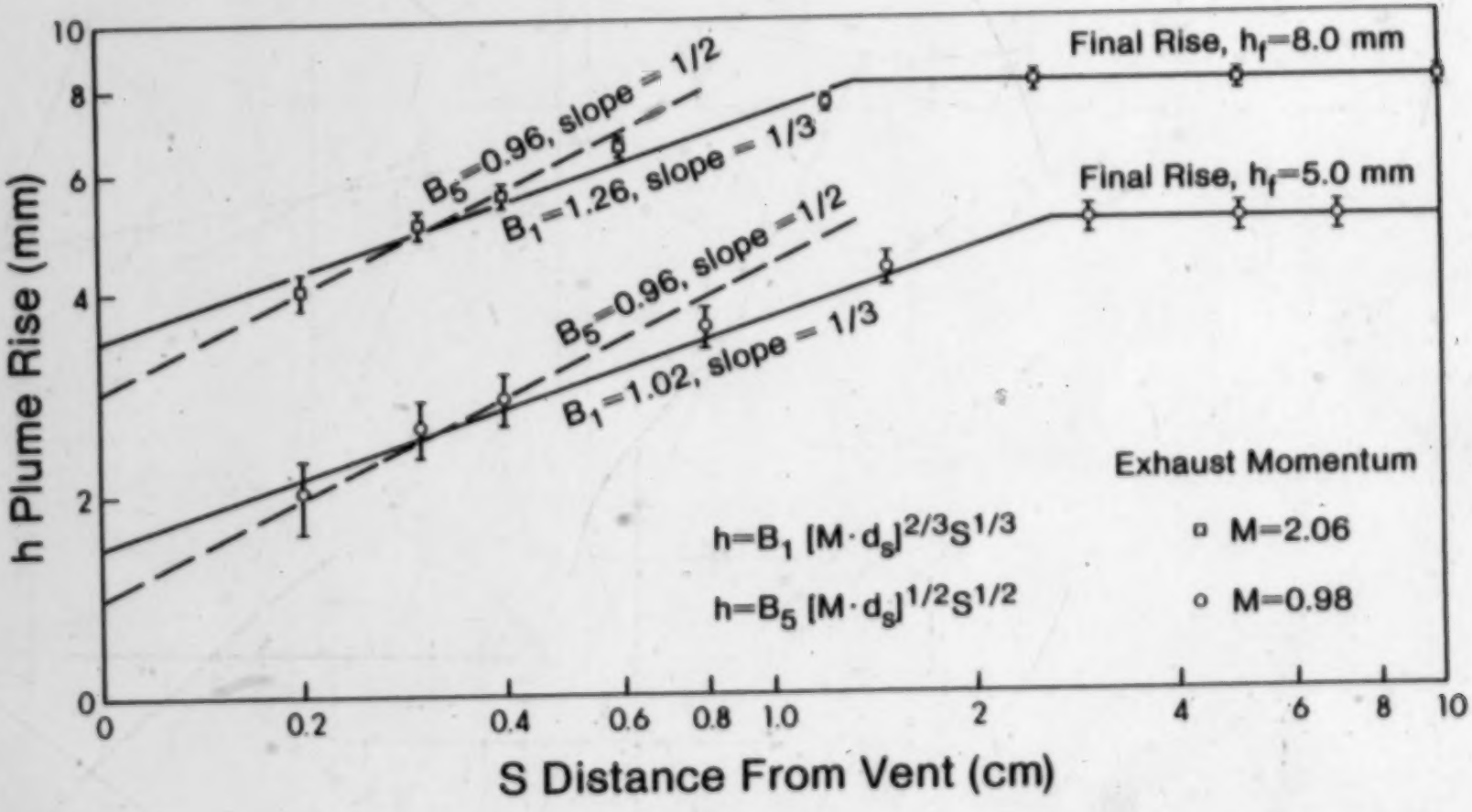

Figure 3-2a Plume rise of exhaust gas jets emitted from a flush, vertically directed vent on a two dimensional roof at two different exhaust momentum conditions

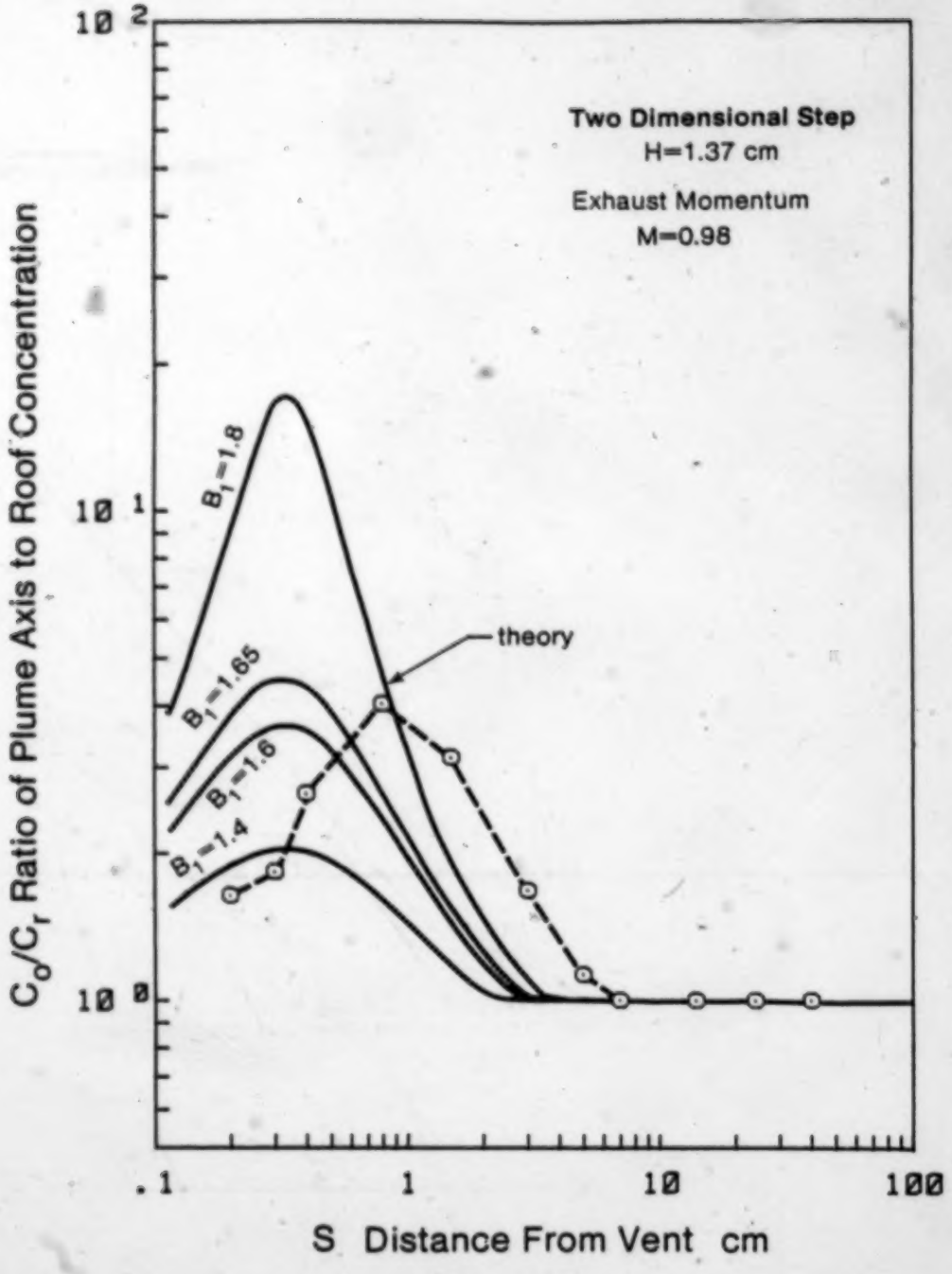

Figure 3-3 Use of $h \alpha S^{1/3}$ power law for plume rise to estimate the effect of plume rise on concentration at roof level. Dashed line represents experimental data and solid lines, theoretical predictions based on linear plume concentration profiles with different values of plume rise constant, B_1

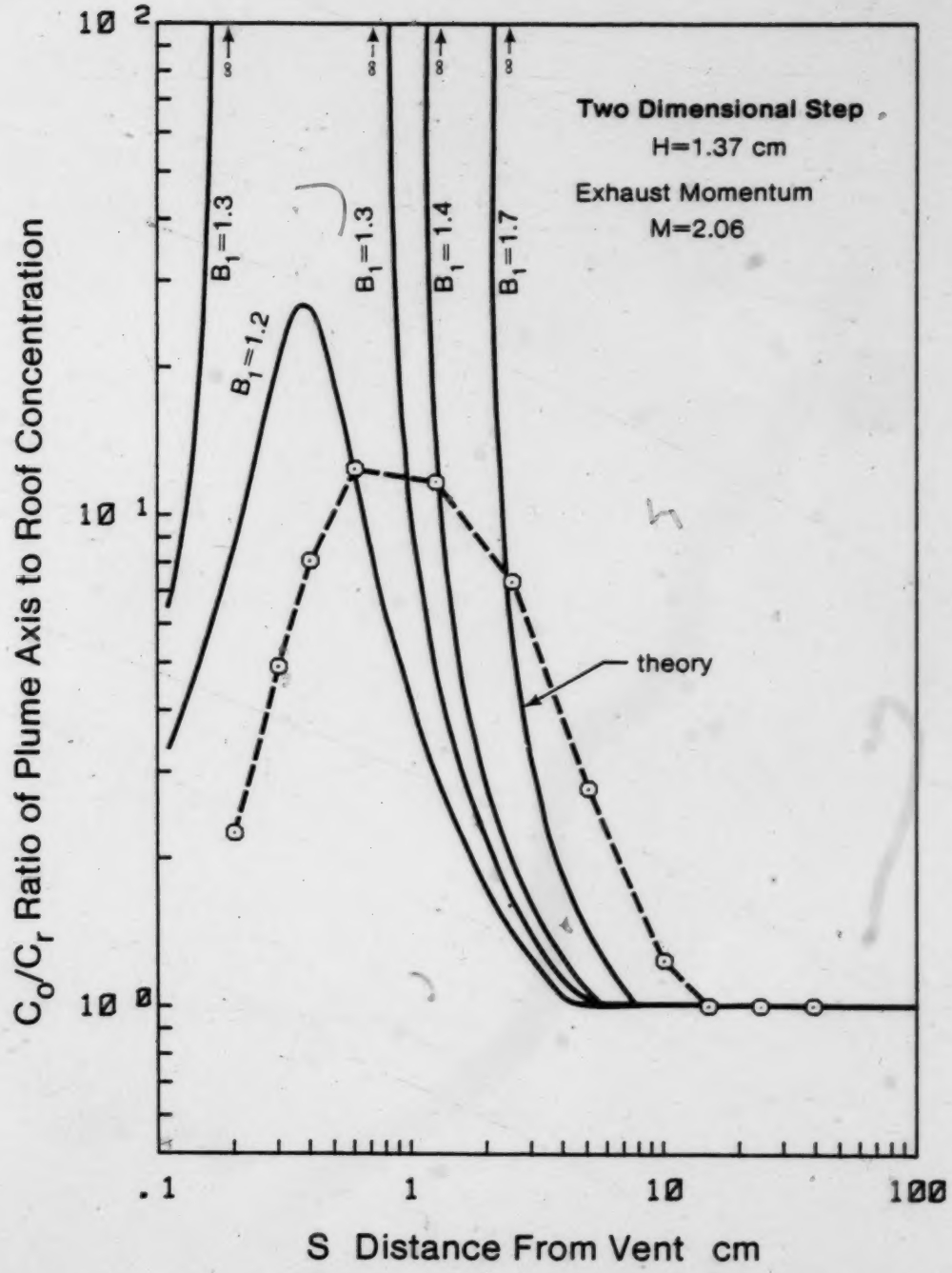

Figure 3-4 Use of $h \alpha S^{1/3}$ power law for plume rise to estimate the effect of plume rise on concentration at roof level. Dashed line represents experimental data and solid lines, theoretical predictions based on linear plume concentration profiles with different values of plume rise constant, B_1

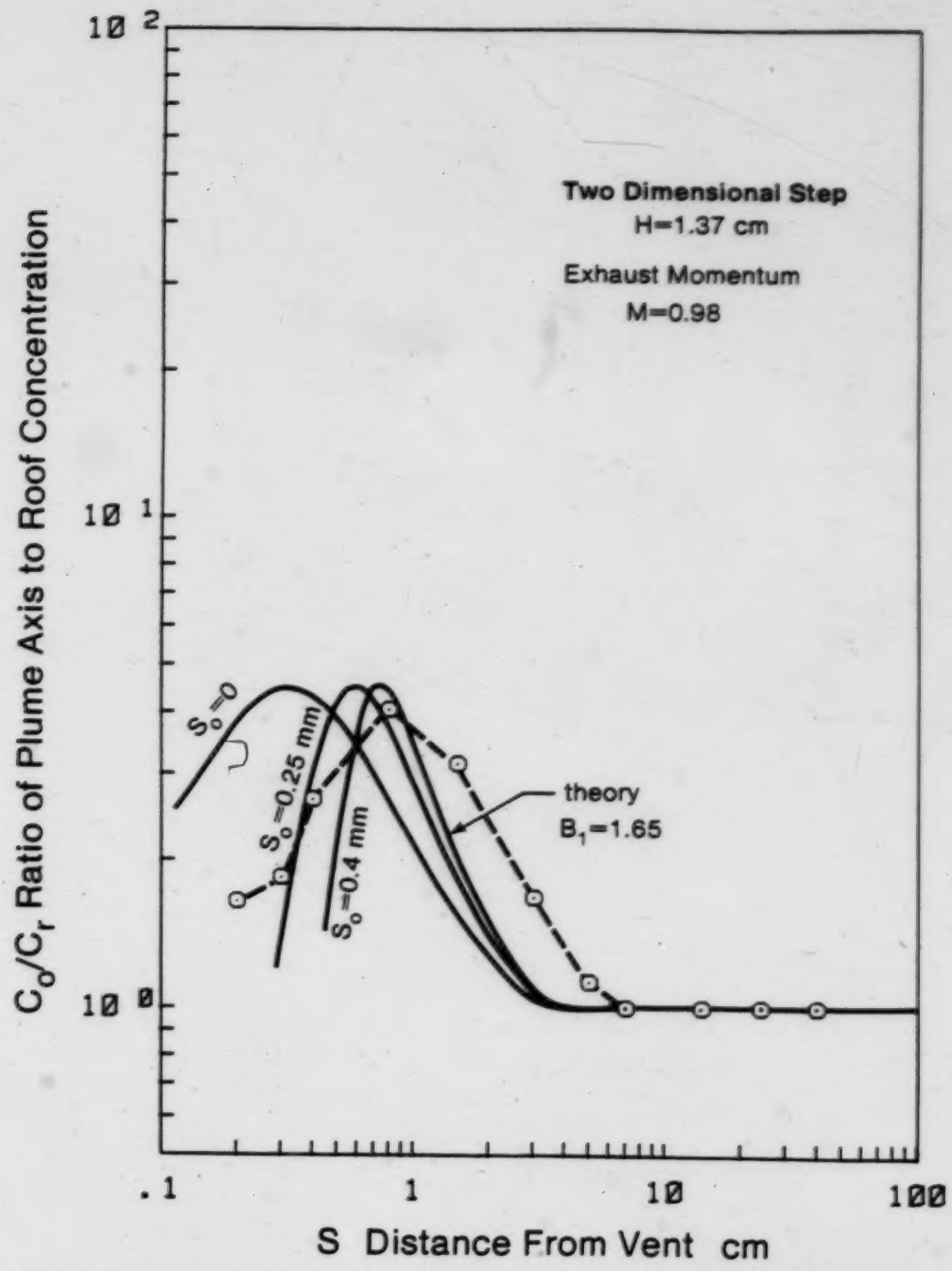

Figure 3-5 Use of $h \alpha S^{1/3}$ power law for plume rise to estimate the effect of plume rise on concentration at roof level assuming a virtual origin at downwind distance, S_o in the plume rise formulation equation (3-9) with linear plume concentration profiles

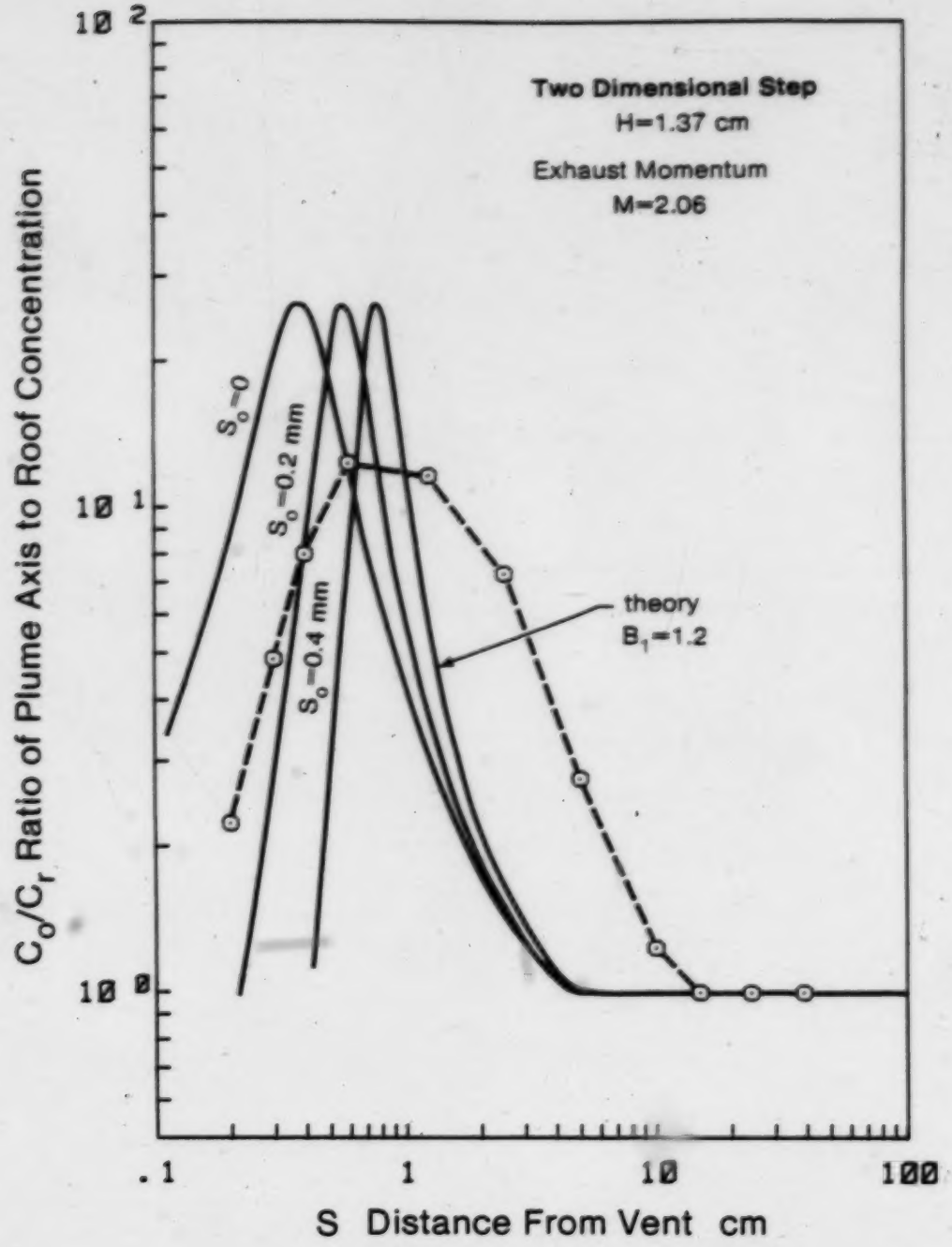

Figure 3-6 Use of $h \alpha S^{1/3}$ power law for plume rise to estimate the effect of plume rise on concentration at roof level assuming a virtual origin at downwind distance, S_o in the plume rise formulation equation (3-9) with linear plume concentration profiles

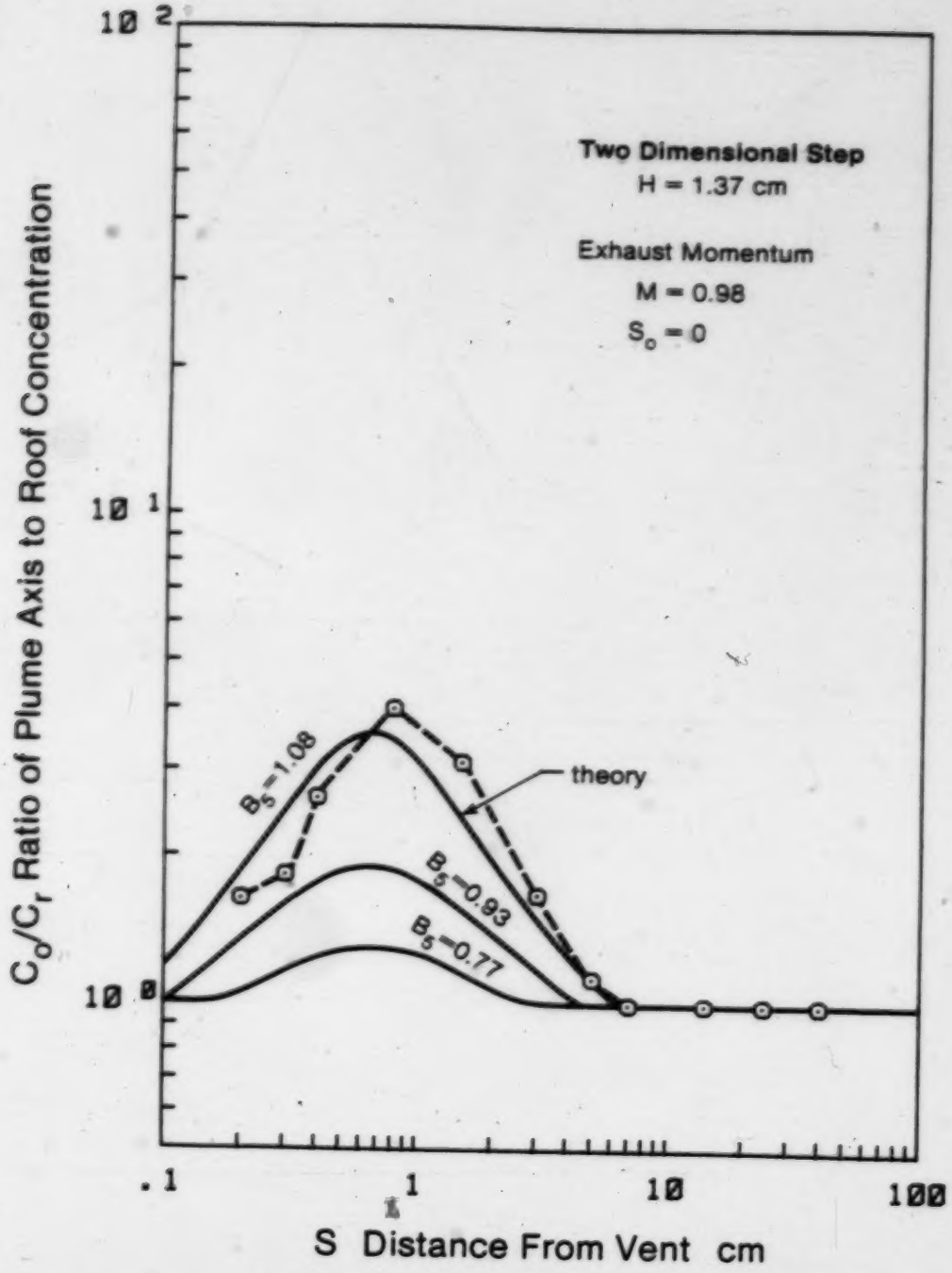

Figure 3-7 Use of $h \alpha S^{1/2}$ power law for plume rise to estimate the effect of plume rise on concentration at roof level. Dashed line represents experimental data and solid lines, theoretical predictions based on linear plume concentration profiles with different values of plume rise constant, B_5

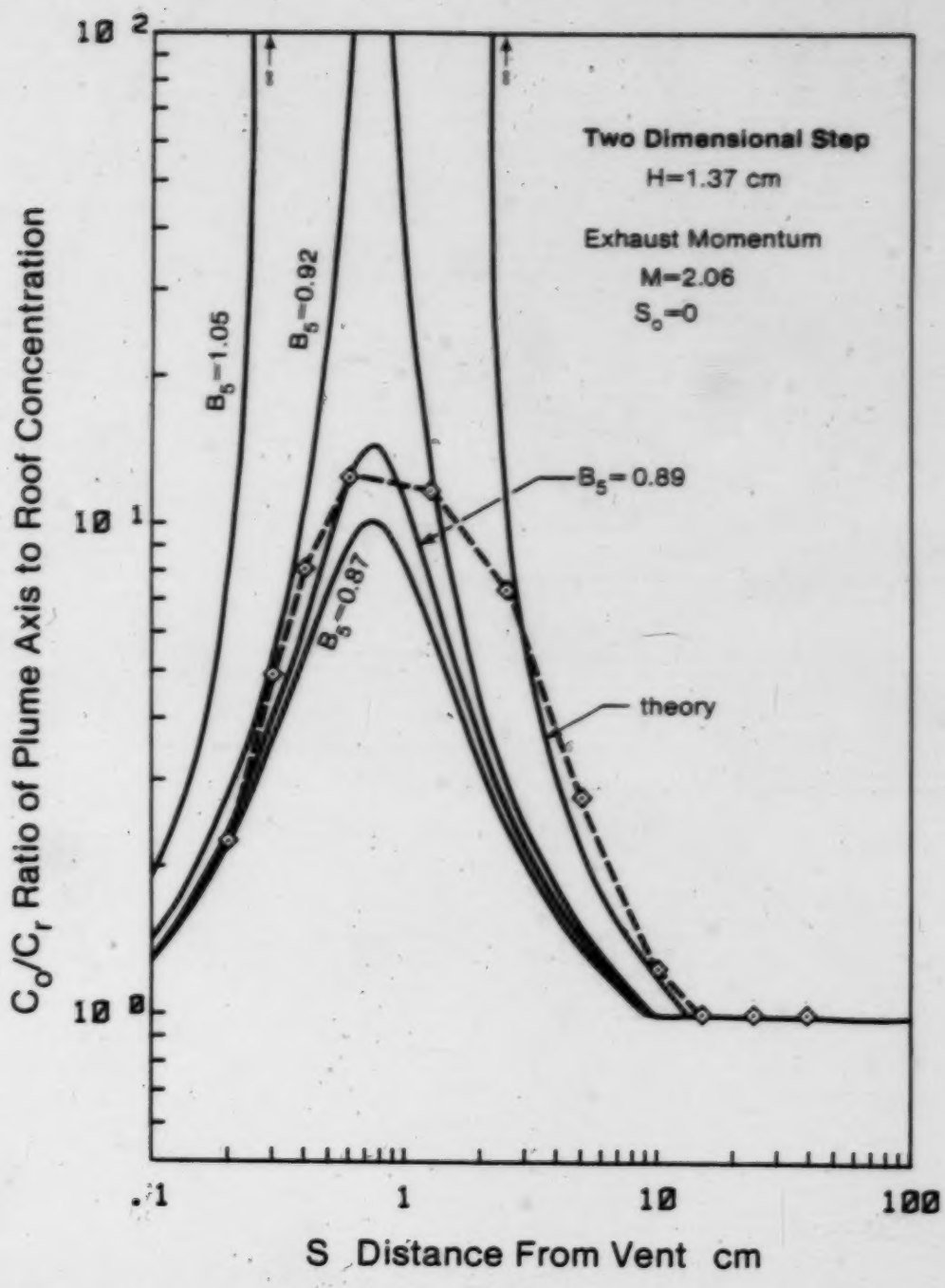

Figure 3-8 Use of $h \alpha S^{1/2}$ power law for plume rise to estimate the effect of plume rise on concentration at roof level. Dashed line represents experimental data and solid lines, theoretical predictions based on linear plume concentration profiles with different values of plume rise constant, B_5

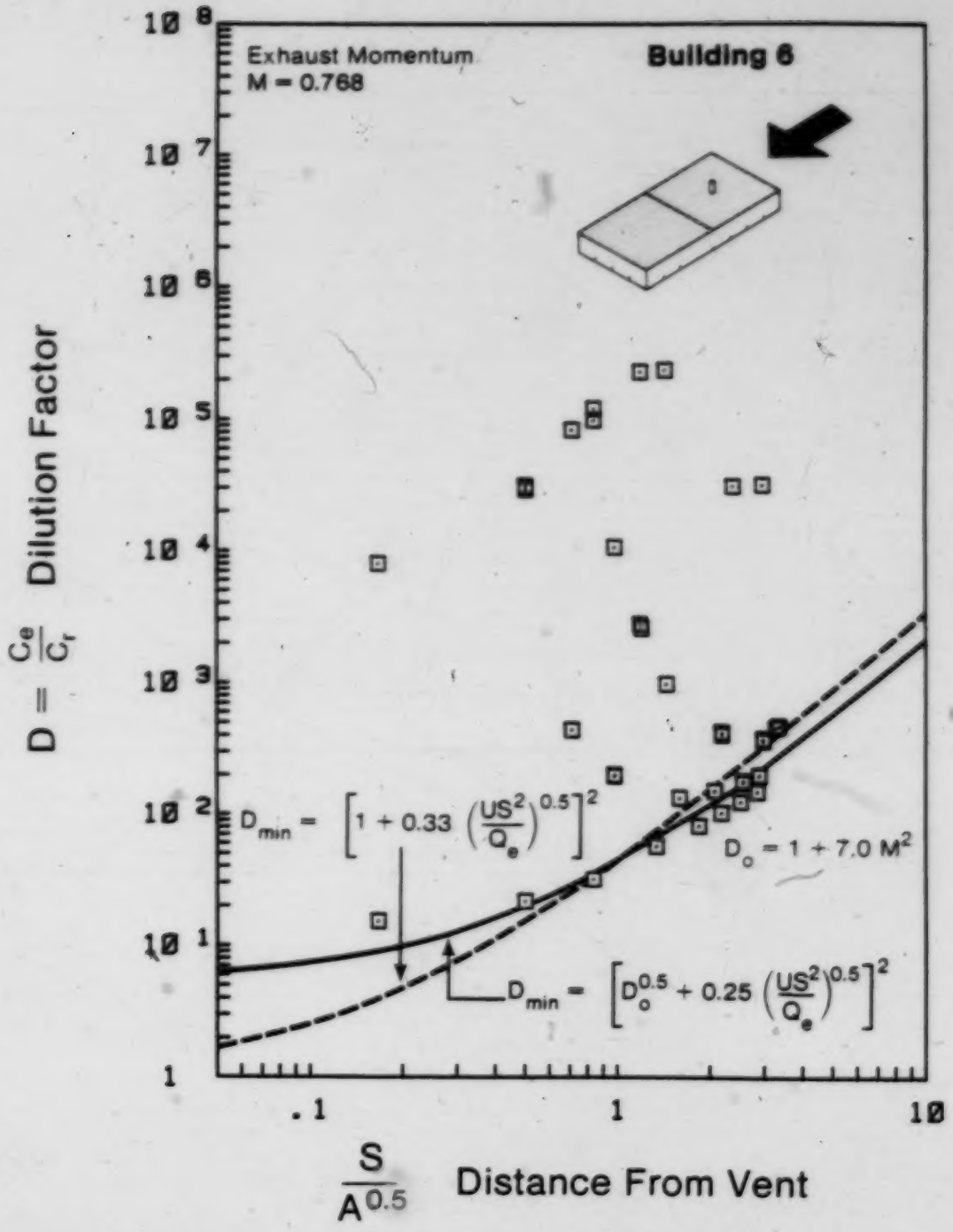

Figure 3-9 Effect of vertical exhaust momentum on minimum dilution for M = 0.768 and wind angle θ = 0°

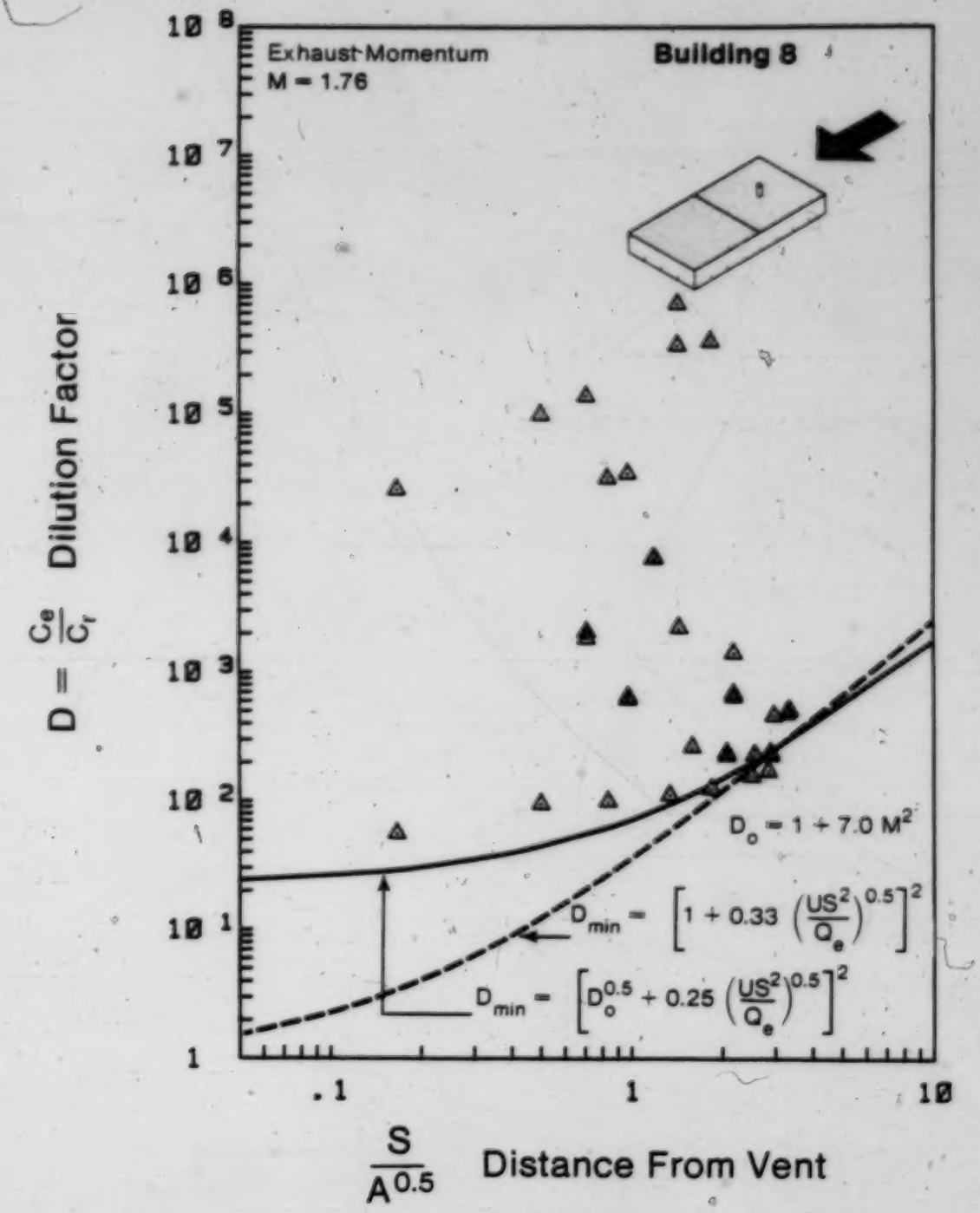

Figure 3-10 Effect of vertical exhaust momentum on minimum dilution for M = 1.76 and wind angle θ = 0°

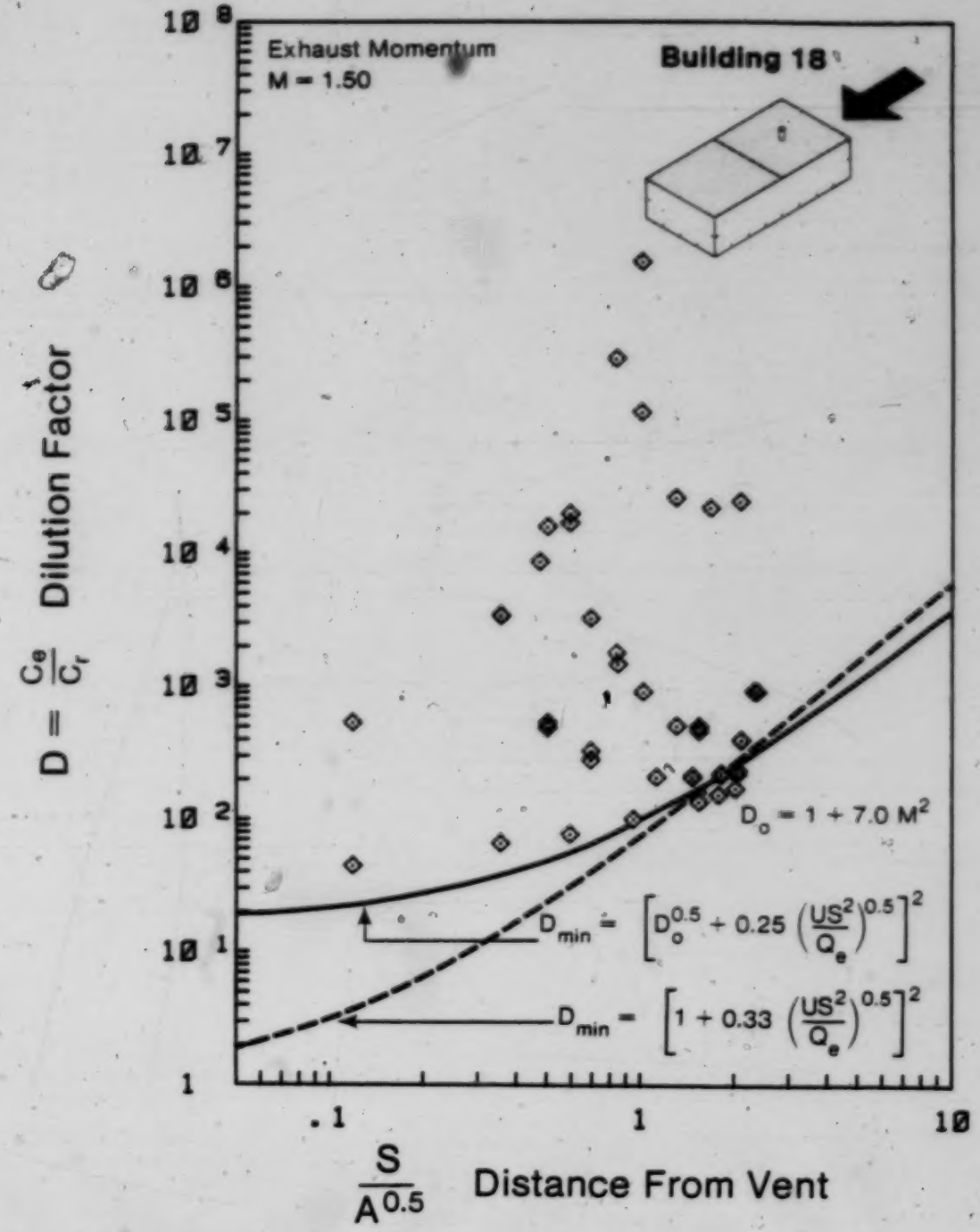
Exhaust Momentum
M = 1.50
Building 18
$D = \frac{C_e}{C_r}$ Dilution Factor
$D_o = 1 + 7.0\ M^2$
$D_{min} = \left[D_o^{0.5} + 0.25\left(\frac{US^2}{Q_e}\right)^{0.5}\right]^2$
$D_{min} = \left[1 + 0.33\left(\frac{US^2}{Q_e}\right)^{0.5}\right]^2$
$\frac{S}{A^{0.5}}$ Distance From Vent

Figure 3-11 Effect of vertical exhaust momentum on minimum dilution for M = 1.50 and wind angle θ = 0°

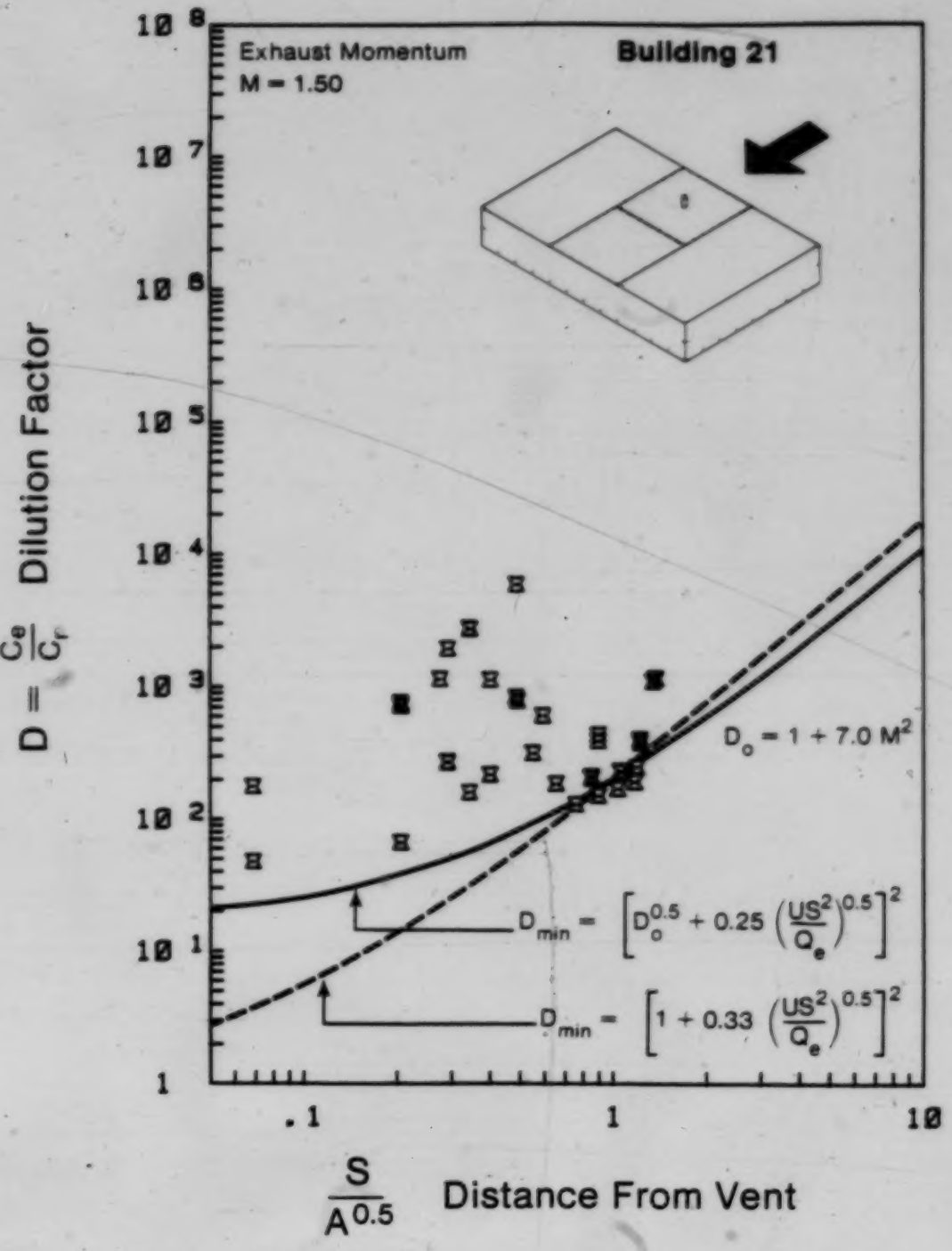

Figure 3-12 Effect of vertical exhaust momentum on minimum dilution for M = 1.50 and wind angle θ = 0°

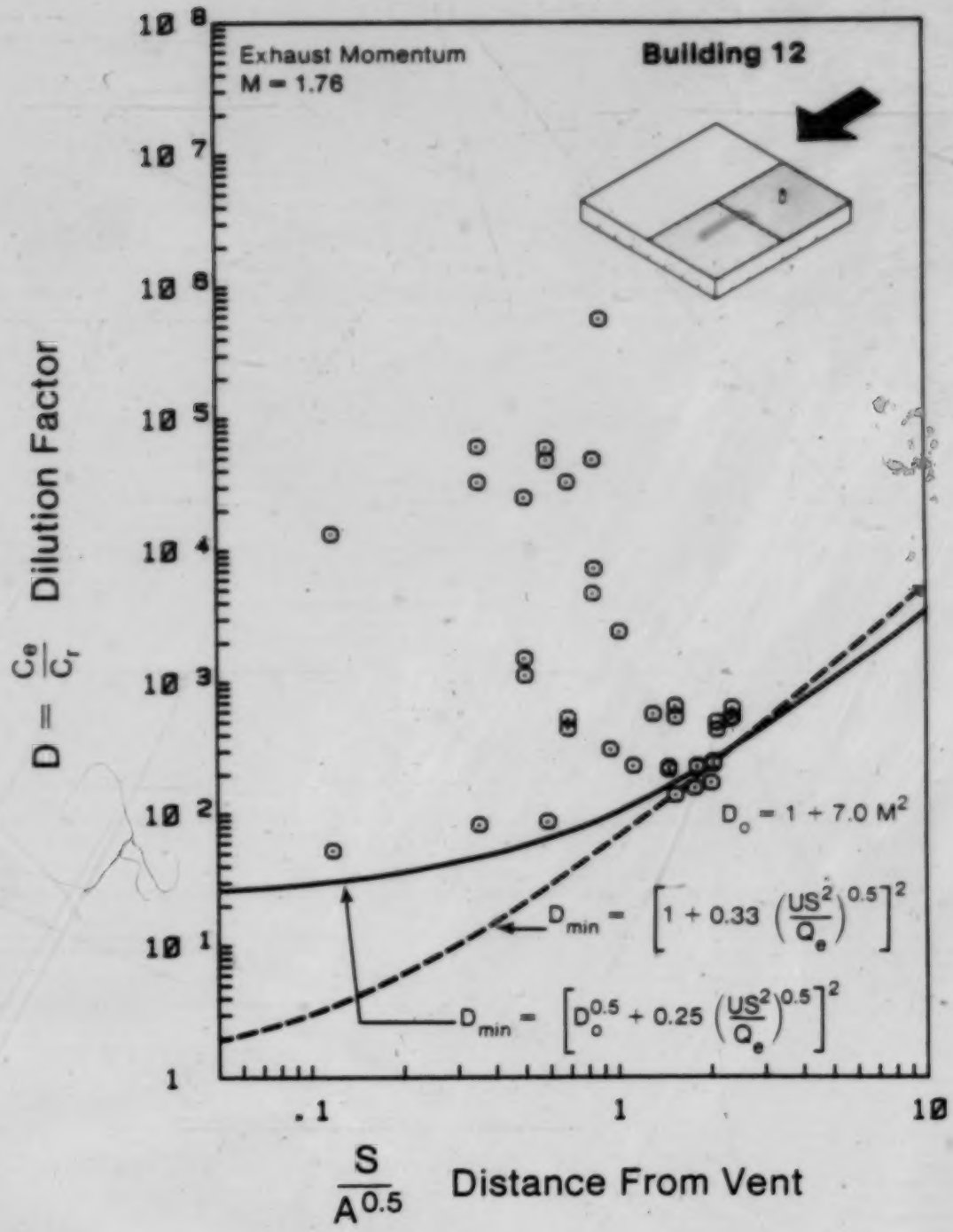

Figure 3-13 Effect of vertical exhaust momentum on minimum dilution for M = 1.76 and wind angle θ = 0°

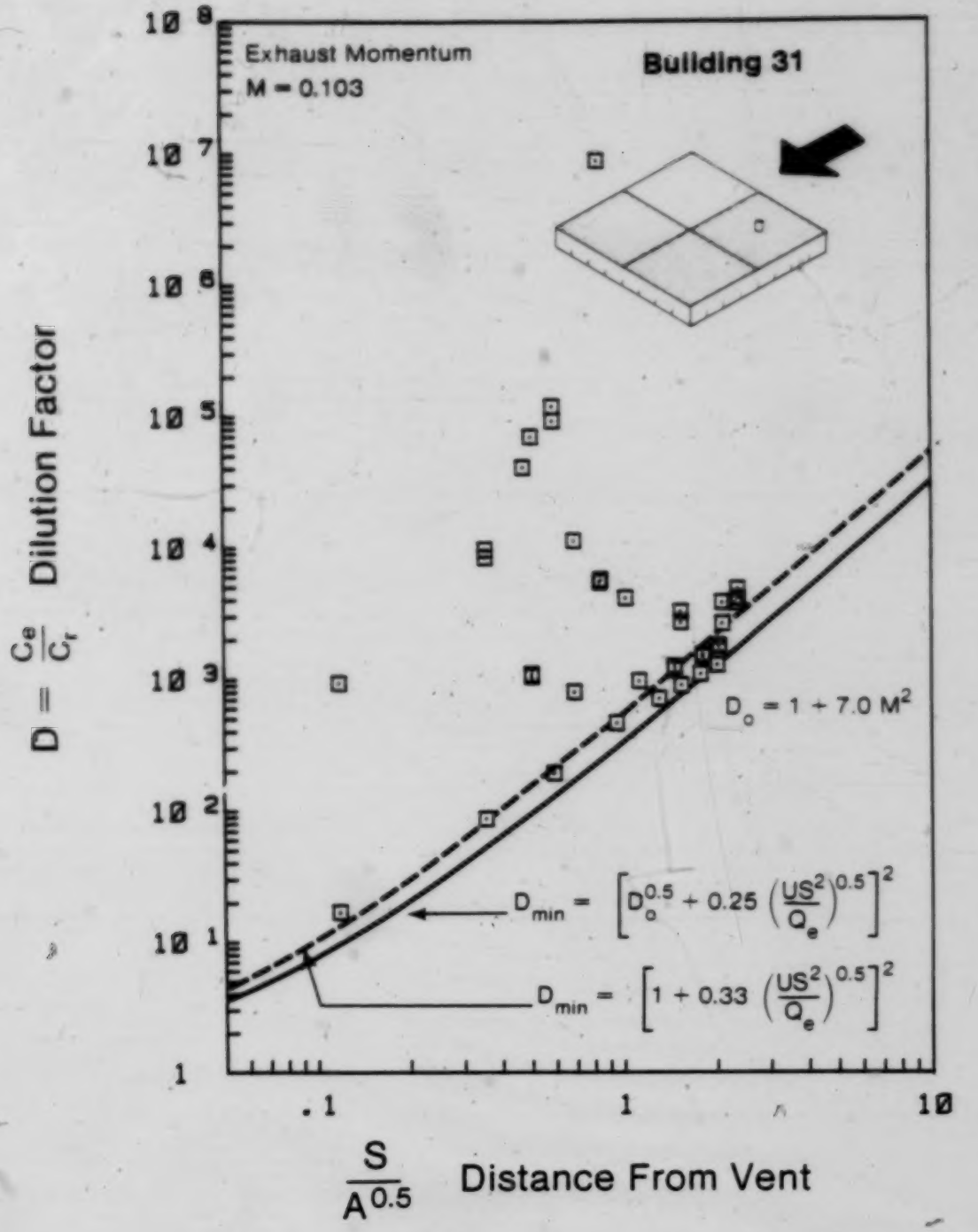

Figure 3-14 Effect of vertical exhaust momentum on minimum dilution for M = 0.103 and wind angle θ = 0°

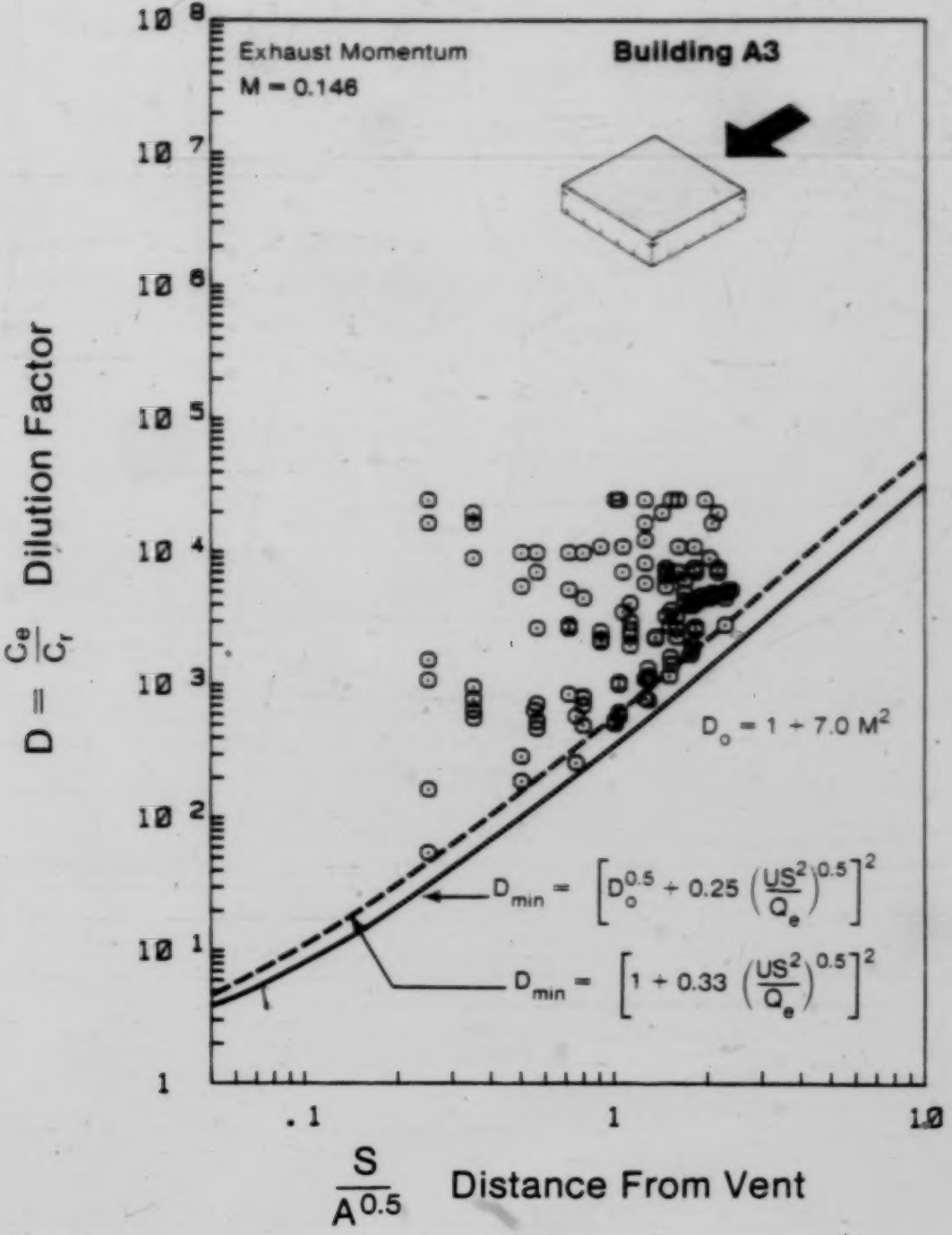
Exhaust Momentum
M = 0.146
Building A3
$D = \frac{C_e}{C_r}$ Dilution Factor
$D_o = 1 + 7.0\ M^2$
$D_{min} = \left[D_o^{0.5} + 0.25\left(\frac{US^2}{Q_e}\right)^{0.5}\right]^2$
$D_{min} = \left[1 + 0.33\left(\frac{US^2}{Q_e}\right)^{0.5}\right]^2$
$\frac{S}{A^{0.5}}$ Distance From Vent

Figure 3-15 Dilution from vents located on upwind half of building roof with exhaust momentum M = 0.146

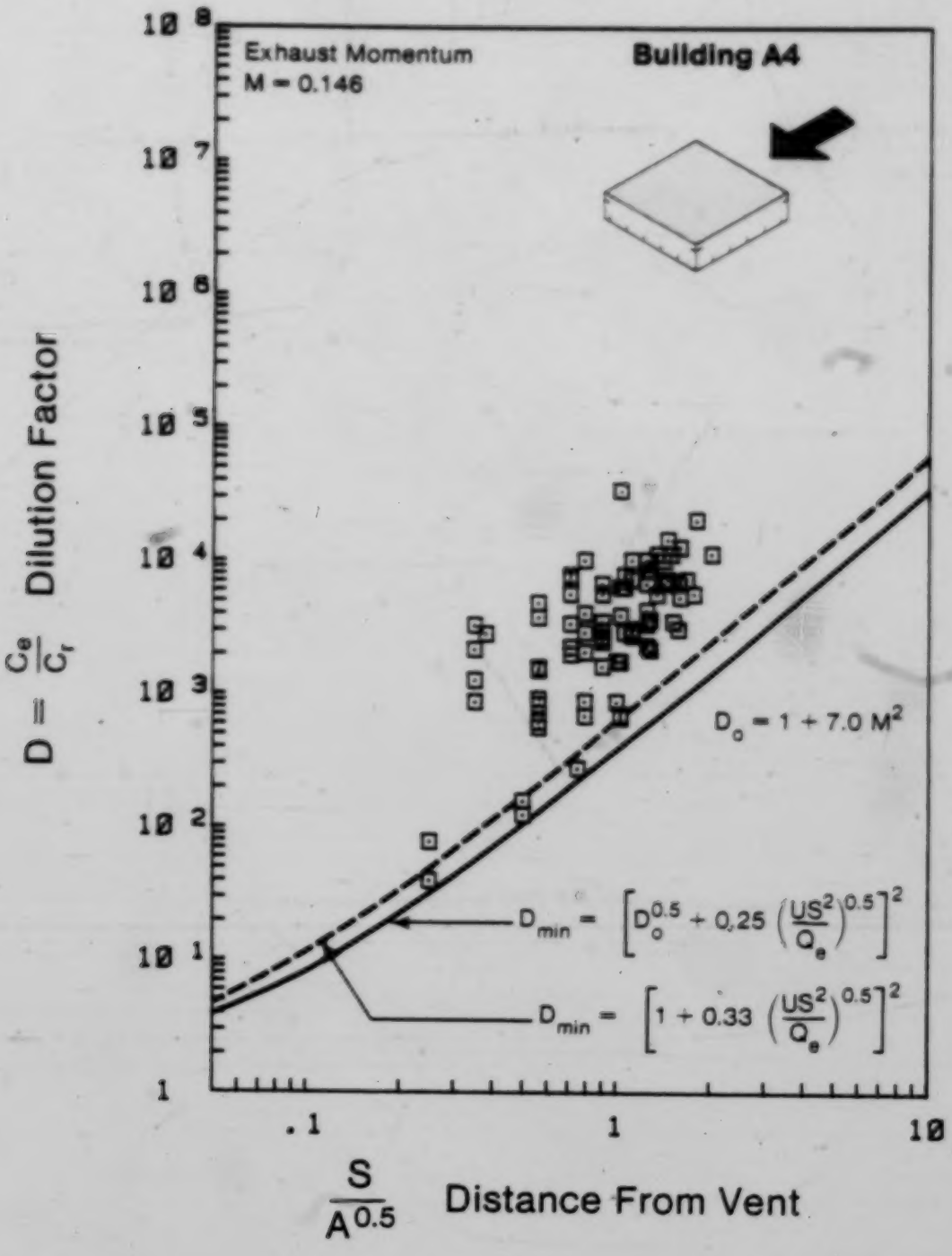
Exhaust Momentum
M = 0.146
Building A4
$D = \frac{C_e}{C_r}$ Dilution Factor
$D_o = 1 + 7.0\ M^2$
$D_{min} = \left[D_o^{0.5} + 0.25\left(\frac{US^2}{Q_e}\right)^{0.5}\right]^2$
$D_{min} = \left[1 + 0.33\left(\frac{US^2}{Q_e}\right)^{0.5}\right]^2$
$\frac{S}{A^{0.5}}$ Distance From Vent

Figure 3-16 Dilution from vents located on downwind half of building roof with exhaust momentum M = 0.146

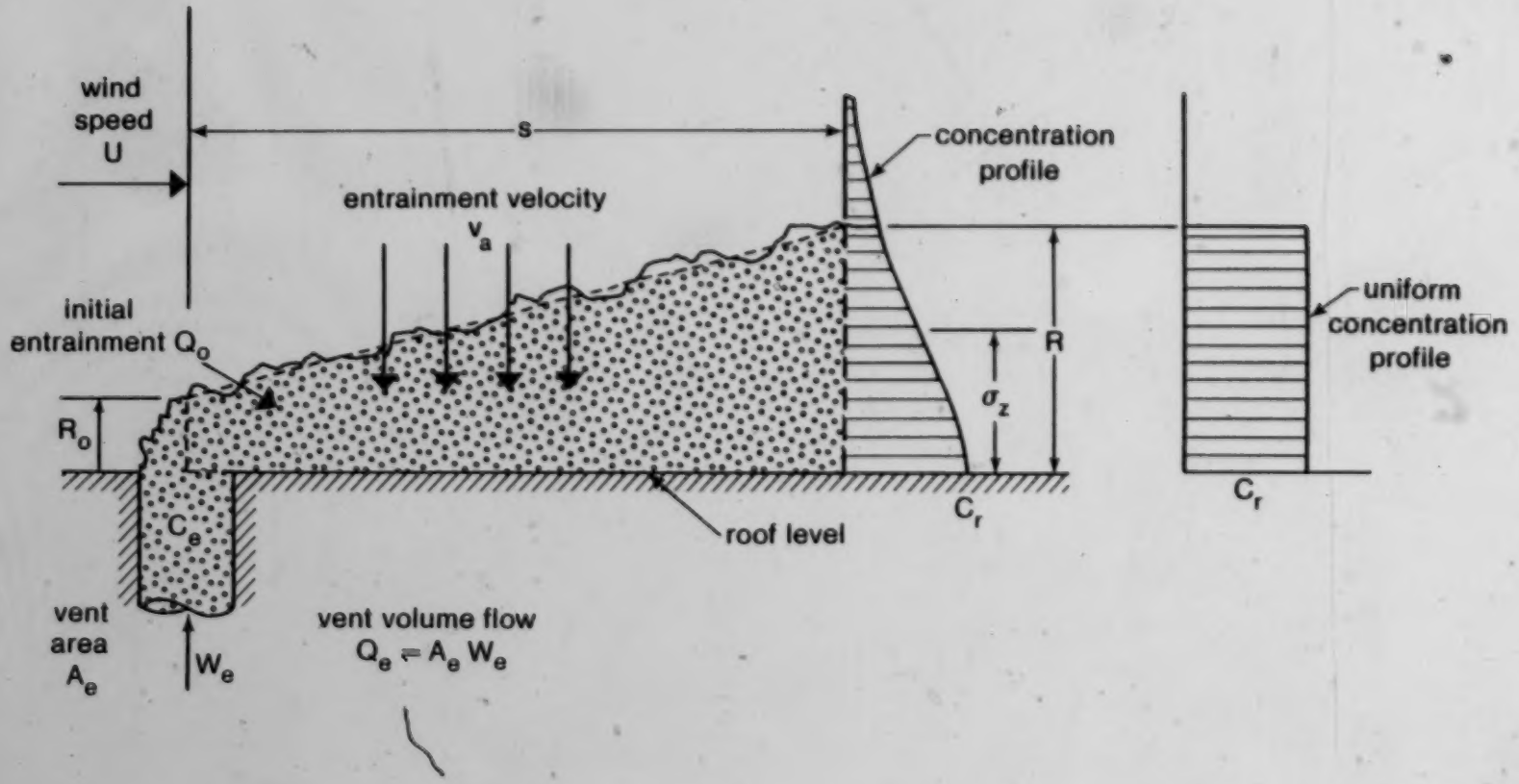

Figure 3-17 Air entrainment into the exhaust gas plume from a flush, vertically directed roof vent

CHAPTER IV

Effect of Wind Incidence Angle on Dilution of Effluent at Roof Level

Introduction

All the minimum dilution models discussed so far were developed with the approach wind perpendicular to the upwind face of the building, in other words at wind incidence angle θ equal to 0°. In reality, wind direction does shift from time to time and the complex flow pattern on the building surface changes with it. According to a flow visualization study reported by Wilson (1979), when wind incidence angle θ is zero, the flow separates from the upwind edges of the building and later reattaches to the building, forming the peculiar flow pattern as shown in Figure 4-1. But, when θ is greater than 20°, the recirculation cavity on the building roof becomes very small and two intense counter-rotating vortices are induced at the upwind edges of the roof as indicated in Figure 4-2. Evidently, the change in flow pattern with wind direction is substantial and may significantly affect the minimum dilution level on building roofs. This chapter will discuss how the existing minimum dilution model, equation (3-14) can be modified to accommodate the influence of wind incidence angle.

4.1 A Theory to Account for Wind Incidence Angle Effect

For a building skewed to wind, exactly how the intricate flow patterns influence vent gas dilution is not well understood. Most likely, the dominant effect originates from the two counter-rotating

vortices induced at the upwind roof edges. These vortices enhance turbulent mixing and generate intense downwash which returns the emitted exhaust gas from roof vents to the building roof. As a result, a high concentration of exhaust gas may be present at roof level. Because of the complexity of the flow, the author attempted to modify the existing minimum dilution model, equation (3-14), determined at zero incidence wind angle instead of formulating a completely new model for angled buildings. The reason for doing so is twofold:

a) The existing model has already incorporated the influence of windspeed, vent-to-intake distance, source strength and initial entrainment on dilution. These effects are probably an integral part of the total dilution of vent gases whether or not the building is skewed to wind. So, using the existing model as a basis for modification seems reasonable.

b) This approach will yield a dilution model in which the contribution due to wind angle can readily be identified. From a designer's point of view, this seems more desirable than having two different, unrelated models: one for θ at 0° and one for angled buildings.

The modification to include wind angle effect was based on the basic assumption that the overall significance of wind angle on dilution can be summarized by the change in entrainment constant, α. Mathematically, the postulation can simply be represented by

$$\alpha(\theta) = B_2 \alpha(0°)$$

and with $\alpha(0°)$ defined as α_o

$$\alpha(\theta) = B_2 \alpha_o \qquad (4\text{-}1)$$

Intuitively B_2 should be a multi-variable function because the efficiency with which the two roof edge vortices trap exhaust gas at roof level depends on a number of factors. Some fundamental ones are:

1) The wind angle, θ, and possibly building geometry which determine the size, pattern and strength of the vortices that in turn may affect the degree of meandering of the exhaust plume.
2) The vent location in relation to the vortices: the closer to the vortices, the stronger the influence.
3) The exhaust momentum factor, M, which governs the degree of exhaust gas penetration above the roof will almost certainly limit the amount of exhaust gas that will be trapped by the two vortices.

These various factors are probably interrelated and their complex interplay determines the extent of wind angle effect on dilution. For a first estimation of this effect, only two of these factors were isolated to be studied - the wind angle θ and exhaust velocity ratio M. Thus, B_2 is expressed as

$$B_2 = f(\theta, M) \tag{4-2}$$

Substituting equation (4-1) into the existing dilution model, equation (3-14), the modified dilution model with wind angle effect included can be written using $\alpha_o = 0.2$ at $\theta = 0°$,

$$D_{min} = [D_o^{0.5} + 0.25\, B_2 (\frac{US^2}{Q_e})^{0.5}]^2 \tag{4-3}$$

where

$$D_o = 1 + 7.0\, M^2 \tag{3-15}$$

Experimental measurements were made to verify if this model adequately describes the influence of wind incidence angle on dilution.

4.2 Wind Tunnel Tests

The data collected for this analysis can be classified into two distinct sets according to exhaust momentum factor, M:

a) High exhaust momentum (M = 1.28 to 1.76)

This set included buildings 12 through 15, 19, 20, 23 and 24, see Figure 2-10, chapter II. They were part of the zero stack height baseline data set used by Wilson and Winkel (1982) in their investigation of stack height effects. All data were taken from a sampling grid with 24 to 41 sampling intake locations.

b) Low exhaust momentum (M = 0.073 to 0.103)

Buildings 31, 43 to 46 and 48 through 62 belonged to this set see Figure 2-10, chapter II. They were data taken by the author using the same wind tunnel model employed in the Wilson and Winkel's study (1982). Six more intake locations were added to provide a finer sampling grid to pick up the points of minimum dilution. Table 4.1 indicates their relative positions with the building roof vent location.

All the buildings tested had a flat roof, a square top section (i.e. W/L = 1.0) and a vertically directed roof vent of zero stack height. Each building was tested in the wind tunnel at a single wind speed, U, wind angle θ and rate of exhaust gas Q_e, see Table 4-2. In each case, concentration measurements of vent gas dispersion were performed in accordance with the procedures described in section 2.3, chapter II.

4.3 Wind Angle Effect at Low Exhaust Momentum (M = 0.073 to 0.103)

A sample of the dilution measurements taken at low exhaust momentum is shown in Figures 4-3 to 4-7. These show data gathered from a single building geometry at five different wind angles, θ = 0°, 15°, 22.5°, 30° and 45° respectively. In each figure the dilution measurements on the plume centerline define a distinct lower bound to the data set.

A close look into the data reveals that at a fixed distance S from the vent, the minimum dilution decreases with increasing wind angle θ. From 0° to 15°, the decrease is about 20%, followed by a 40% drop from minimum dilution at 0° when θ = 22.5° and the reduction levels off at 50 to 55% for θ between 30° and 45°. In other words, if wind direction shifts by 30° or more, a doubling of the contaminant concentration level can be expected.

This finding is not peculiar to only one building geometry. Similar results were obtained from three other building configurations at about the same exhaust momentum, see Figures A 4-1 to A 4-15 in Appendix A 4. Actually these figures show that the reduction of minimum dilution with θ is more severe for buildings with smaller width to height ratios like 2:1 and 1:1. Four to eight times smaller dilutions were observed with a θ of 30°. However, in the present study, special provision will not be made in the minimum dilution model for these extreme cases.

4.3.1 Data Correlation

The modified minimum dilution model, equation (4-3), was found to correlate very well with experimental data taken from a building with W/H = 8 (see Figures 4-3 to 4-7) when B_2 of equation (4-3) took on the following values:

For M = 0.1

B_2 = 1.0 at θ = 0°

B_2 = 0.95 at θ = 15°

B_2 = 0.75 at θ = 22.5°

B_2 = 0.7 at θ = 30°

B_2 = 0.65 at θ = 45°

The prediction came within $\pm$ 5% of actual measurements. The dilution model for θ = 0°, equation (3-14) or equation (4-3), with B_2 = 1.0, was also plotted in these figures for comparison. For $\theta \leq 15°$, equation (3-14) is satisfactory. However, when $\theta \geq 22.5°$, equation (3-14) consistently overestimates the minimum dilution and the improvement gained by using equation (4-3) is unquestionable.

Having determined the values of B_2 at M = 0.1, an attempt was made to search for a simple function to represent equation (4-2). Wilson (1984, private communication) suggested the following expression:

$$B_2 = \frac{\alpha}{\alpha_o} = \frac{1 + \theta}{1 + B_4\theta} \qquad (4\text{-}4)$$

where B_4 is assumed to be a function of M. Letting B_4 = 2.2 at M = 0.1, equation (4-4) shown in Figure 4-8 agrees reasonably well with the observed behavior of B_2. Equation (4-4) is conservative for $\theta \leq 22.5°$. When $\theta \geq 22.5°$, it gives a very close approximation of the variation of B_2 with θ, within 1% of the experimentally determined values.

This simple relationship, equation (4-4), can be very useful. When it is coupled with equation (4-3), a prediction of the minimum dilution at low exhaust momentum (M = 0.1) can be made for <u>any</u> wind angle between 0° and 45°.

Although equation (4-4) suggests a decrease in α when θ is greater than 0°, this does not necessarily mean a reduction in actual air entrainment. The definition of α in section 4.1 inherently accounts for other effects on dilution caused by plume meandering, as well as trapping in the roof edge vortices. So, a decrease in α could be a result of downwash and/or less meandering of the exhaust plume due to changes in the surface flow pattern on building roof.

4.3.2 Sensitivity to Building Shape

Using the above B_2 values, equation (4-3) was also tested on three other building configurations which had similar exhaust momentum conditions but smaller aspect (i.e. width to height) ratios: 4:1, 2:1, and 1:1. The results are shown in Figures A4-1 to A4-15 of Appendix A4. In all cases equation (4-3) gave more accurate predictions than equation (3-14). However, the accuracy of equation (4-3) diminishes for buildings with an aspect ratio of 2:1 or smaller. Particularly when wind angle θ, is greater or equal to 30°, instead of having a $\pm$ 5% uncertainty, plus 30% is observed. This may have been caused by the uncertainty of data measurement, but more likely is due to the fact that the dependence of dilution on building size and shape is ignored in equations (4-3), and (4-4). Further studies are needed to formulate a more realistic model to account for this dependence. Since this study aims at making a first approximation of the influence of wind angle on dilution, the simple and convenient model represented by equations (4-3) and (4-4) is quite adequate, with a maximum uncertainty of $\pm$ 30% in estimating the minimum dilution for varying wind angle.

4.3.3 Comparison with Other Investigations

Li and Meroney (1983) in their study on gas dispersion near buildings also found that wind angle had a significant effect on minimum dilution. They tested a cubical building with almost negligible momentum (M = 0.07) in a simulated atmospheric boundary layer very close to the one in this study with similar boundary layer thickness, Reynolds number, turbulence intensity and scale, and building height. According to their observations, a correction factor to account for the wind angle effect was found to be:

$$(D_{min})_\theta = (D_{min})_{\theta=0^\circ} f(\theta)$$

where

$$f(\theta) = \frac{1}{1 + \frac{4\theta}{\pi}} \qquad (4\text{-}5)$$

with θ in radians. For $(D_{min})_{\theta=0^\circ}$, they used Wilson's (1976) formulation,

$$(D_{min})_{\theta=0^\circ} = 0.11 \frac{US^2}{Q_e} \qquad (1\text{-}3)$$

From which they obtained,

$$(D_{min})_\theta = (0.11\frac{US^2}{Q_e})(\frac{1}{1 + \frac{4}{\pi}\theta}) \qquad (4\text{-}6)$$

which reduces to

$$(D_{min})_\theta = [0.33 (\frac{1}{1 + \frac{4\theta}{\pi}})^{0.5} (\frac{US^2}{Q_e})^{0.5}]^2 \qquad (4\text{-}7)$$

This predicts a factor of 2 decrease in minimum dilution for a shift in wind direction by 45° from $\theta = 0^\circ$. This finding is appreciably close to

the present study which predicts the same drop in minimum dilution for $\theta = 30°$. Figure 4-8 shows a more complete comparison by plotting equation (4-5) in a form comparable to B_2 of equation (4-4). The two curves display very similar trends with equation (4-4) being consistently lower, leading to a difference of about 20% in their respective predictions on minimum dilution.

Considering that these two models came from two independent studies with data taken using different sampling techniques, it is remarkable to have such a small difference. This consistency in findings from these independent experiments lends credibility to the experimental results in the present study and suggests that the minimum dilution model being employed has some physical basis.

A large disparity between equations (4-6) and (4-3) is expected when exhaust momentum factor M increases, because equation (4-6) completely ignores the initial entrainment induced by exhaust momentum which was discussed in the previous chapter.

4.4. Wind Angle Effect at High Exhaust Momentum (M = 1.28 to (1.76)

Figures 4-9 to 4-12 show a set of dilution measurements taken at the high exhaust momentum condition (M = 1.76). Rather suprisingly, the data do not indicate any dependence of minimum dilution on wind angle. So, no adjustment was needed for B_2 in equation (4-3), with $B_2 = 1.0$ irrespective of the wind angle, θ. The same phenomenon was observed in two other test buildings having similar magnitudes of exhaust momentum factor M, but very different frontal areas and vent locations (see Appendix A4, Figures A4-16 to A4-19). Although the data was collected without the six additional intake locations specified in Table 4-1, it

still seems unlikely that the original sampling grid of about 41 locations would not have been adequate to identify the minimum dilution points.

Considering that the only parameter which was changed in this set of tests was the exhaust momentum factor, M, it appears logical to conclude that the independence of minimum dilution on θ is due to M. Wilson and Chui (1985) state that the high vertical momentum in the exhaust plume causes considerable penetration above the roof which may be the factor responsible for reducing the influence of the two roof edge vortices. Alternately, the high exhaust momentum may result in such a large initial dilution by enhanced entrainment that any wind angle effect is overshadowed.

Given that B_4 is about 2.2 for $M \approx 0.1$ from the previous section and it is 1.0 for $M \geq 1.28$, a plausible functional form for B_4 is

$$B_4 = 1.0 + 1.7 \exp(-3.5M) \qquad (4\text{-}8)$$

This is shown in Figure 4-13. It should be emphasized that equation (4-8) is not based on any specific physical principle. Further studies are required to investigate its range of validity.

4.5 Summary

Significant changes in roof flow patterns with wind incidence angle lead us to suspect that the minimum dilution evaluation at roof level may be affected considerably. Experimental data at negligible exhaust momentum ($M \approx 0.1$) confirm this suspicion. For low rise, flat roofed buildings having aspect ratios of 4:1 to 8:1, a factor of 2 reduction in minimum dilution was observed with wind angle $\theta \geq 30°$, while for buildings of smaller aspect ratios (1:1 to 2:1), a factor of 4 to 8 decrease

was noted at $\theta \geq 30°$. However, when exhaust momentum was high (M = 1.28 to 1.76) there was no conclusive evidence that minimum dilution was sensitive to wind angle θ.

A simple minimum dilution model was proposed to account for the above effect and is represented by equations (4-3), (4-4) and (4-8). Data correlation indicates that when θ is between 22.5° and 45°, the model is accurate to $\pm$5% in general. The only exception is when θ is greater than 30° for buildings of aspect ratio 2:1 or smaller, the accuracy error increases to about $\pm$ 30%. When θ is small i.e. $\theta \leq 15°$, the prediction by the model tends to be conservative and equation (3-14) is recommended instead. In other words, wind angle effect is small enough to be neglected in this range of θ.

It is important to note that the above model was developed based on data taken from square topped buildings (i.e. W/L = 1.0) with flush, vertically directed roof vents. It does not account for the variation caused by changing the position of vent location, stack heights or building shapes. Further systematic studies are needed to incorporate these effects. However, this model does provide a first estimation of wind angle effect and forms a useful foundation upon which further studies can be based.

TABLE 4-1

Locations of the New Sampling Ports

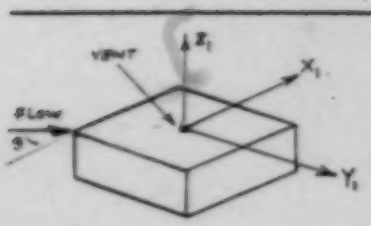	Intake Locations Relative to Vent		
	X_1 (cm)	Y_1 (cm)	Z_1 (cm)
Vent Number			
30	2.5	0.67	0.0
31	2.5	1.00	0.0
32	1.5	0.40	0.0
33	1.5	0.87	0.0
34	0.5	0.21	0.0
35	0.5	0.50	0.0

TABLE 4-2

Conditions for Wind Tunnel Tests

BUILDING NUMBER	WIND ANGLE θ	FLOW PARAMETERS: EXHAUST FLOW RATE Q_e — Helium flowrate $\left(\frac{cm^3}{min}\right)$	EXHAUST FLOW RATE Q_e — Air flowrate $\left(\frac{cm^3}{min}\right)$	DENSITY RATIO $\frac{\rho_e}{\rho_a}$	WIND SPEED AT ROOF HEIGHT U $\left(\frac{m}{s}\right)$	STACK DIAMETER d_s (cm)	EXHAUST MOMENTUM FACTOR $M=\left(\frac{\rho_e}{\rho_a}\right)^{0.5}\frac{W_e}{U}$
12	0°						
13	30°						
14	45°	1000	385	0.378	5.89	0.132	1.76
15	15°						
19	0°						
20	45°	1000	385	0.378	6.91	0.132	1.50
23	0°						
24	45°	1000	385	0.378	8.10	0.132	1.28
31	0°						
43	15°						
44	22.5°	195	0	0.138	8.56	0.132	0.103
45	30°						
46	45°						
48	0°						
49	45°						
50	30°	195	0	0.138	8.56	0.132	0.103
51	15°						
52	22.5°						
53	0°						
54	45°						
55	22.5°	195	0	0.138	10.2	0.132	0.087
56	30°						
57	15°						
58	0°						
59	45°						
60	15°	195	0	0.138	12.1	0.132	0.073
61	30°						
62	22.5°						

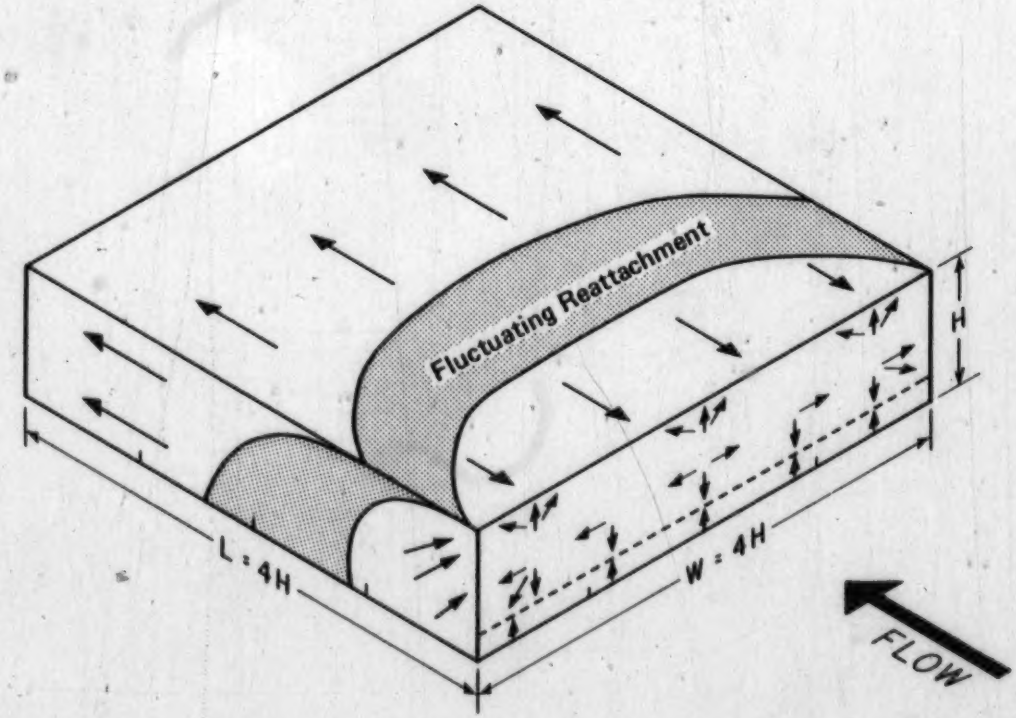

Figure 4-1 Surface flow patterns on a wide flat-roofed building with wind incidence angle of $\theta = 0°$

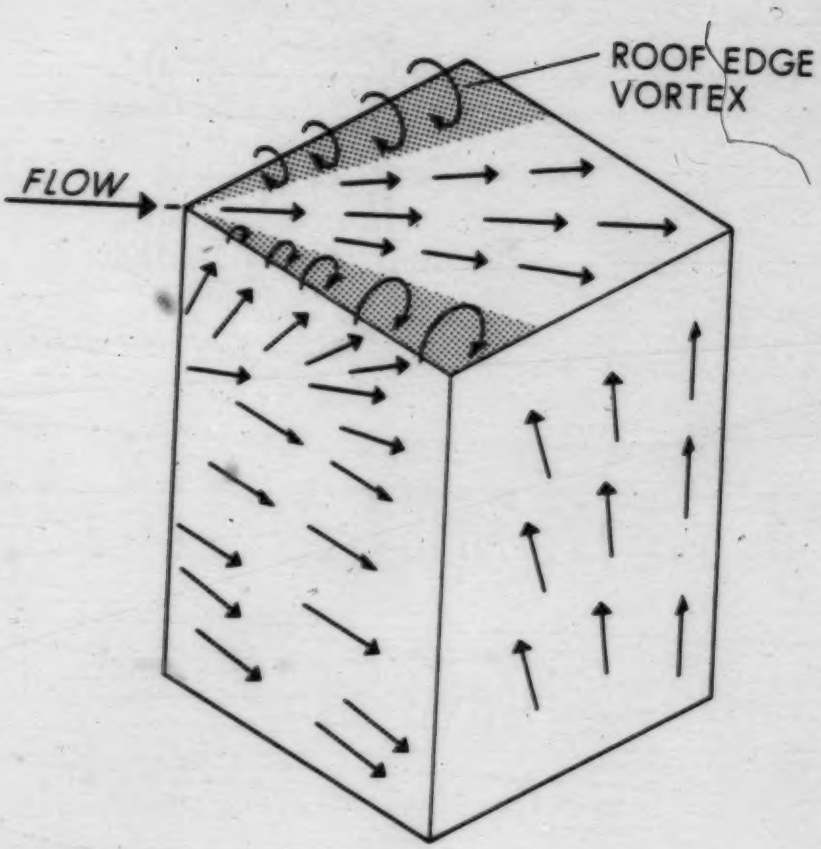

Figure 4-2 Surface flow pattern on a tall flat-roofed building with wind incidence angle of $\theta = 45°$

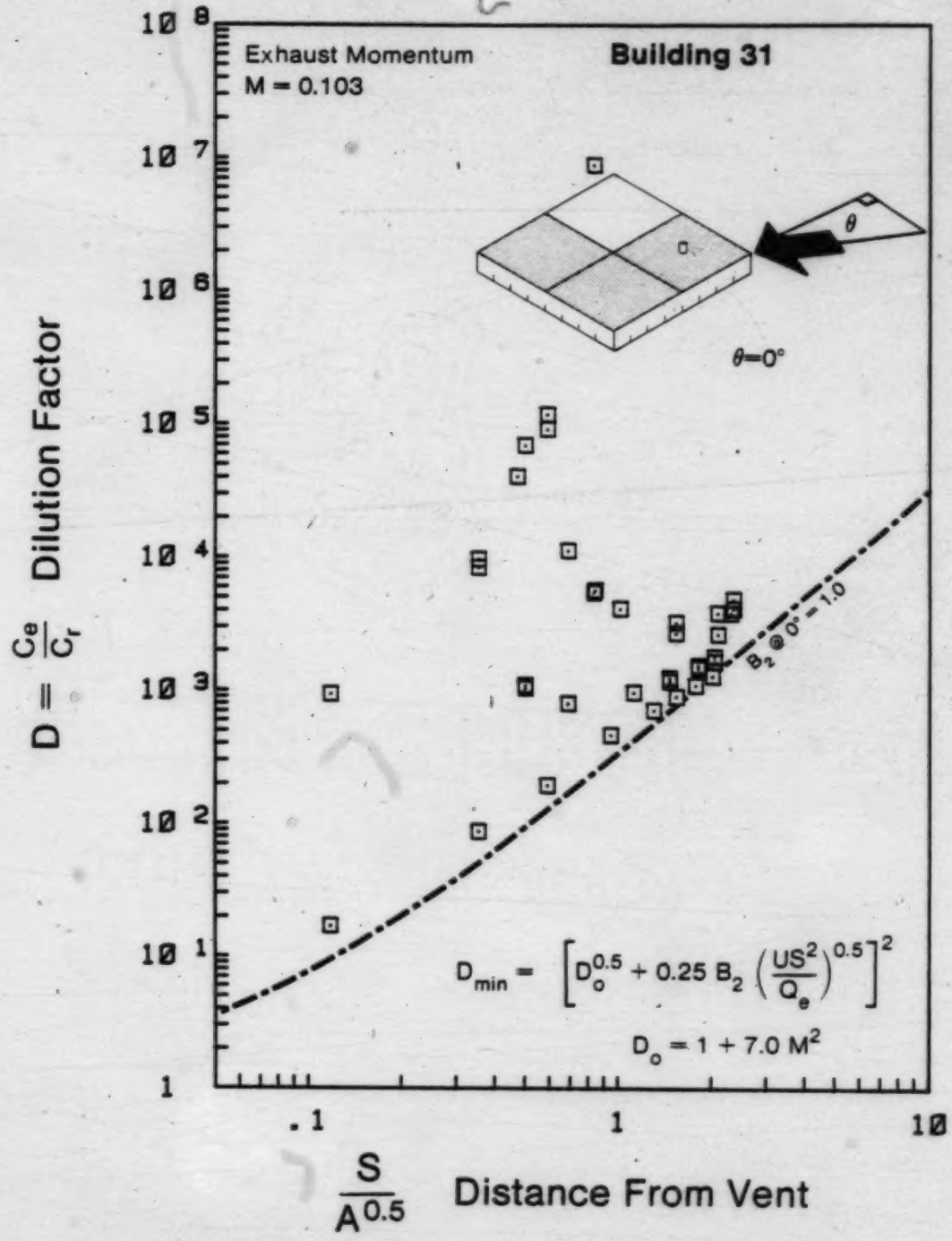

Figure 4-3 Effect of wind angle on minimum dilution for a low rise building with low exhaust momentum, M = 0.103 and wind angle θ = 0°

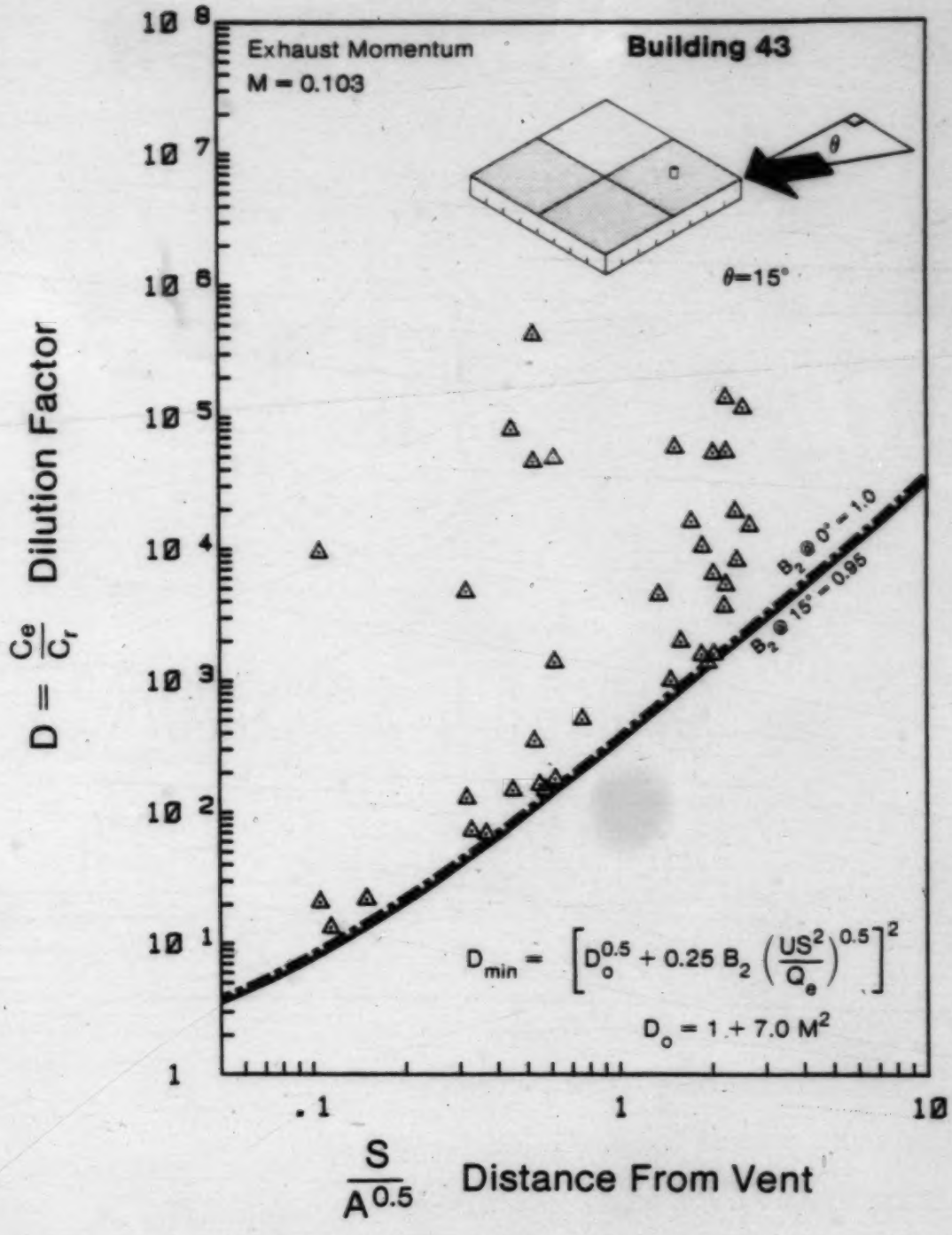

Figure 4-4 Effect of wind angle on minimum dilution for a low rise building with low exhaust momentum, M = 0.103 and wind angle θ = 15°

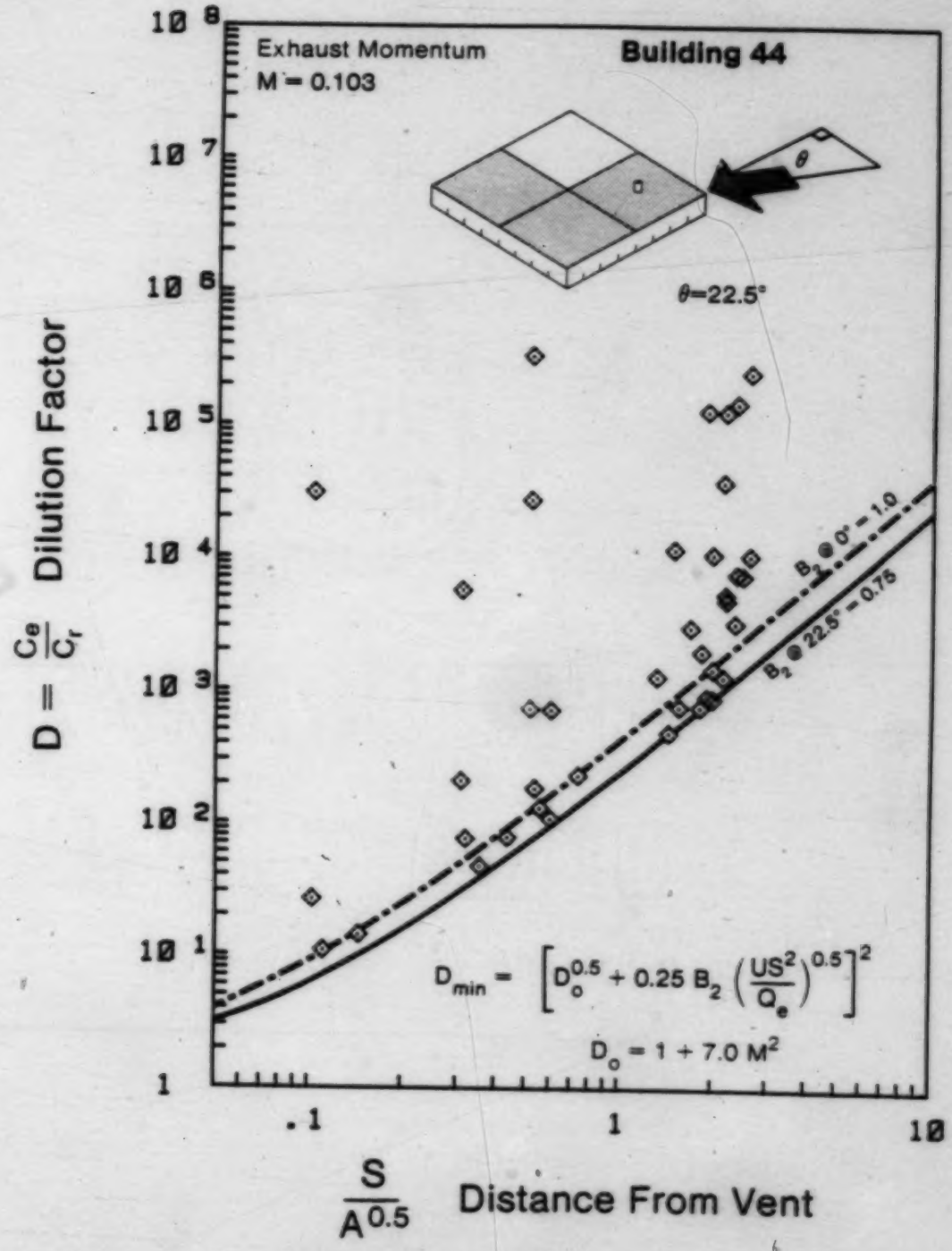

Figure 4-5 Effect of wind angle on minimum dilution for a low rise building with low exhaust momentum, M = 0.103 and wind angle θ = 22.5°

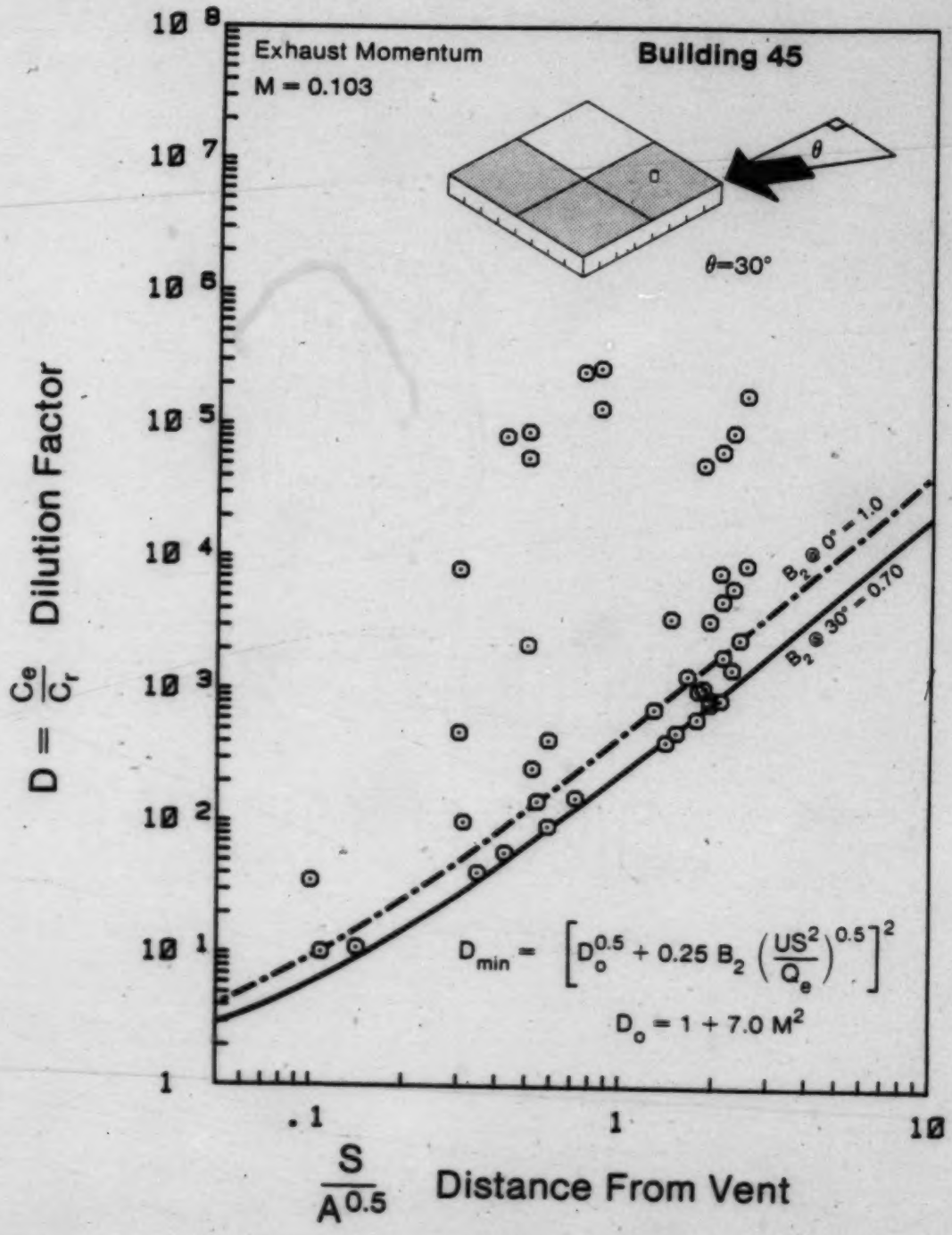

Figure 4-6 Effect of wind angle on minimum dilution for a low rise building with low exhaust momentum, M = 0.103 and wind angle θ = 30°

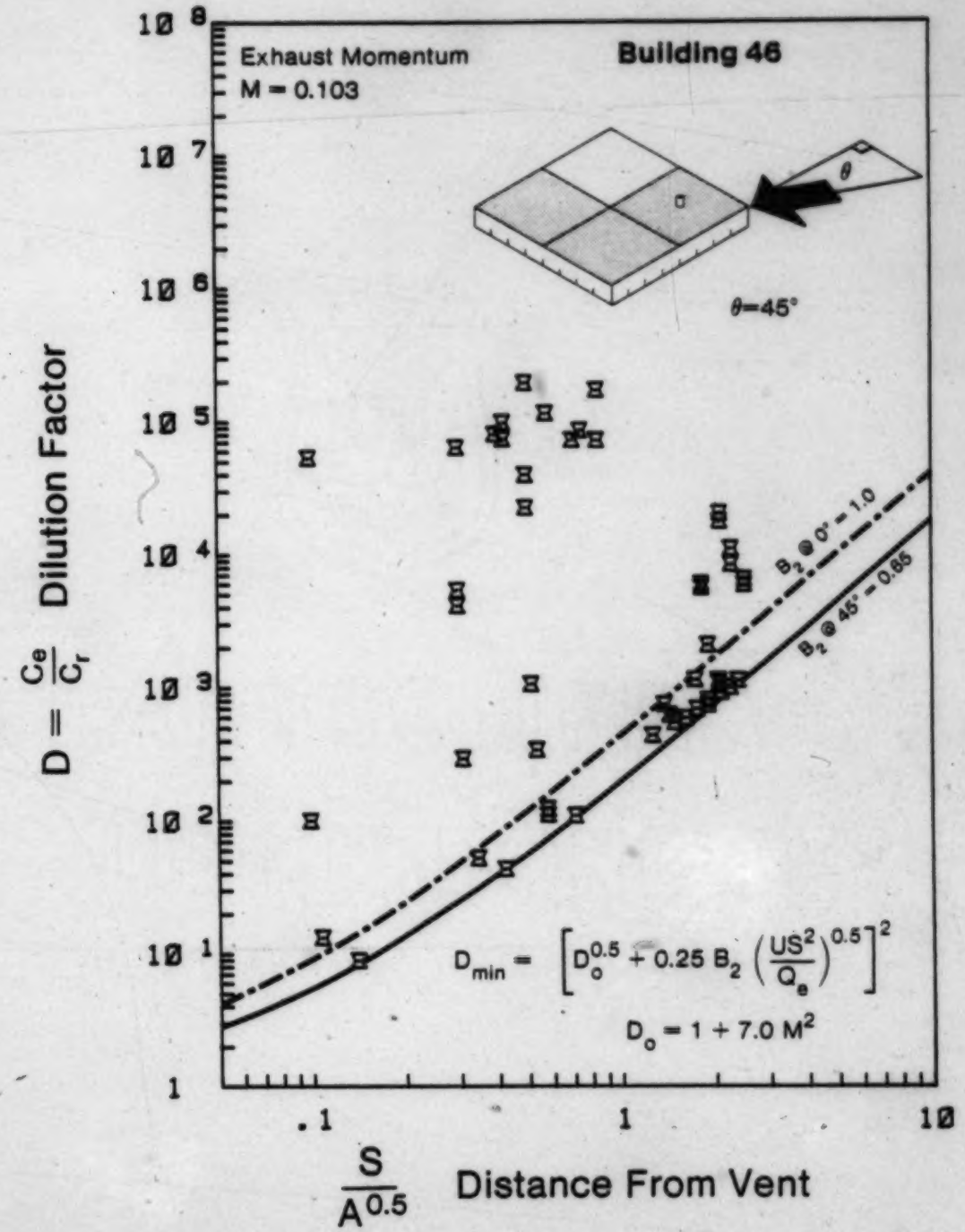

Figure 4-7 Effect of wind angle on minimum dilution for a low rise building with low exhaust momentum, M = 0.103 and wind angle θ = 45°

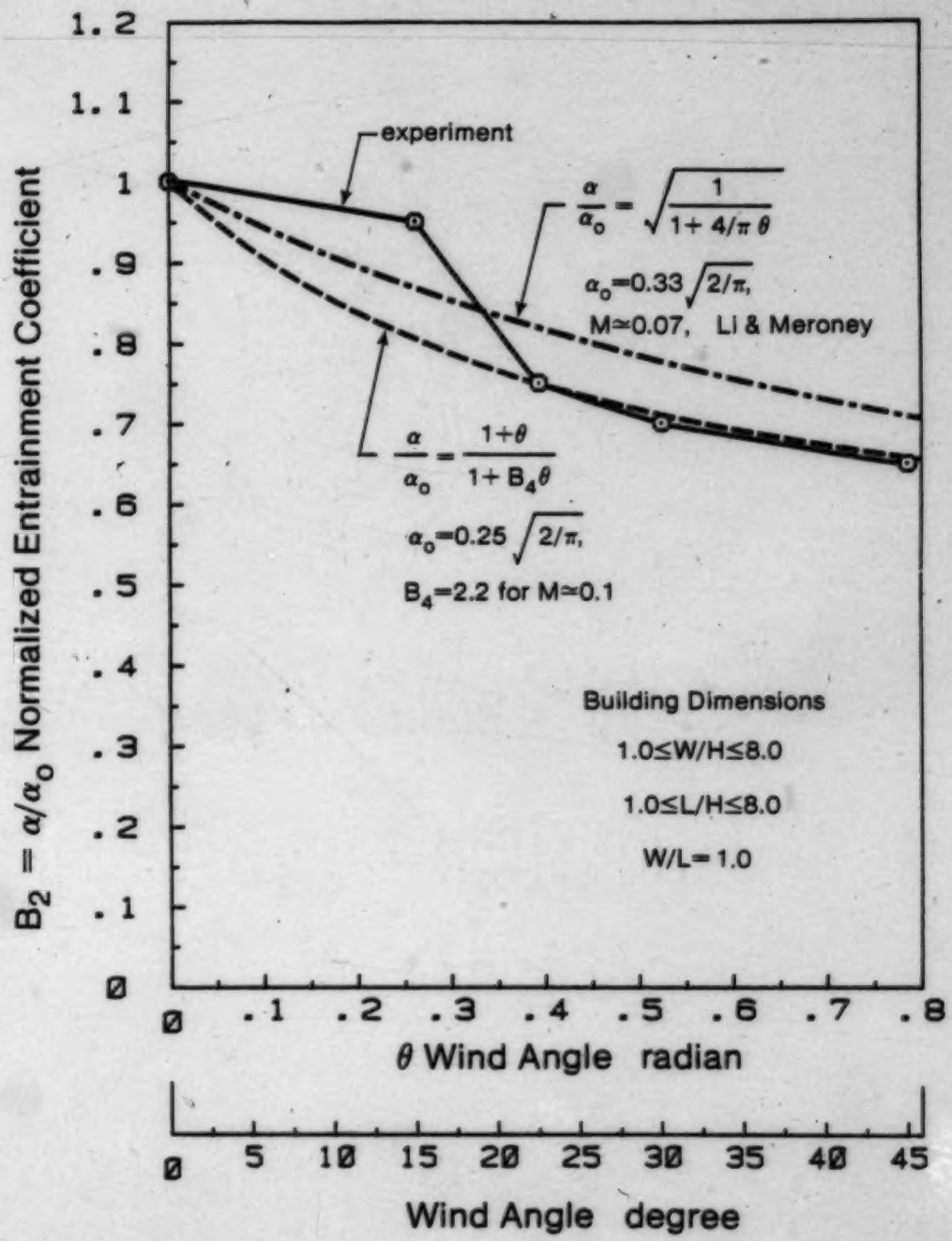

Figure 4-8 Effect of wind incidence angle on air entrainment coefficient, α at low exhaust momentum condition, M = 0.1

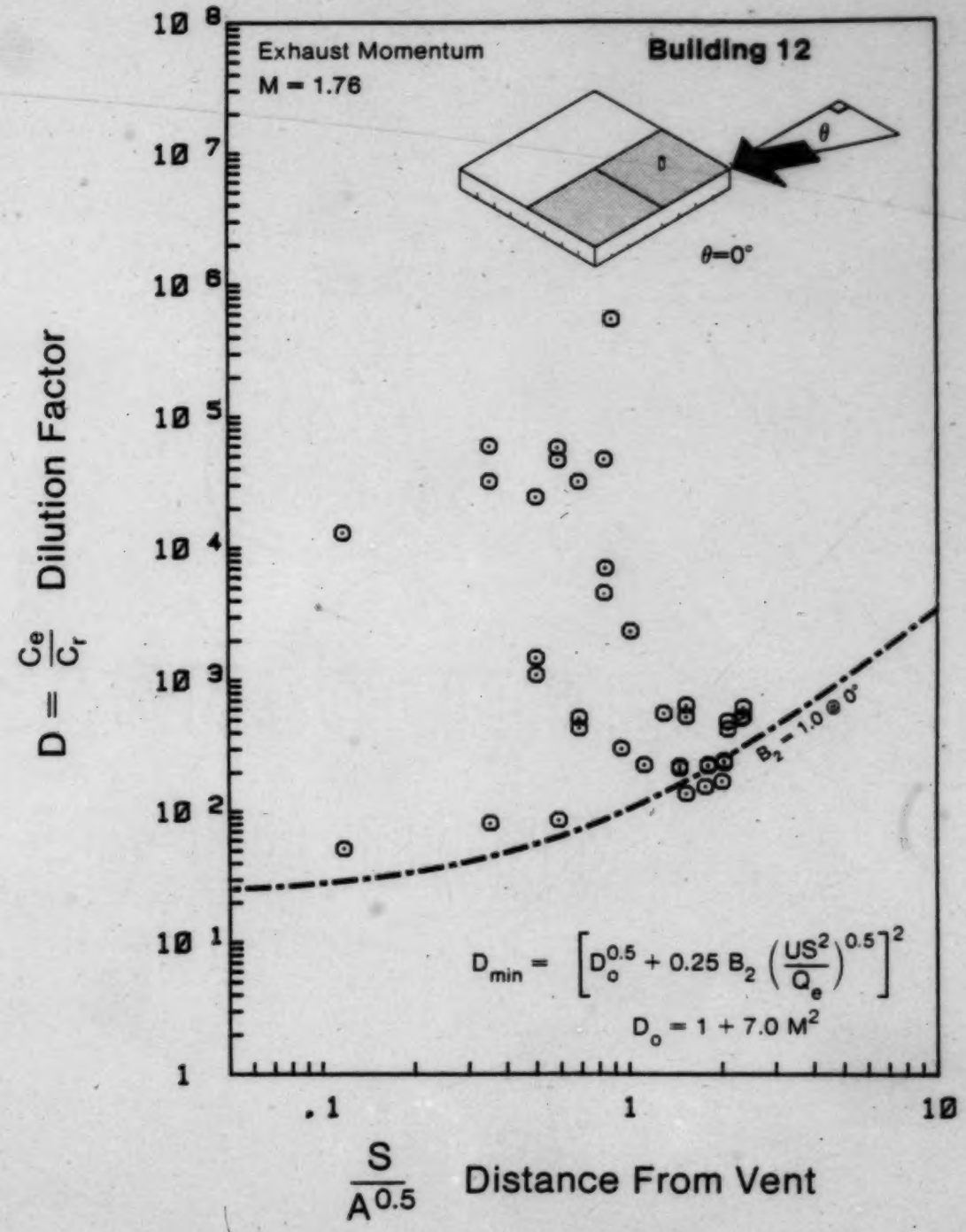

Figure 4-9 Effect of wind angle on minimum dilution for a low rise building with high exhaust momentum M = 1.76 and wind angle θ = 0°

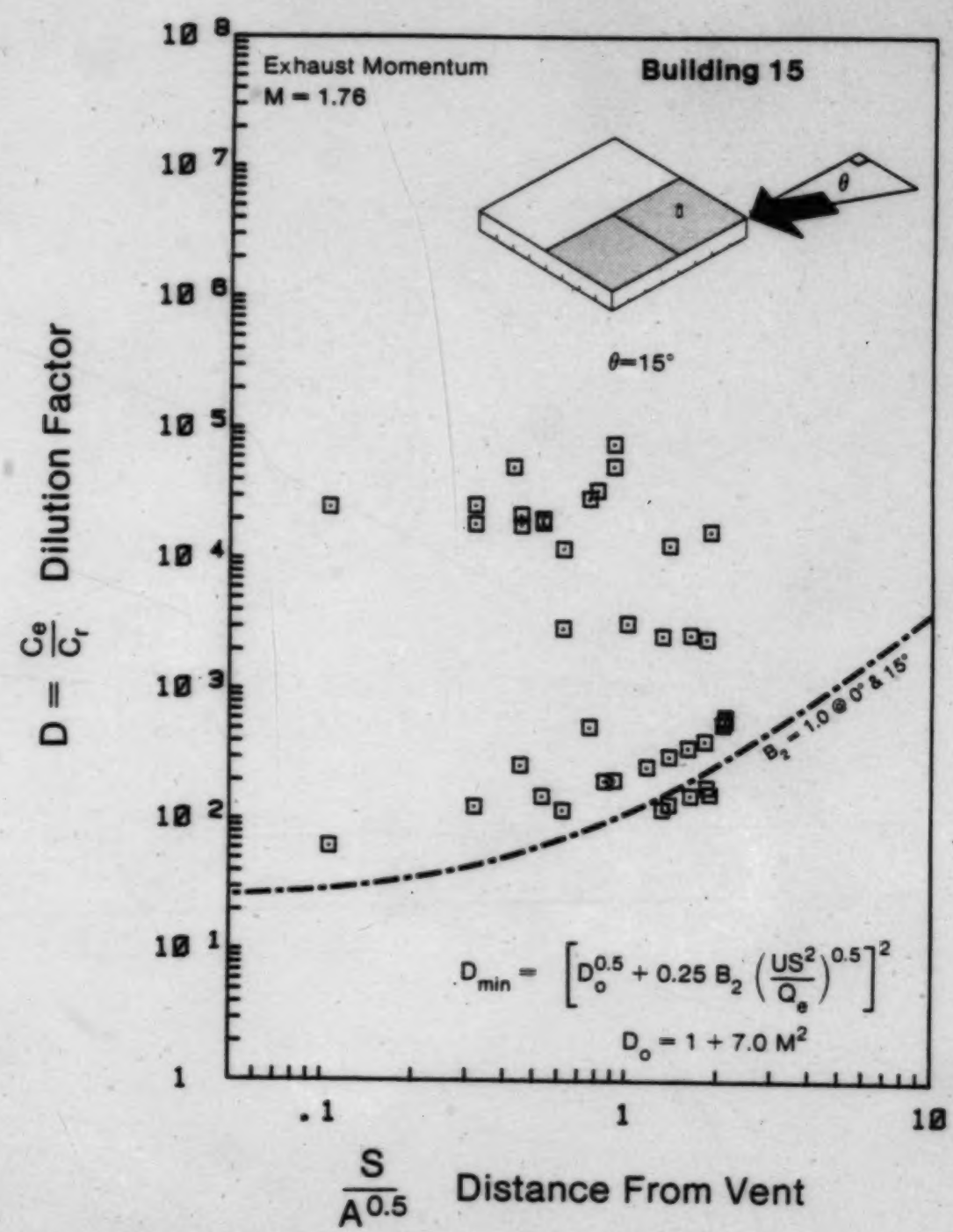

Figure 4-10 Effect of wind angle on minimum dilution for a low rise building with high exhaust momentum M = 1.76 and wind angle θ = 15°

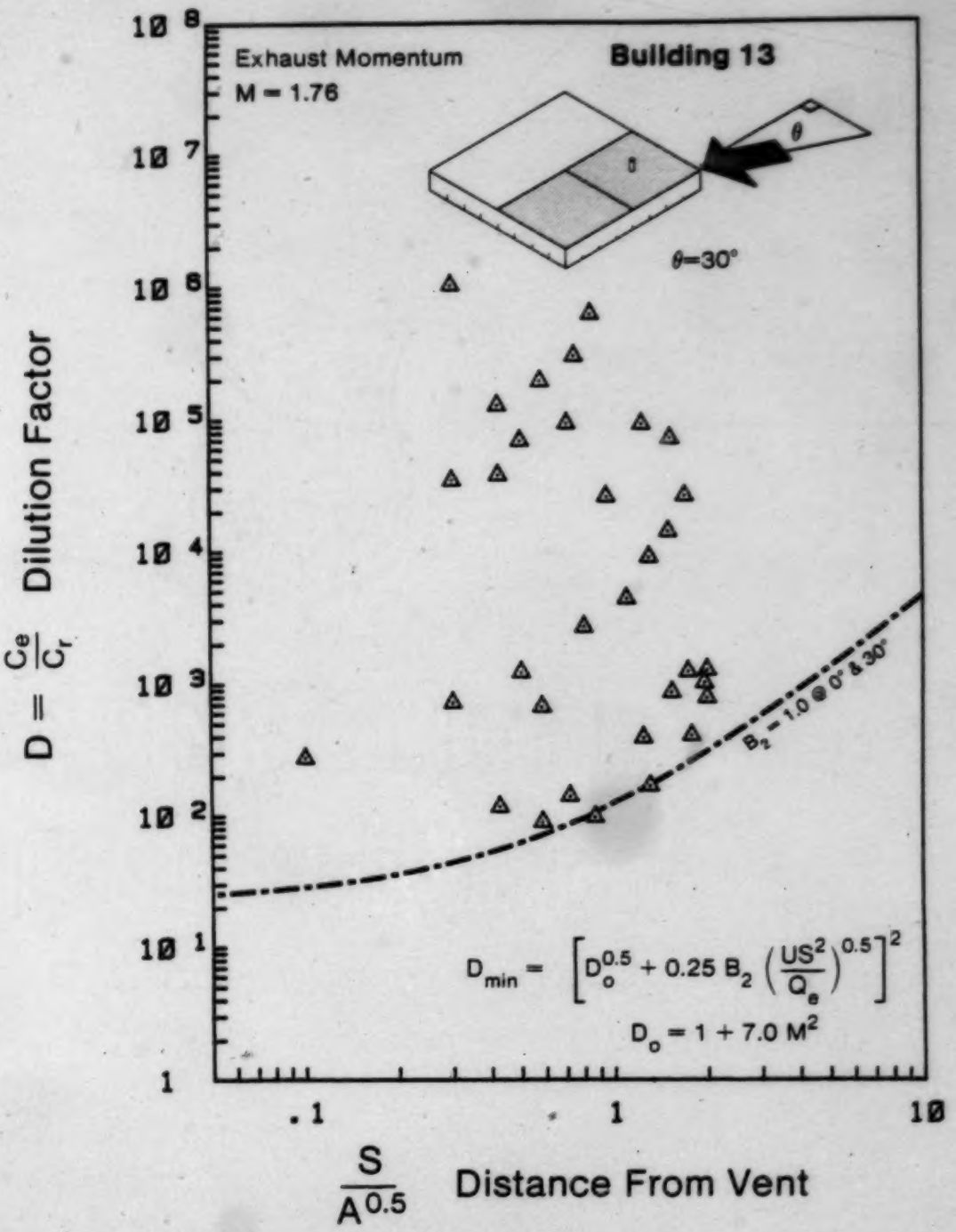

Figure 4-11 Effect of wind angle on minimum dilution for a low rise building with high exhaust momentum M = 1.76 and wind angle θ = 30°

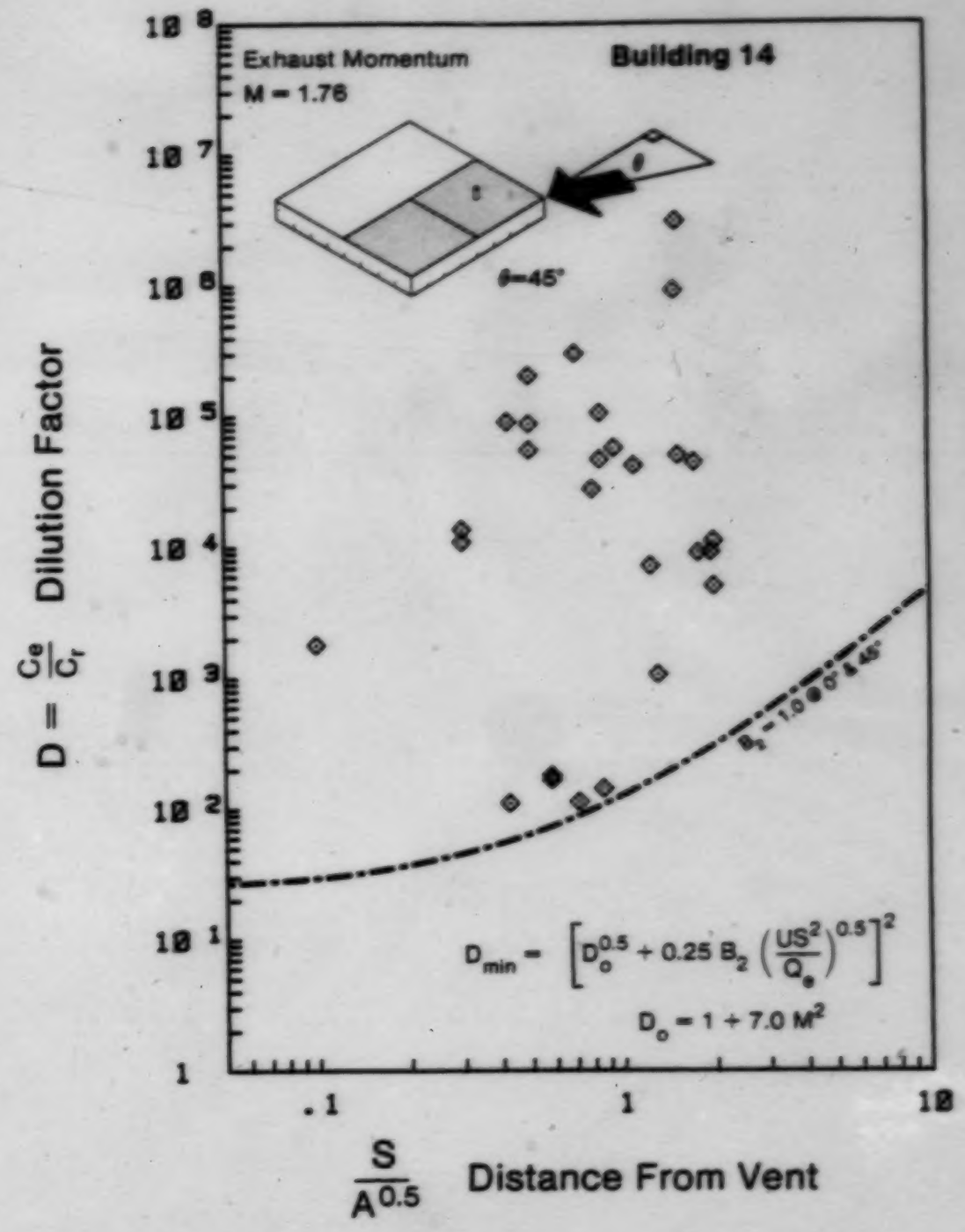

Figure 4-12 Effect of wind angle on minimum dilution for a low rise building with high exhaust momentum M = 1.76 and wind angle θ = 45°

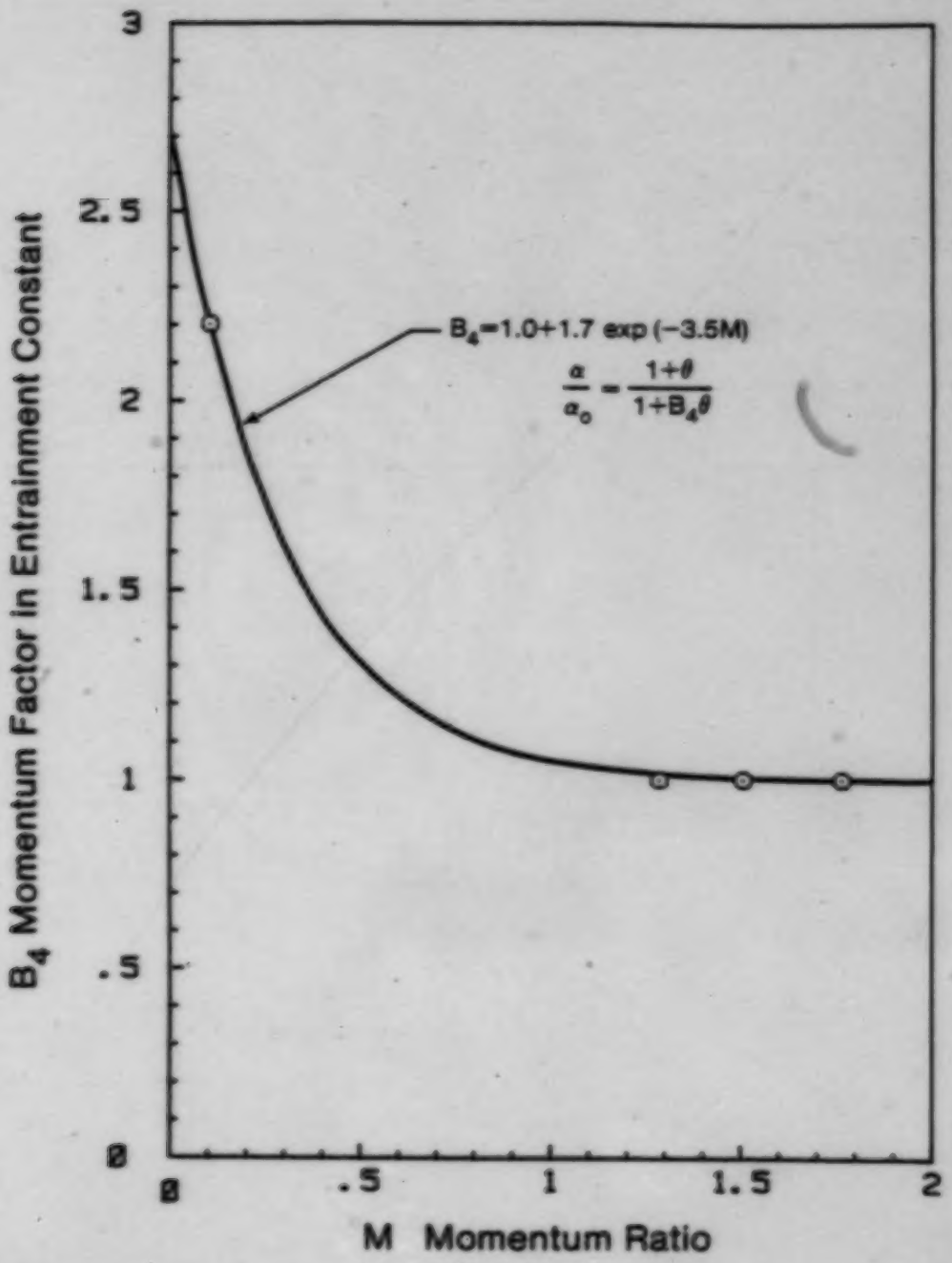

Figure 4-13 Observed effect of vertical exhaust momentum on air entrainment coefficient. Best fit to all wind angles combined

Chapter V

Summary, Recommendations and Further Studies

5.1 The Wind Tunnel Model

In this study, a wind tunnel system was used to simulate the dispersion of vent gases exhausted from the roof of a building in an atmospheric boundary layer. Turbulence measurements confirmed that this wind tunnel system, previously developed by Wilson (1976) was able to generate a shear layer that has the same turbulence characteristics as a neutrally stable atmospheric boundary layer in a lightly built-up urban area and an overall model scale of about 2000:1. This simulation ensured that the effects of the random fluctuations of atmospheric turbulence on the dilution of vent gas would be incorporated in the study. The simulated atmospheric boundary layer displayed three distinct regions: a smooth inner wall layer of 2 cm thick (40 m full scale), a rough outer wall layer from z = 2 to 15 cm (40 to 300 m full scale) and an outer zone for z = 15 to 25 cm (300 to 500 m full scale). The presence of a smooth inner wall layer was encouraging because it was characteristic of the site that the model tried to reproduce: an isolated region in an urban area free of nearby building influences. However, the use of a small wind tunnel model had its limitations in scaling, due to Reynolds number mismatch (by a factor of about 2000 in this case) which led to a reduction of the range of eddy sizes. However, it was found that the equivalent full scale eddies that were missing in the simulation were those smaller than about 0.2 m which were not expected to make significant contribution to the spread of a contaminant in the atmosphere.

By using sharp edged buildings and keeping the Reynolds number above 10^4, as suggested by Golden (1961), dynamic similarity of flow was preserved in the model. So, the simulation remained credible and effective despite the Reynolds number mismatch.

5.2 Results From Wind Tunnel Studies

Data collected from the above wind tunnel simulations in three different studies - Wilson (1976), Wilson and Winkel (1982) and the present investigation, were used to evaluate the influence of exhaust momentum and wind angle on dilution of vent gases.

It was evident that additional dilution was induced by the vertical exhaust momentum. Two theoretical models were developed to account for this additional dilution:

a) Plume Rise Model

This model assumed the plume to have a linear crosswind concentration profile with roof level reflection. When coupled with a plume rise formulation it provided a theoretical prediction of the plume rise effect on dilution in equations (3-6a) through (3-6c). Plume rise measurements showed that the initial stage of rise followed an $h \alpha S^{0.5}$ power law in equation (3-8) whereas the overall rise behavior was better described by the one-third power law where $h \alpha S^{0.33}$, see equation (3-7). A prediction within a factor of 2 of the plume rise effect was achieved by either using the one-half power law or by introducing a virtual origin to the one-third power law. Unfortunately, data correlations indicated that the "constants" B_1 and B_5 in the plume rise formulations, equations (3-7) and (3-8), were not really true constants. In addition, the predictions were extremely sensitive to the

variation of B_1 and B_5 and could not be generalized for design purposes. The breakdown of the model could possibly be due to the fact that the entrainment constant, α_o, instead of being constant as the model assumed, did vary with downwind distance, S. Also the assumption that the plume crosswind concentration profile was linear might not be realistic.

b) Initial Entrainment Model

This model assumed a hypothetical initial dilution to account for the extra entrainment in the initial bending-over of plume, with plume rise included implicitly. It not only accounts for the influences of wind speed, vent-to-intake distance, and source strength but also the additional dilution caused by the vertical momentum in the exhaust gas. This led to a dilution model represented by equations (3-14) and (3-15). For the range of momentum ratios tested, (M = 0.103 to 1.76), the model predicted a minimum dilution within a factor of 2 of the actual dilution measurements, independent of vent locations and building shape. It was evidently superior to the old dilution model, equation (1-4) which did not account for the additional dilution due to exhaust momentum and underestimated the minimum dilution by a factor as high as 16. This improved performance, plus the fact that B_3 in equation (3-13) was found to be a true constant, demonstrated that this dilution model seems to have some physical basis, although the concept of initial dilution is a hypothetical one. This initial dilution model, equations (3-14) and (3-15), is recommended for the estimation of minimum dilution.

As stated by Wilson and Chui (1985) this dependence of minimum dilution on exhaust momentum can be very useful for design, particularly

when a designer has to upgrade an existing ventilation system where vent-to-intake distance cannot be altered. Extra dilution near the source can be obtained by using a higher vertical exhaust velocity, to increase the ratio W_e/U.

However, this dilution model is only recommended for use where distances from the vent are greater than 10 stack diameters, because the actual initial dilution, D_o at vent exit should be 1.0 to be physically correct. Also, equation (3-15), $D_o = 1 + 7.0\ M^2$, is not expected to be applicable for very large exhaust momentum ratios. If M is sufficiently large, the plume will completely detach from the building roof due to increased plume rise thus changing the form of the equation. Additional experiments are required to determine this upper bound. For most industrial applications, M rarely exceeds 2.0, and equation (3-15)'s usefulness is not impaired even if there is an upper limit on the value of M.

Orientation of building with respect to the wind direction was found to have a significant effect on the minimum dilution of vent gases at the building roof when exhaust momentum was small (M = 0.1). A doubling of contaminant concentration level was observed with $\theta \geq 30°$ for low rise buildings having a width to height ratio, W/H, greater than 4, while for buildings with smaller W/H (≤ 2), 4 to 8 times higher concentrations were seen. However, at high exhaust momentum (M = 1.28 to 1.76), minimum dilution was no longer sensitive to θ.

The above wind angle effect was incorporated in a simple dilution model represented by equations (4-3), (4-4) and (4-8), a modified version of the initial dilution model, equation (3-14). As a first approximation to wind angle effect with θ between 22.5° and 45°, this model predicts minimum dilution with a maximum uncertainty of $\pm$ 30%.

For smaller wind angle ($\theta \leq 15°$) the model tends to be slightly conservative and equation (3-14) is recommended for $0° \leq \theta \leq 15°$ as a better estimate.

5.3 Recommendations for Further Studies

a) Effects of Building Shape and Size

The initial dilution model, equation (3-14), proposed in this study assumes that plume radius, R, increases linearly with downwind distance, S, so that equation (3-14) is conveniently independent of turbulence length scale, characterized by $\sqrt{A}$, i.e., building size. Data correlations in this study did indicate that this was an acceptable assumption for all the buildings tested (with aspect ratios, $8 \geq W/H \geq 2$). However, Wilson and Winkel (1982) found that roof level concentrations from vent stack suggest a plume growth $R \propto S^{0.75}$, which transforms equation (3-14) into

$$D_{min} = \left[D_o^{0.5} + 0.25 \left(\frac{UA}{Q_e}\right)^{0.5} \left(\frac{S}{A^{0.5}}\right)^{0.75}\right]^2 \qquad (5\text{-}1)$$

This does depend weakly on building size, with $D_{min} \propto A^{0.25}$ far from the vent. In a preliminary study, equation (5-1) was compared with equation (3-14) for a number of building shapes, see Figures 5-1 to 5-3 and Appendix A5. Equation (5-1) seemed to correlate better with the measurements especially in the case of a cubical building (Figure 5-3) and at large $S/A^{0.5}$ distances. An interesting topic for future studies would be to consider the importance of building size and shape and determine whether equation (5-1) is indeed superior to equation (3-14).

b) Effect of Stack Height

As noted before, only flush, vertically directed roof vents of zero stack height were used in this study. A logical continuation of the present investigation would be to consider the case of non-zero stack heights which in fact is more common in most large industrial ventilation systems. Wilson and Winkel (1982) reported the effect of varying stack heights on contaminant concentration at roof level. They proposed a design equation in the form of (D_{stack}/D_{min}). A question left for other researchers to answer is whether the actual dilution at roof level when stack height is non-zero can be obtained as follows:

$$(D_{stack})_{actual} = (D_{min}) \left| \begin{matrix} \\ \text{this study} \end{matrix} \cdot \left(\frac{D_{stack}}{D_{min}}\right) \right| \begin{matrix} \\ \text{Wilson \& Winkel (1982)} \end{matrix}$$

c) Effect of Vent Location

The dominant wind angle effect on dilution likely originates from the two upwind roof edge vortices, see Figure 4-2. It is expected that vent location in relation to these vortices may have an influence on vent gas dilution. This study only considered exhaust vents located at or near the center of building roof. A systematic study should be carried out on the variation of vent location with wind angle effect.

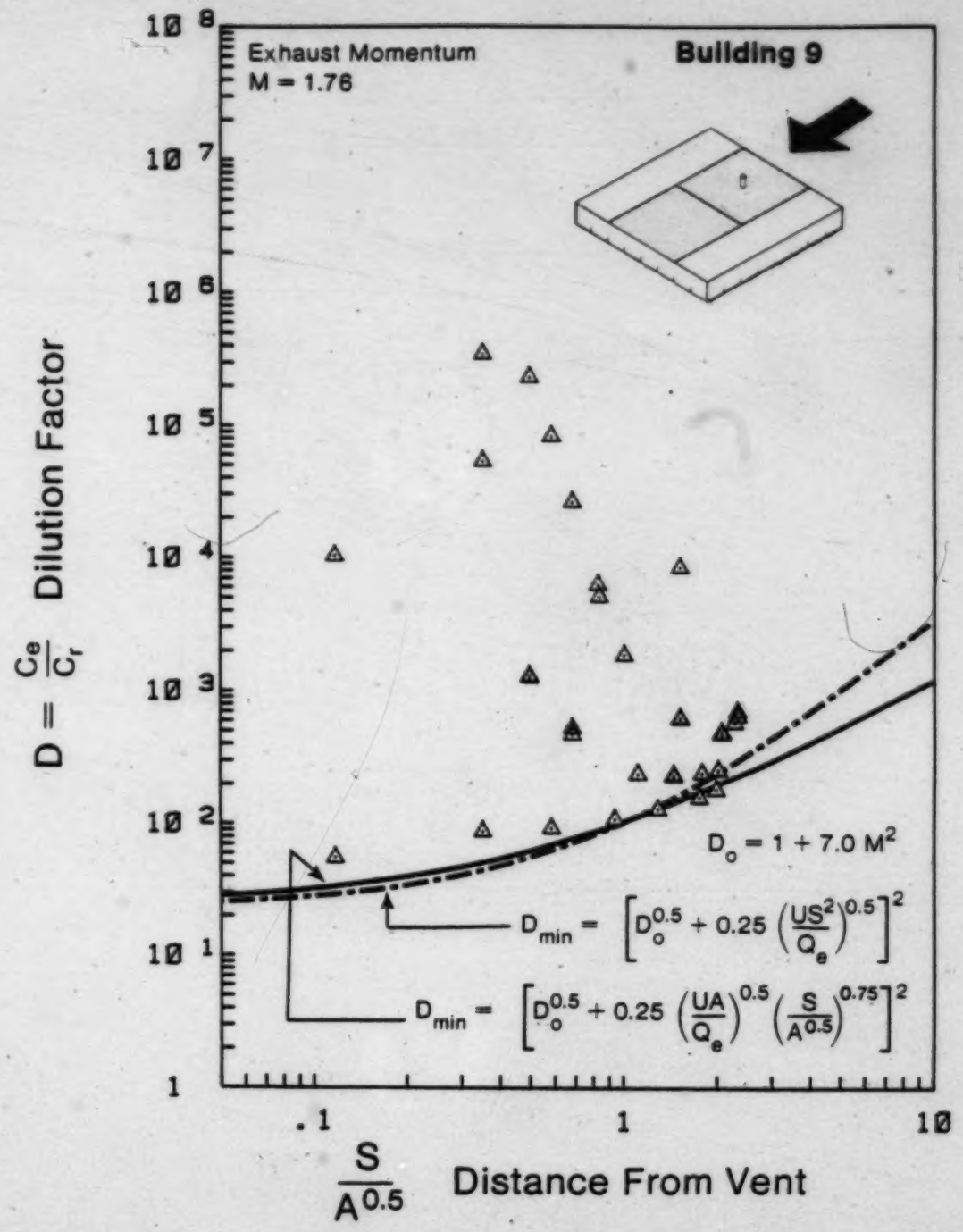

Figure 5-1 Effect of building shape on minimum dilution for a low rise building with high exhaust momentum M = 1.76

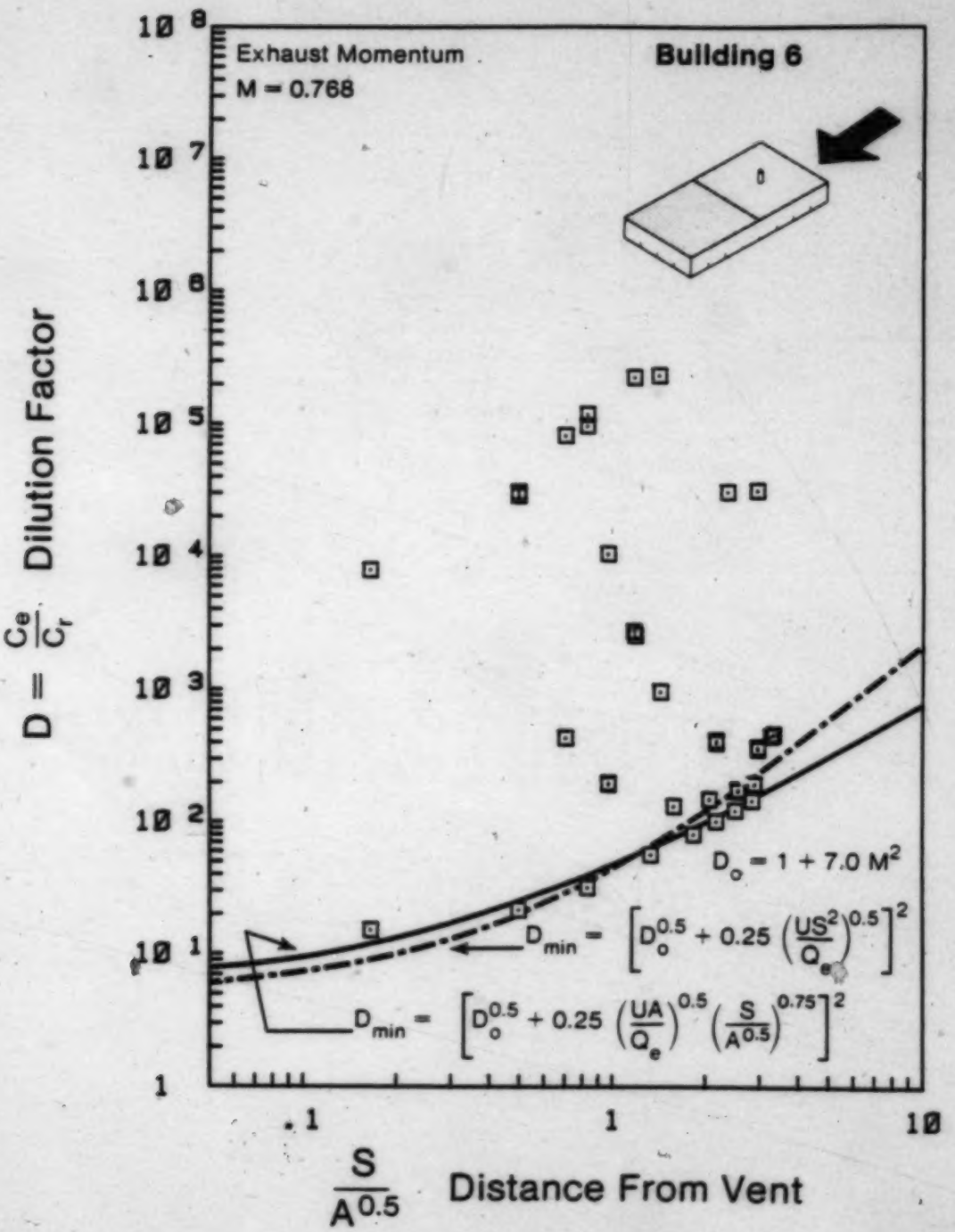
Exhaust Momentum
M = 0.768
Building 6
$D = \frac{C_e}{C_r}$ Dilution Factor
$D_o = 1 + 7.0\ M^2$
$D_{min} = \left[D_o^{0.5} + 0.25\left(\frac{US^2}{Q_e}\right)^{0.5}\right]^2$
$D_{min} = \left[D_o^{0.5} + 0.25\left(\frac{UA}{Q_e}\right)^{0.5}\left(\frac{S}{A^{0.5}}\right)^{0.75}\right]^2$
$\frac{S}{A^{0.5}}$ Distance From Vent

Figure 5-2 Effect of building shape on minimum dilution for a low rise building with medium exhaust momentum M = 0.768

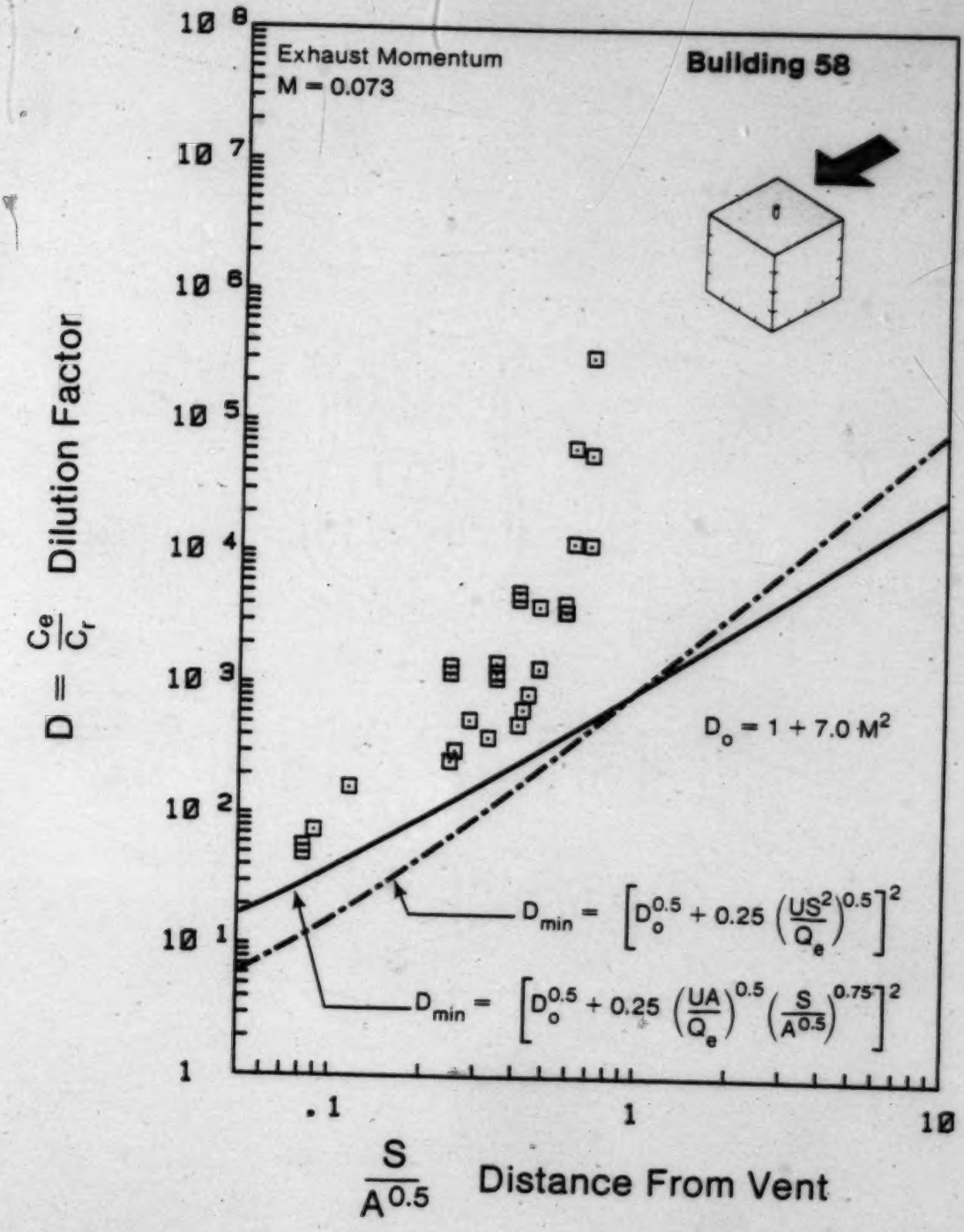

Figure 5-3 Effect of building shape on minimum dilution for a cubical building with low exhaust momentum M = 0.073

References

ASHRAE. (1981) "Air Flow Around Buildings." ASHRAE Handbook-1981 Fundamentals Chapter 14, p. 6 and pp. 12-14.

Briggs, G.A. (1969) Plume Rise. U.S. Atomic Energy Commission, Div. Tech. Information TID-25075.

Briggs, G.A. (1975) "Plume Rise Predictions". In Lectures on Air Pollution and Environmental Impact Analysis. American Meteorological Society, September 1975, Boston, Mass.

Counihan, J. (1973) "Simulation of an Adiabatic Urban Boundary Layer in a Wind Tunnel". Atmospheric Environment 7, pp. 673-689.

Counihan, J. (1975) "Adiabatic Atmospheric Boundary Layers: A Review and Analysis of Data from Period 1880-1972." Atmospheric Environment 9, pp. 871-905.

Csanady, G.T. (1973) Turbulent Diffusion in the Environment, Reidel, pp. 66-71.

Golden, J. (1961) "Scale Model Techniques". M.S. Thesis, College of Engineering, New York University.

Halitsky, J. (1962) "Diffusion of Vented Gas Around Buildings", Journal of the Air Pollution Control Association 12, pp. 74-80.

Halitsky, J. (1963) "Gas Diffusion Near Buildings". ASHRAE Transactions 69, pp. 464-484.

Halitsky, J. (1968) "Gas Diffusion Near Buildings". In Slade, D. (ed) Meteorology and Atomic Energy 1968, U.S. Atomic Energy Commission document, TID-24190, pp. 221-252.

Henry, R.M. (1959) "A Study of the Effects of Wind Speed, Lapse Rate and Altitude on the Spectrum of Atmospheric Turbulence at Low Altitude." I.A.S. Rep. 59-43.

Hill, B.J. (1972) "Measurement of Local Entrainment Rate in the Initial Region of Axisymmetric Turbulent Air Jets." Journal of Fluid Mechanics 51(4), pp. 773-779.

Hinze, J.O. (1975) Turbulence 2nd edition, McGraw-Hill, New York, pp. 66-67.

Jones, P.M., de Larringa, M.A.B. and Wilson, C.B. (1971) "The Urban Wind Velocity Profile." Atmospheric Environment 5, pp. 89-102.

Kaimal, J.C., Wyngaard, J.C., Izumi, Y. and Cote, O.R. (1972) "Spectral Characteristics of Surface Layer Turbulence." Quarterly Journal Royal Meteorological Society 98, pp. 563-589.

Li, W.W. and Meroney, R.N. (1983) "Gas Dispersion Near a Cubical Model Building ." Journal of Wind Engineering and Industrial Aerodynamics 12, pp. 15-23.

Lumley, J.L. and Panofsky, H.A. (1964) The Structure of Atmospheric Turbulence. Interscience, New York, p. 239.

Meroney, R.N. (1982) "Turbulent Diffusion Near Buildings." In Engineering Meteorology, edited by E.J. Plate. Elsevier, Amsterdam.

Notess, C.B. (1957) "A Study of the Nature of Atmospheric Turbulence Based on Flight Measurements of the Gust Velocity Components." W.A.D.C. Tech. Rep. 57-256, ASTIA Doc. No. AD 118242, U.S.A.F.

Notess, C.B. (1959) "Analysis of Turbulence Data Measured in Flight at Altitudes up to 1600 Ft. Above Three Different Types of Terrain." Cornell Aero. Rep. T.E.-1215-F-1.

Pai, S.I. (1954) Fluid Dynamics of Jets. D. Van Nostrand Co. Inc., New York.

Pasquill, R. (1974) Atmospheric Diffusion, Halstad Press, pp. 365-378.

Sagendorf, J.F., Ricks, N.R., Start, G.E. and Dickson, C.R. (1979) "Near Building Diffusion Determined from Atmospheric Tracer Experiments." Proceedings, Fourth Symposium on Turbulence, Diffusion and Air Pollution, Jan. 1979, Reno, NV: American Meteorological Society

Singer, I.A., Busch, N.E. and Frizzola, J.A. (1967) "The Micrometerology of the Turbulent Flow Field in the Atmospheric Surface Boundary Layer." Paper 21. Conf. on Wind Loads on Buildings, University of Toronto Press, Toronto.

Synder, W.H. (1972) "Similarity Criteria for the Application of Fluid Models to the Study of Air Pollution Meteorology". Boundary Layer Meteorology 3, pp. 113-134.

Taylor, G.I. (1945) "Dynamics of a Mass of Hot Gas Rising in the Air." USAEC Report MDDC-919 (LADC-276). Los Alamos Scientific Laboratory.

Wilson, D.J. (1976) "Contamination of Air Intakes from Roof Exhaust Vents." ASHRAE Transactions, 82:1, pp. 1024-1038.

Wilson, D.J. (1977) "Dilution of Exhaust Gases from Building Surface Vents." ASHRAE Transactions, 83:1, pp. 168-176.

Wilson, D.J. (1977) "Effect of Vent Stack Height and Exit Velocity on Exhaust Gas Dilution." ASHRAE Transactions, 83:1.

Wilson, D.J. (1979) "Flow Patterns Over Flat-Roofed Buildings and Application to Exhaust Stack Design." ASHRAE Transactions, 85:2, pp. 284-295.

Wilson, D.J. (1983) "A Design Procedure for Estimating Air Intake Contamination from Nearby Exhaust Vents." ASHRAE Transactions, 89:2.

Wilson, D.J. and Chui, E.H. (1985) "Influence of Exhaust Velocity and Wind Incidence Angle on Dilution from Roof Vents." ASHRAE Symposium on Air Flow Around Buildings. Honolulu, Hawaii, June 1985.

Wilson, D.J. and Winkel, G. (1982) "The Effect of Varying Exhaust Stack Height on Contaminant Concentration at Roof Level." ASHRAE Transactions, 88:1.

Winkel, G. (1979) M.Sc. Thesis. Department of Mechanical Engineering, University of Alberta, Edmonton, Alberta.

APPENDIX A2

Comparison of the Smallest Eddy Size η in the Model and its Full Scale Equivalent

Appendix A2

Comparison of the Smallest Eddy Size η in the Model and its Full Scale Equivalent

Full scale estimation:

Assuming integral length scale Λ_u = 120 m.

turbulence intensity, $\frac{u'}{U}$ = 0.1

mean flow velocity, U = 11.25 m/s

According to Wilson (1983, private communication)

$$\frac{\ell}{\eta} = 0.95 \left[\frac{u_s \ell}{\nu}\right]^{0.75} \qquad \text{(A2-1)}$$

where ℓ = large eddy scale = 1.33 Λ_u

u_s = turbulent velocity scale = $U(\frac{u'}{U})$ = 1.125 m/s

η = Kolmogoroff microscale

ν = kinematic viscosity of air = $10^{-5} m^2/s$

therefore, $$\left(\frac{\Lambda_u}{\eta}\right)_{\text{full scale}} = \frac{0.95}{1.33}\left(\frac{1.125(1.33)(120)}{10^{-5}}\right)^{0.75}$$

$$= 1.97 \times 10^5$$

$$\eta_{\text{full scale}} = 0.6 \text{ mm}$$

Model Estimation:

Assuming model scale = 2000:1

$$(\Lambda_u)_{\text{model}} = 0.06 \text{ m}$$

Since $\left(\frac{\Lambda_u}{\eta}\right)_{model} = \frac{1}{300}\left(\frac{\Lambda_u}{\eta}\right)_{f.s.}$

$$= \frac{1.97 \times 10^5}{300}$$

$$\eta_{model} = 0.09 \text{ mm}$$

Full scale equivalent of $\eta_{model} = 0.09 \times 2000 = 0.18$ m. Therefore all eddy sizes smaller than 0.18 m in the atmosphere are not modelled.

APPENDIX A3-1

Growth of a Plume with Linear Crosswind Concentration Profile

Appendix A3-1

Growth of a Plume with Linear Crosswind Concentration Profile

Consider an exhaust plume that has been bent over and is being carried horizontally at the local wind speed, U. To analyze the growth of an unconfined and bent-over plume, the following assumptions are made:

1. The horizontal velocity of the bent-over jet is everywhere equal to the local wind speed, U..
2. The crosswind concentration profile of the jet drops linearly from C_m at plume centerline to zero at plume radius, R.
3. The variation of plume centerline concentration, C_m with downwind distance from the exhaust, S is predicted by the plume entrainment model proposed by Wilson (1983).
4. The turbulent entrainment velocity, v_a of air into the plume is some fraction, α_o of the wind speed, U.

For each plume cross section, if t is the radial distance from the plume centerline, then concentration at t is

$$C_t = C_m \left(1 - \frac{t}{R}\right) \qquad \text{(A3-1-1)}$$

Given at the vent exit, concentration is C_e and total exhaust gas flow rate, Q_e, then for the mass of exhaust contaminant to be conserved, the mass flux through each plume cross section is

$$C_e Q_e = \int_o^R C_t (U \cdot 2\pi t \, dt) \qquad \text{(A3-1-2)}$$

Substituting equation (A3-1-1) into equation (A3-1-2)

$$C_e Q_e = \int_0^R C_\infty \left(1 - \frac{t}{R}\right) U \, 2\pi t \, dt \qquad \text{(A3-1-3)}$$

Integrating from t = 0 to t = R,

$$C_e Q_e = \pi U C_\infty \frac{R^2}{3}$$

Therefore, the plume radius at each plume cross section is

$$R = \left[\frac{3 C_e Q_e}{\pi U C_\infty}\right]^{0.5} \qquad \text{(A3-1-4)}$$

Applying his plume entrainment model [see Wilson (1983)] to an unconfined plume, Wilson (1983, private communication) showed that the plume centerline concentration C_∞ at downwind distance, S from the exhaust is given by

$$\frac{C_e}{C_\infty} = \left[1 + \sqrt{\pi}\, \alpha_o \left(\frac{US^2}{Q_e}\right)^{0.5}\right]^2 \qquad \text{(A3-1-5)}$$

Using this in equation (A3-1-4), the plume radius at downwind distance, S becomes

$$R = \left[\frac{3 Q_e}{\pi U}\right]^{0.5} \left[1 + \sqrt{\pi}\, \alpha_o \left(\frac{US^2}{Q_e}\right)^{0.5}\right] \qquad \text{(A3-1-6)}$$

APPENDIX A3-2

Entrainment Model for Initial Dilution

Appendix A3-2

Entrainment model for Initial Dilution

(from Wilson and Chui (1985))

The plume entrainment model proposed by Wilson (1983) accounts for the exhaust gas volume flow contribution to the total plume volume flow, and has the correct concentration limit C_e at the vent exit. However, the model does not account for the initial high rate of air entrainment that occurs when the exhaust gas is released as a jet with appreciable crosswind momentum. As this crosswind jet is bent over by the wind, it will entrain an initial volume flow rate of air Q_o. Figure 3-17 shows this process schematically, with the exhaust gas plume growing as a half-cone of radius R over the building roof. Defining an entrainment constant α_o which relates the plume entrainment velocity v_a to the wind speed U

$$v_a = \alpha_o U \qquad \text{(A3-2-1)}$$

Wilson (1983) performed a mass balance on the plume to show that the rate of increase of total volume flow in the plume over a length dS at a distance S downwind from the exhaust is

$$dQ_T = \pi \alpha_o U (R_o + \alpha_o S) dS \qquad \text{(A3-2-2)}$$

The half-conical geometry assumed for the plume results in a linear rate of growth of the plume radius

$$R = R_o + \alpha_o S \qquad \text{(A3-2-3)}$$

Including an initial entrainment flow Q_o, equation (A3-2-2) can be integrated from S = 0 where $Q_T = Q_o + Q_e$, and $R = R_o$ to obtain

$$Q_T = (Q_e + Q_o) + \pi \alpha_o U R_o S + \frac{\pi \alpha_o^2}{2} U S^2 \qquad \text{(A3-2-4)}$$

Because the mass balance assumes that the plume is bent-over and moving with the local wind speed U at each cross section, the initial radius must safisfy

$$\frac{\pi R_o^2}{2} U = (Q_e + Q_o) \qquad \text{(A3-2-5)}$$

Using this in equation (A3-2-4)

$$Q_T = (Q_e + Q_o) + (2\pi \alpha_o^2 (Q_e + Q_o) U S^2)^{0.5} + \frac{\pi \alpha_o^2}{2} U S^2 \qquad \text{(A3-2-6)}$$

The minimum dilution is related to the plume flow by a mass balance on the exhaust contaminant

$$C_e Q_e = C_r Q_T \qquad \text{(A3-2-7)}$$

where C_r is the mean concentration across a uniform top-hat concentration profile at a plume cross section, see Figure 3-17. Dividing Equation (A3-2-6) by Q_e using Equation (A3-2-7) gives the minimum dilution $D_{min} = C_e/C_r$

$$D_{min} = D_o + \left(2 \pi \alpha_o^2 D_o \frac{US^2}{Q_e}\right)^{0.5} + \frac{\pi \alpha_o^2}{2} \frac{US^2}{Q_e} \qquad \text{(A3-2-8)}$$

where D_o is the initial dilution near the exhaust,

$$D_o = 1 + \frac{Q_o}{Q_e} \qquad \text{(A3-2-9)}$$

The quadratic in Equation (A3-2-8) can be factored to

$$D_{min} = \left[D_o^{0.5} + \left(\frac{\pi}{2}\right)^{0.5} \alpha_o \left(\frac{US^2}{Q_e}\right)^{0.5}\right]^2 \qquad \text{(A3-2-10)}$$

APPENDIX A3-3

Comparison of Buoyancy Rise and Momentum Rise in the Wind Tunnel Model

Appendix A3-3

Comparison of Buoyancy Rise and Momentum Rise in the Wind Tunnel Model

A helium plume emitted from a vertically directed exhaust vent in the wind tunnel model will rise due to its upward momentum and its buoyancy. Their relative contributions to the combined final rise height will be compared in the following to determine whether a theoretical model which neglects buoyancy is justified.

Plume Rise Due to Buoyancy

According to Briggs (1975), the rise of a buoyant plume has the functional form

$$h_B = 1.2 \frac{F^{1/3} S^{2/3}}{U} \qquad \text{(A3-3-1)}$$

where the buoyancy flux parameter F is

$$F = g\left(1 - \frac{\rho_e}{\rho_a}\right) W \left(\frac{d_s}{2}\right)^2 \qquad \text{(A3-3-2)}$$

It should be noted that the plume rise constants - 1.2 in equation (A3-3-1) and 1.7 in equation (A3-3-5) which will be shown later, are recommended by Alberta Environment in the 1978 Dispersion Guidelines. They are about 75% lower than the values suggested by Briggs (1975).

Typically a plume will level off after a certain rise distance, S_{fB} because atmospheric turbulence tends to break up the conically shaped plume to pockets of plume materials scattered in space by inducing a large amount of entrained air. The magnitude of S_{fB} is governed by F and the level of atmospheric turbulence. Briggs (1969) made the following estimates for S_{fB} in an adiabatic atmosphere:

$$S_{fB} = 49\ F^{5/8} \quad \text{for } F \leq 55\ m^4/s^3$$

$$= 119\ F^{2/5} \quad \text{for } F > 55\ m^4/s^3 \qquad \text{(A3-3-3)}$$

(A3-3-1) and (A3-3-3) are combined to give the final rise height due to buoyancy:

$$h_{Bf} = 16\ \frac{F^{3/4}}{U} \quad \text{for } F \leq 55\ m^4/s^3$$

$$= 29\ \frac{F^{3/5}}{U} \quad \text{for } F > 55\ m^4/s^3 \qquad \text{(A3-3-4)}$$

Plume Rise Due to Momentum

The trajectory equation of a rising momentum plume is given by Briggs (1975) as:

$$h_M = 1.7\ \left(M \cdot \frac{d_s}{2}\right)^{2/3} S^{1/3} \qquad \text{(A3-3-5)}$$

where M = momentum ratio = $(\rho_e/\rho_a)^{0.5}\ W_e/U$

As the plume rises and entrains more air, the vertical velocity of the momentum jet decreases. When it reduces to have the same order of magnitude of the vertical turbulent velocity fluctuations in the atmosphere, the plume breaks up and stops rising. The rise distance at which this occurs is represented by

$$S_{fM} = 22\ M\ d_s \qquad \text{(A3-3-6)}$$

Using this in equation (A3-3-5) to give the final momentum rise height

$$h_{Mf} = 3\ M\ d_s \qquad \text{(A3-3-7)}$$

Combined Rise Height

It can be shown that the combined rise height due to momentum and buoyancy is [see Briggs (1975)]:

$$h = [h_M^3 + h_B^3]^{1/3} \qquad \text{(A3-3-8)}$$

Substituting (A3-3-4) and (A3-3-7) into this, the combined final rise height is approximately

$$h_f = \left[\left(16 \frac{F^{3/4}}{U}\right)^3 + (3 M d_s)^3\right]^{1/3} \quad \text{for } F \leq 55 \text{ m}^4/\text{s}^3$$

$$= \left[\left(29 \frac{F^{3/5}}{U}\right)^3 + (3 M d_s)^3\right]^{1/3} \quad \text{for } F > 55 \text{ m}^4/\text{s}^3 \qquad \text{(A3-3-9)}$$

Numerical Examples

Consider two wind tunnel test conditions - one with high exhaust momentum, M = 2.06 and the other at M = 0.103 (see Table 3-1).

Case (i) M = 2.06

$$\frac{\rho_e}{\rho_a} = 0.378$$

$$U = 5.77 \text{ m/s}$$

$$W_e = 19.33 \text{ m/s}$$

$$d_s = 0.216 \text{ cm}$$

Using (A3-3-2), $F = 1.37 \times 10^{-4} \text{ m}^4/\text{s}^3$

Using (A3-3-4), $h_{Bf} = 16 \frac{(1.37 \times 10^{-4})}{5.77}^{3/4}$ m

$= 3.52$ mm

Using (A3-3-7) $h_{Mf} = 3(2.06)(0.216 \times 10^{-2})$ m

$= 13.35$ mm

Using (A3-3-9) $h_f = [3.52^3 + 13.35^3]^{1/3}$

$= 13.43$ mm

Therefore, extra rise due to buoyancy

$= (1 - \frac{h_{Mf}}{h_f}) \times 100\%$

$= \underline{0.6\%}$

Case (ii) M = 0.103

$\frac{\rho_e}{\rho_a} = 0.138$

$U = 8.56$ m/s

$W_e = 2.37$ m/s

$d_s = 0.132$ cm

Similarly,

$F = 8.72 \times 10^{-6}$ m^4/s^3

$h_{Bf} = 0.30$ mm

$h_{Mf} = 0.41$ mm

$h_f = [0.30^3 + 0.41^3]^{1/3} = 0.46$ mm

Extra rise due to buoyancy

$$= \left(1 - \frac{h_{Mf}}{h_f}\right) \times 100\% = 10.9\%$$

In both cases, momentum rise dominates. Even at very small exhaust momentum (M = 0.103), the contribution of buoyancy to total rise height is only about 11%. So, buoyancy effect can reasonably be assumed to be negligible.

Evidently, the above calculations are based on an entrainment constant α_w lower than the actual one in the wind tunnel model because in the case of M = 2.06, the measured h_f is 8.0 mm (see Figure 3-2), 5.4 mm lower than the value obtained from equation (A3-3-9). In other words, the actual plume rise in the model is always less than what equation (A3-3-9) predicts. However, this will not alter the fact that buoyancy effect is negligible in the wind tunnel model for the relative contribution of buoyancy to total rise height is independent of the value of α_w.

APPENDIX A4

Additional Experimental Data on the Effect of Wind Incidence Angle on Dilution

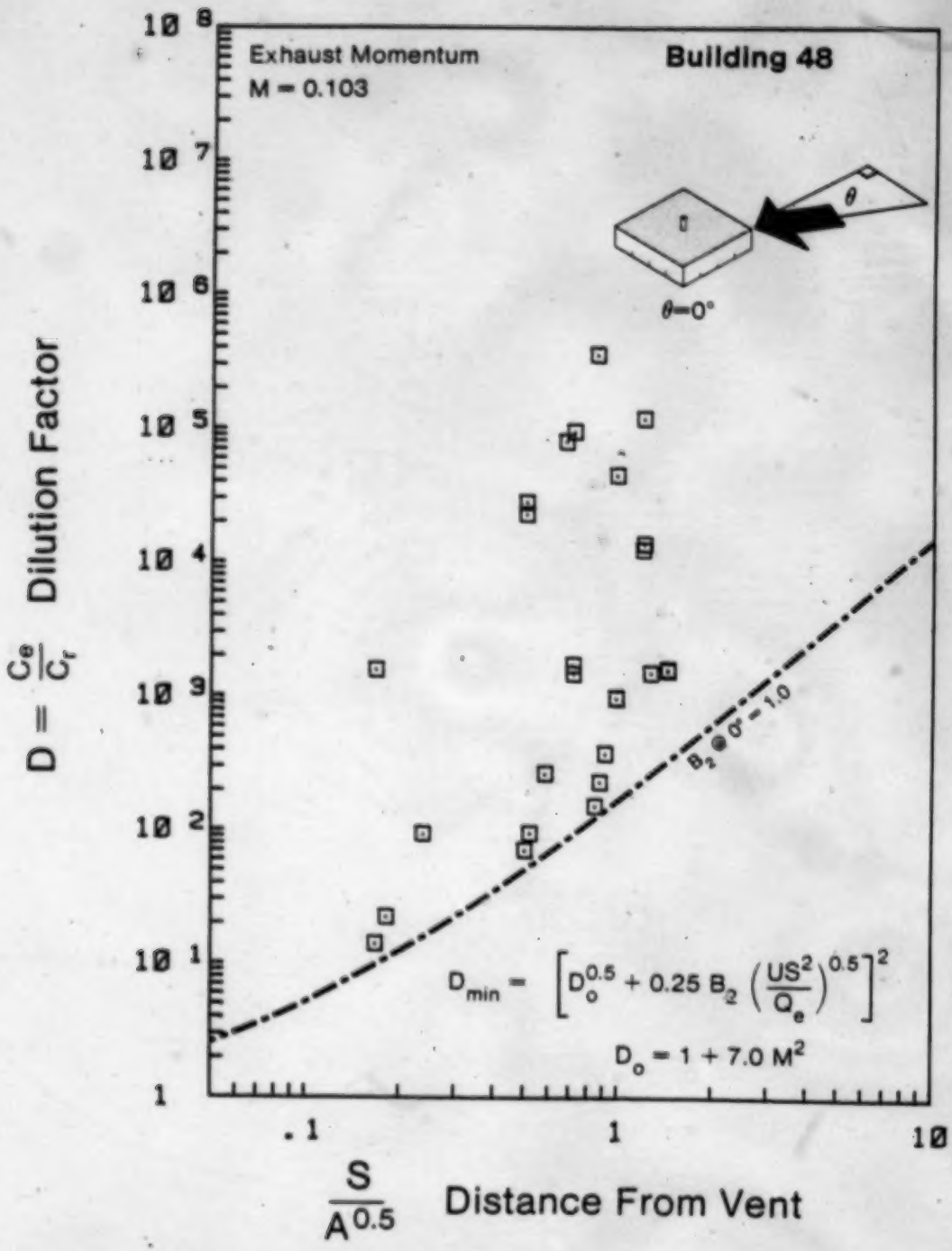

Figure A4-1 Effect of wind angle on minimum dilution for a low rise building with low exhaust momentum M = 0.103 and wind angle θ = 0°

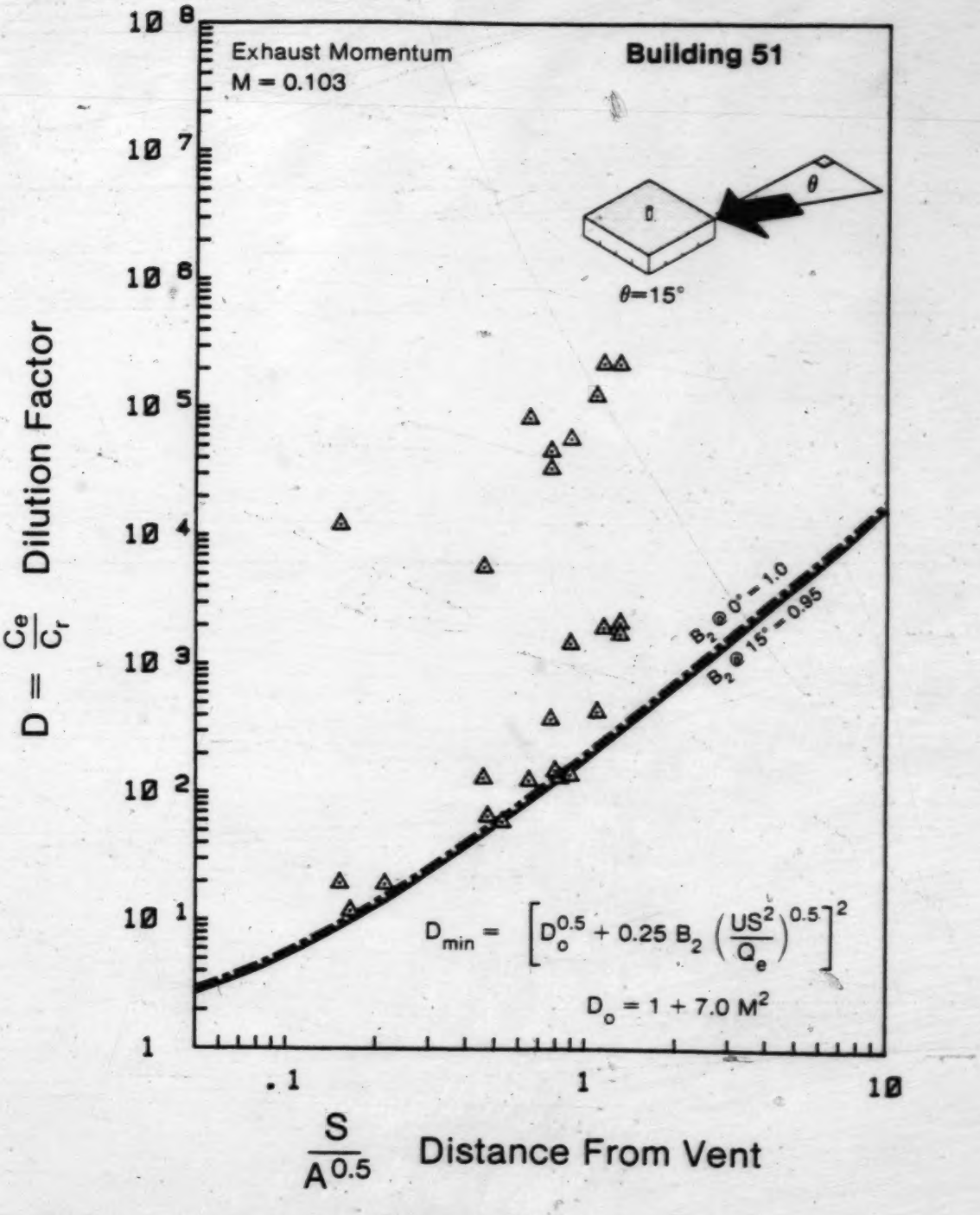

Figure A4-2 Effect of wind angle on minimum dilution for a low rise building with low exhaust momentum M = 0.103 and wind angle θ = 15°

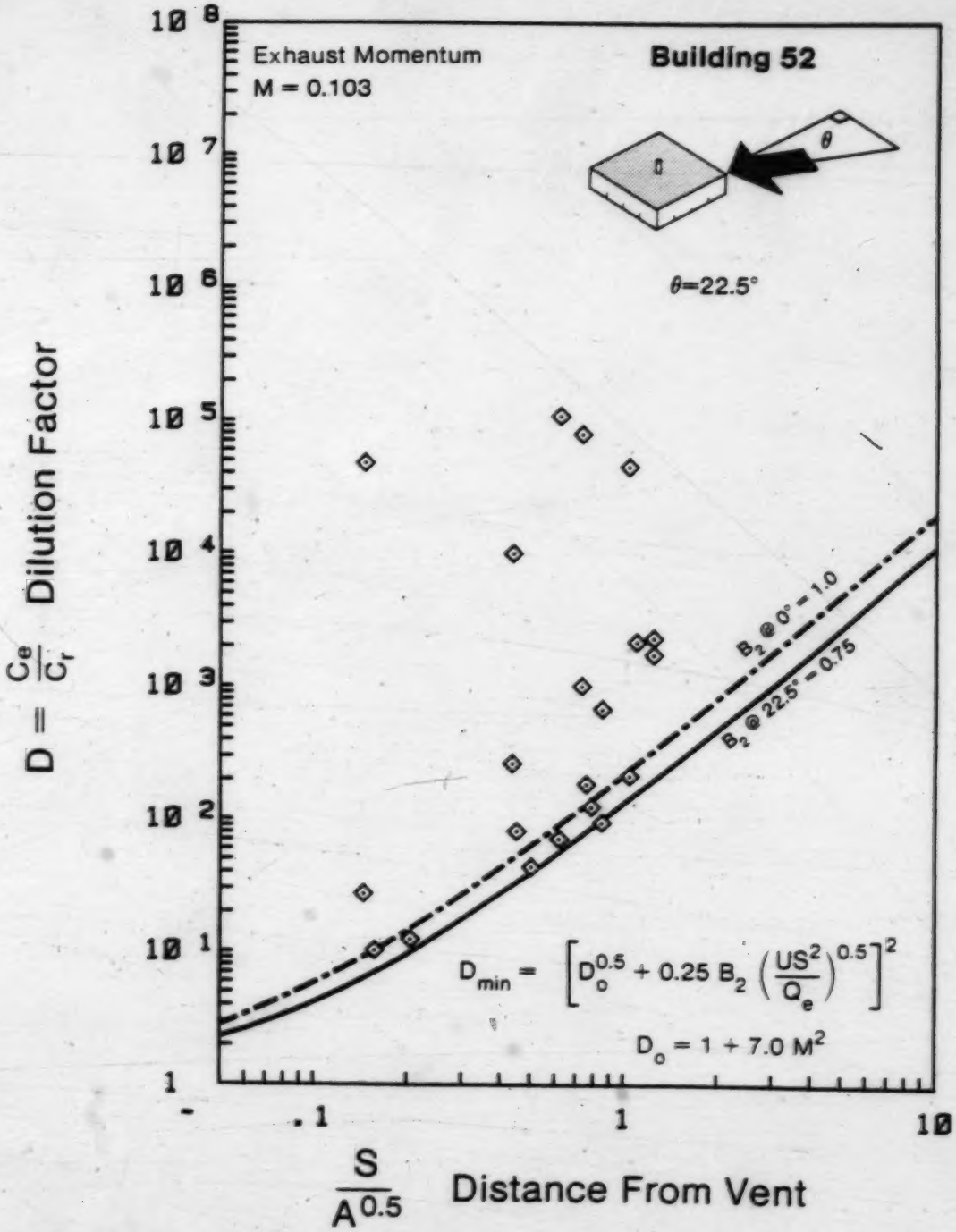

Figure A4-3 Effect of wind angle on minimum dilution for a low rise building with low exhaust momentum M = 0.103 and wind angle θ = 22.5°

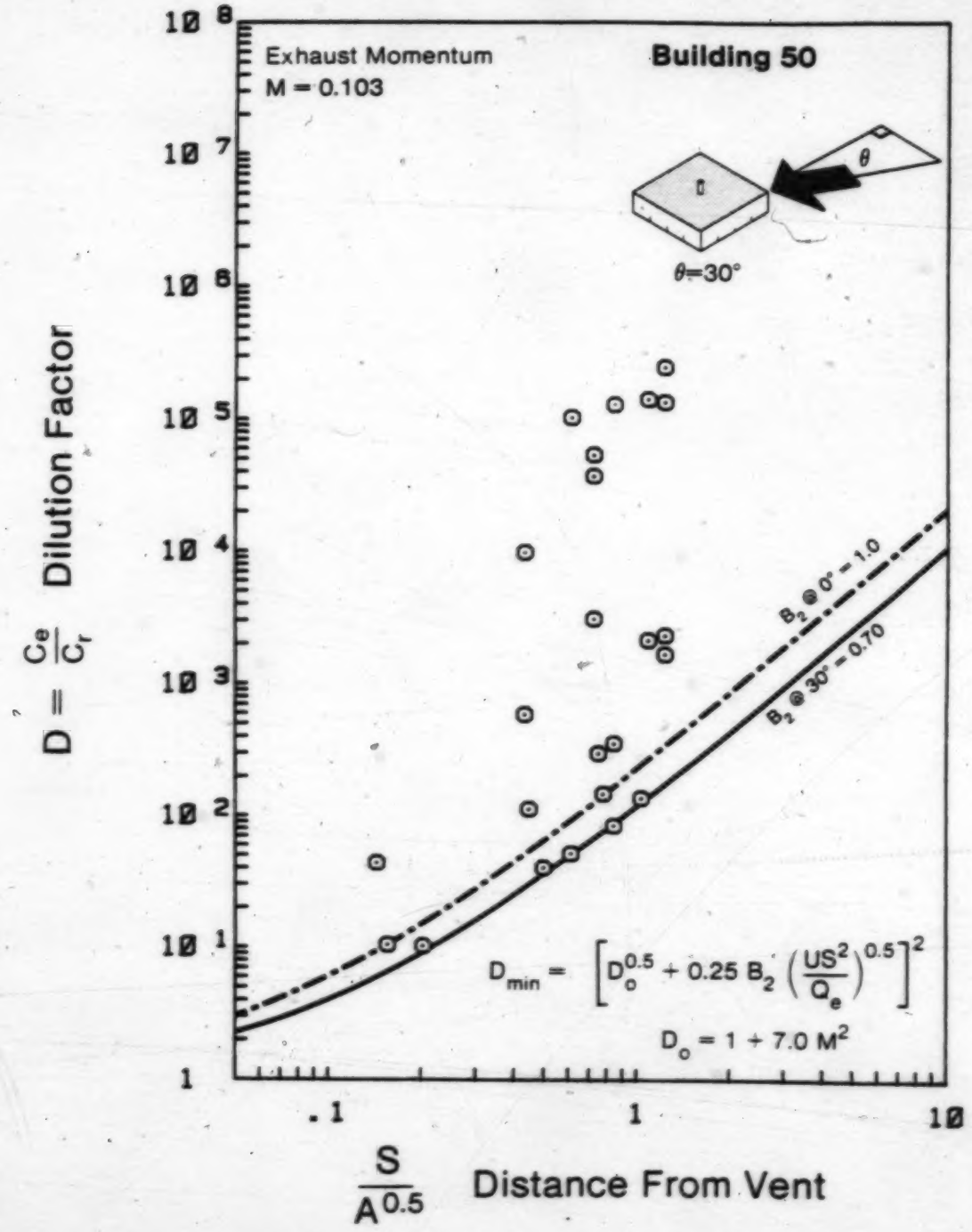

Figure A4-4 Effect of wind angle on minimum dilution for a low rise building with low exhaust momentum M = 0.103 and wind angle θ = 30°

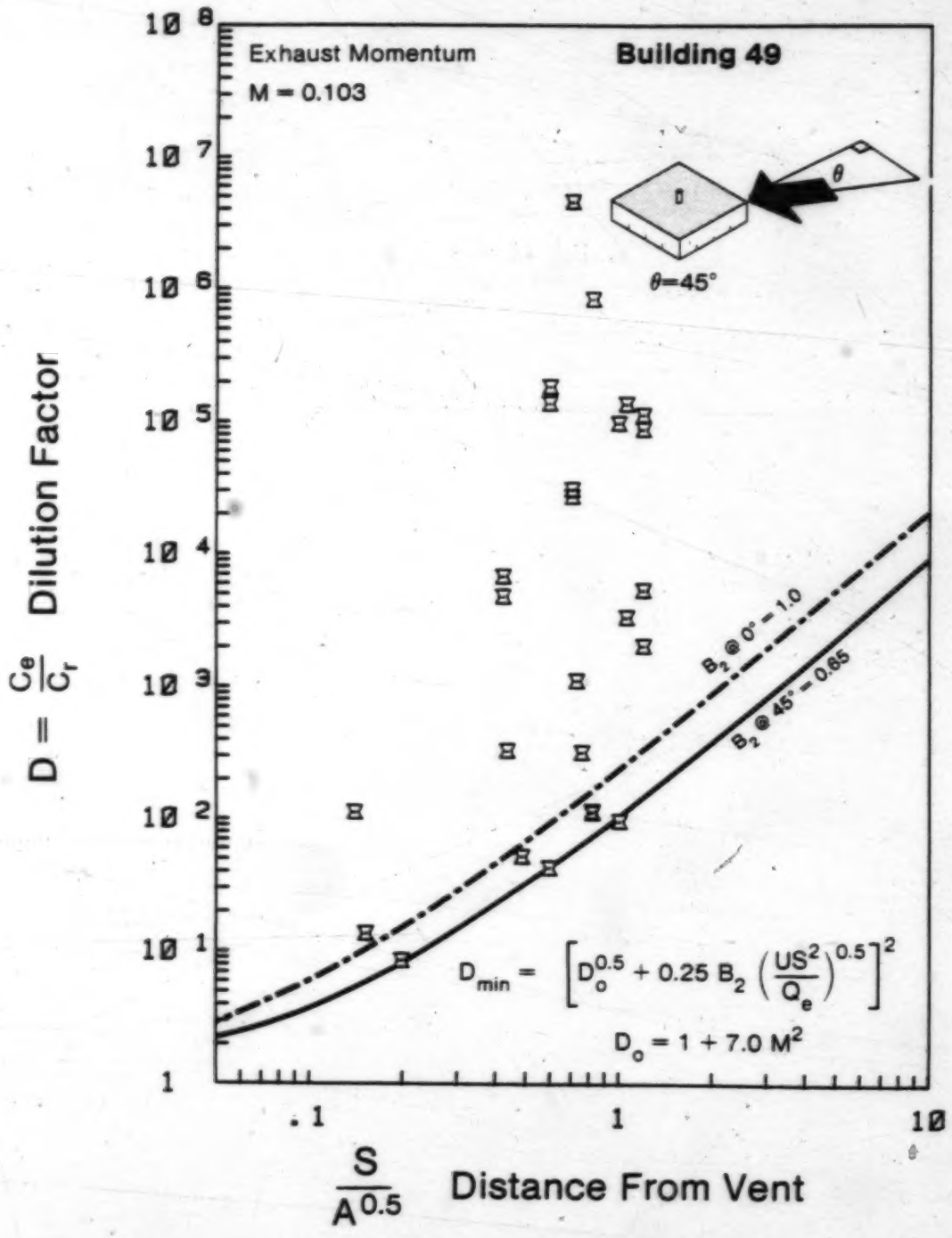

Figure A4-5 Effect of wind angle on minimum dilution for a low rise building with low exhaust momentum M = 0.103 and wind angle θ = 45°

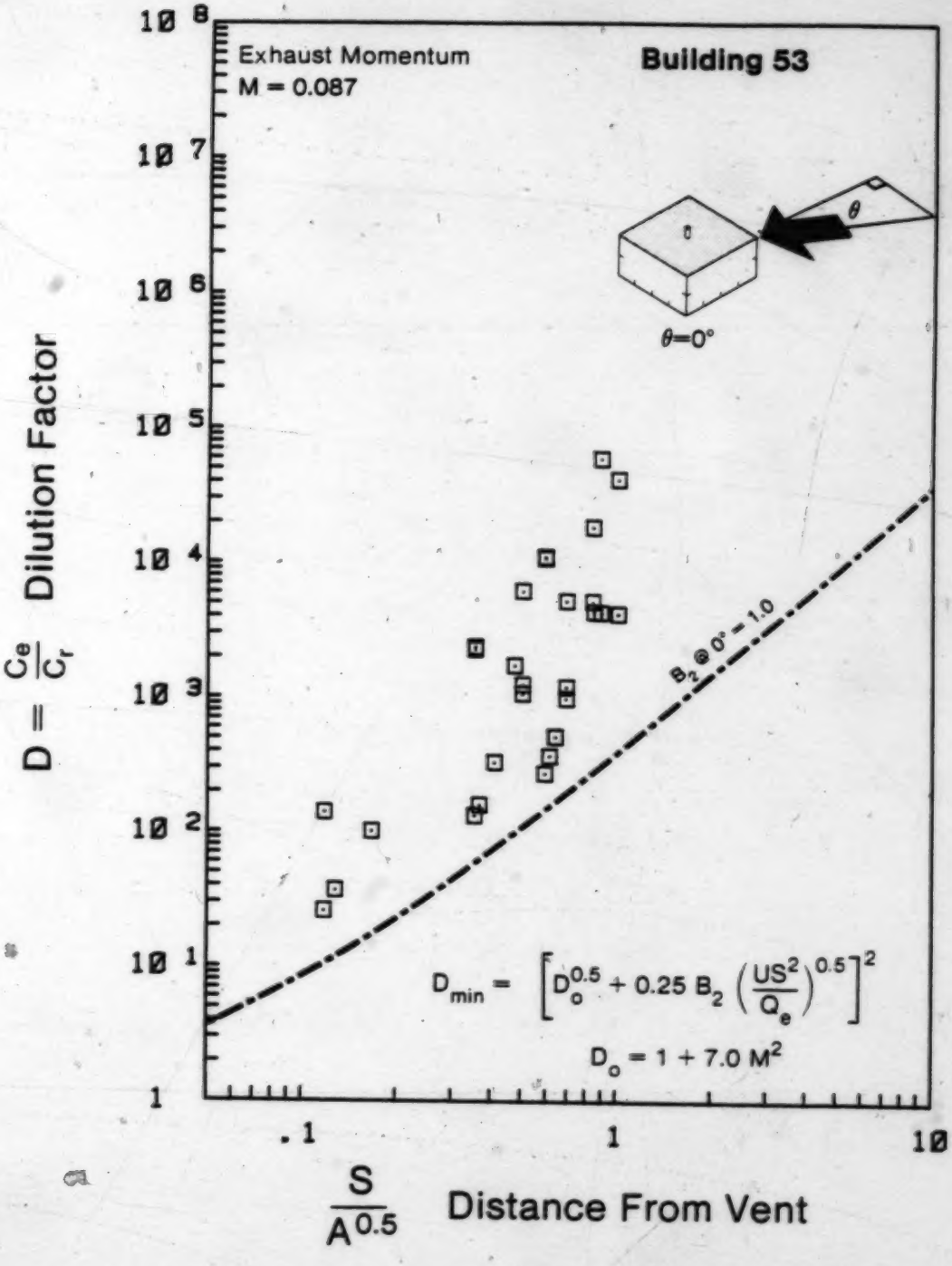

Figure A4-6 Effect of wind angle on minimum dilution for a medium rise building with low exhaust momentum M = 0.087 and wind angle θ = 0°

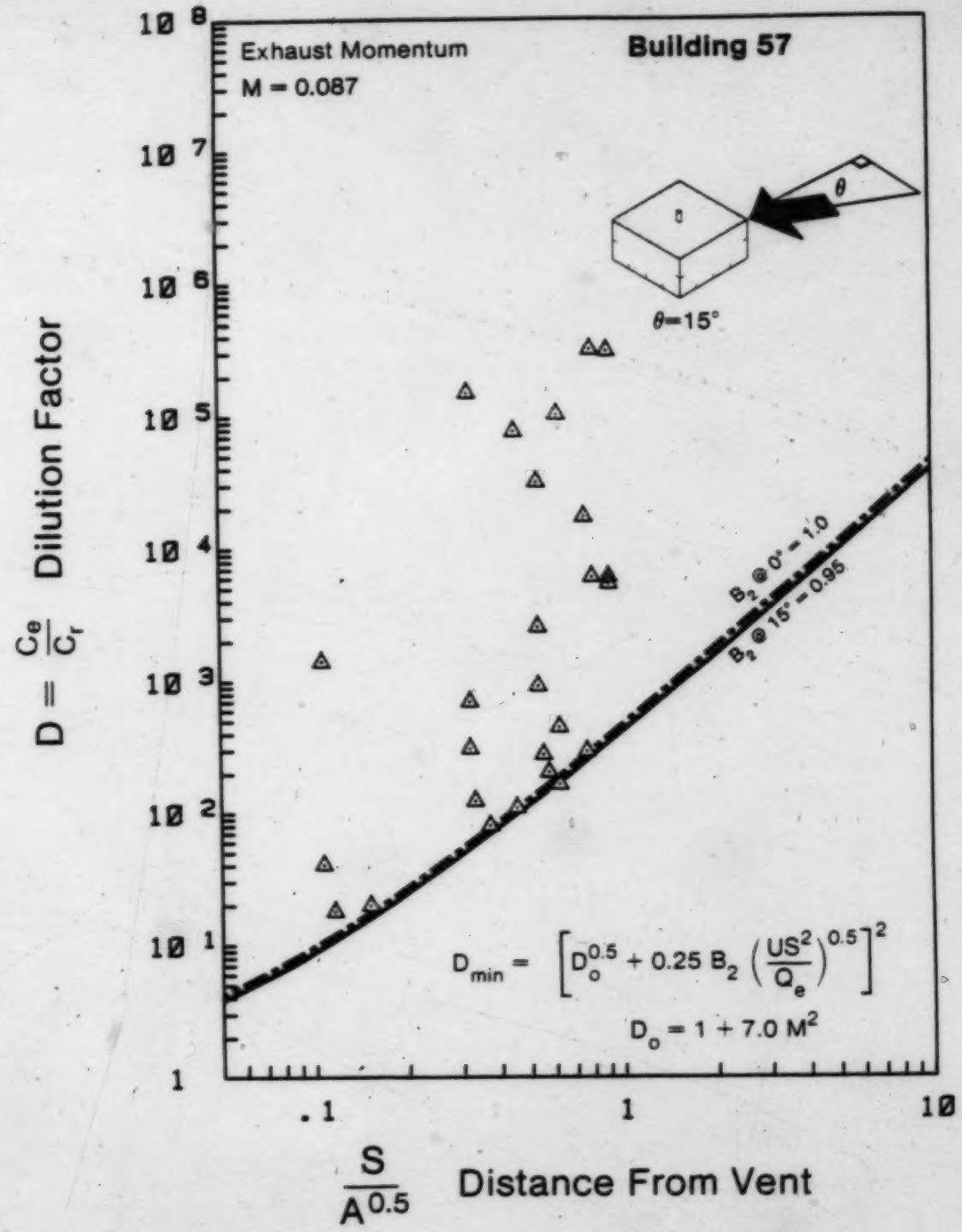

Figure A4-7 Effect of wind angle on minimum dilution for a medium rise building with low exhaust momentum M = 0.087 and wind angle θ = 15°

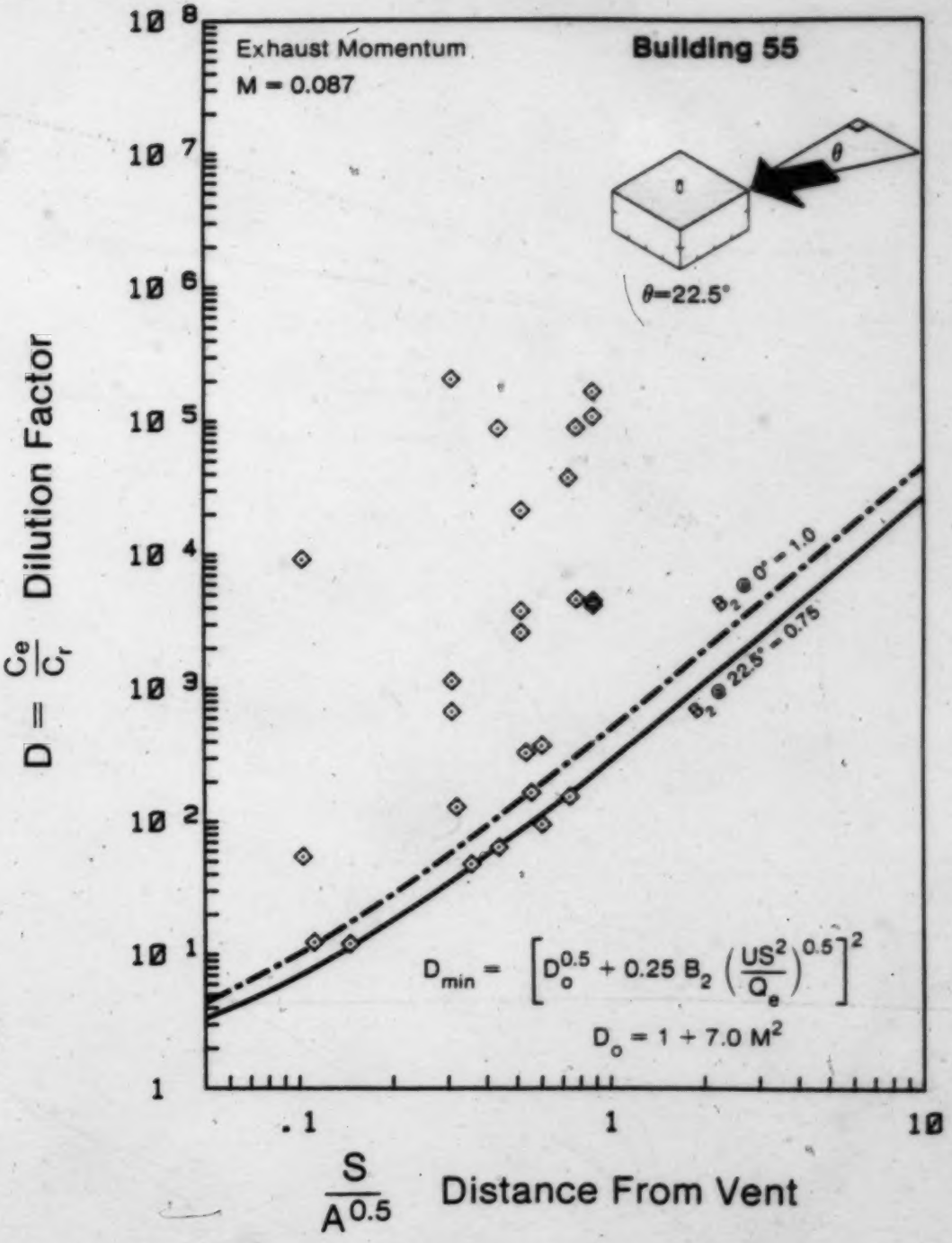

Figure A4-8 Effect of wind angle on minimum dilution for a medium rise building with low exhaust momentum M = 0.087 and wind angle θ = 22.5°

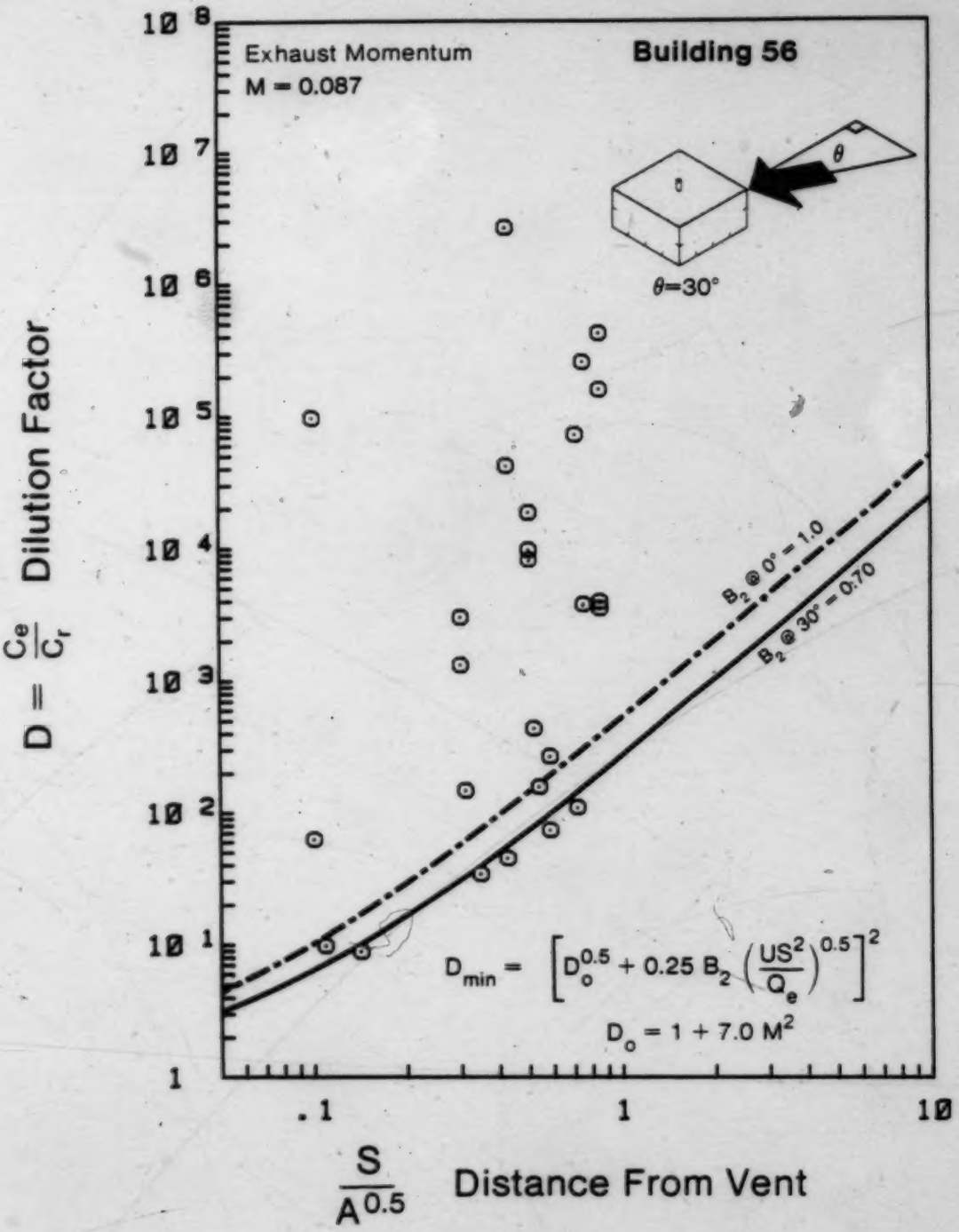

Figure A4-9 Effect of wind angle on minimum dilution for a medium rise building with low exhaust momentum M = 0.087 and wind angle θ = 30°

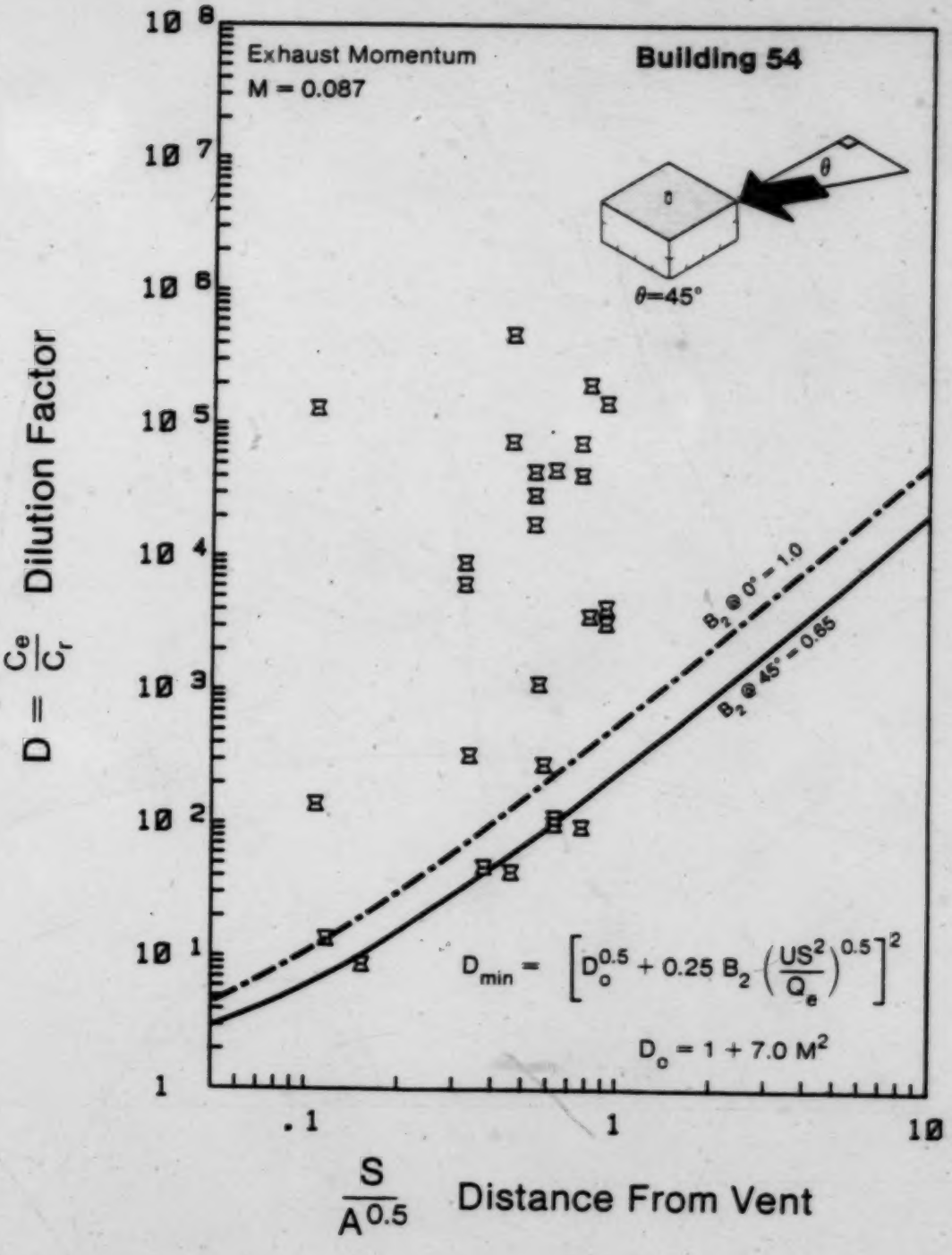

Figure A4-10 Effect of wind angle on minimum dilution for a medium rise building with low exhaust momentum M = 0.087 and wind angle θ = 45°

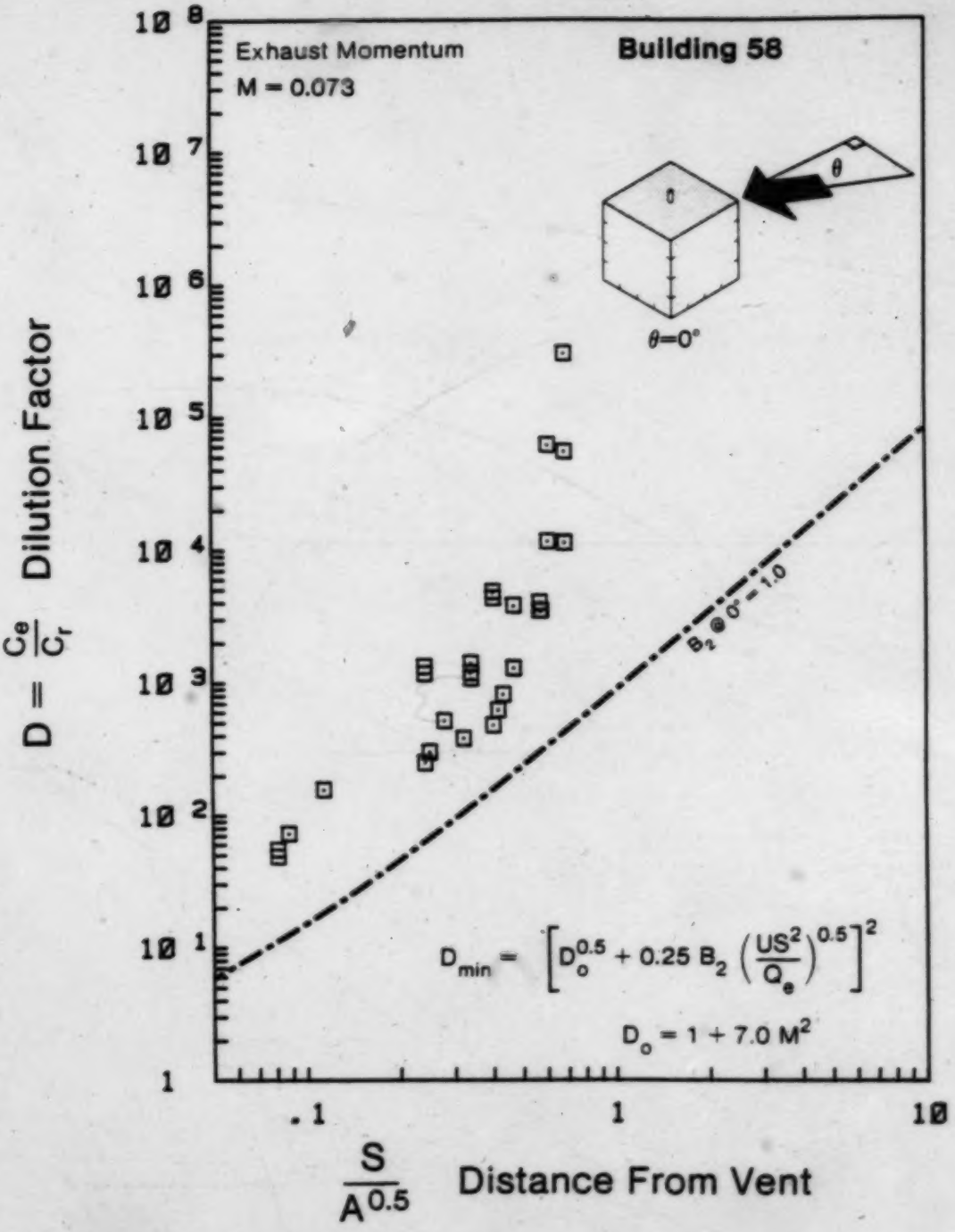

Figure A4-11 Effect of wind angle on minimum dilution for a cubical building with low exhaust momentum M = 0.073 and wind angle θ = 0°

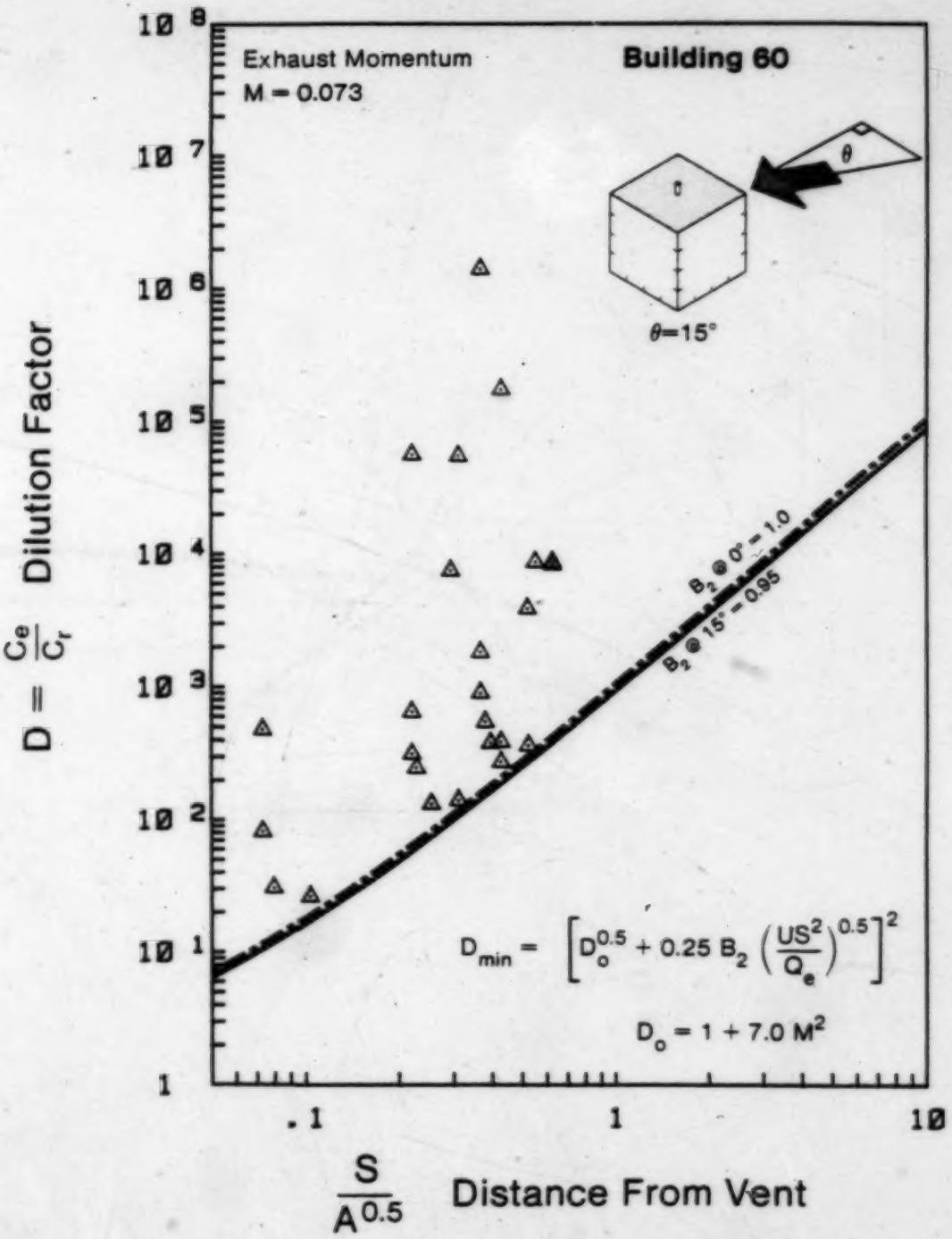

Figure A4-12 Effect of wind angle on minimum dilution for a cubical building with low exhaust momentum M = 0.073 and wind angle θ = 15°

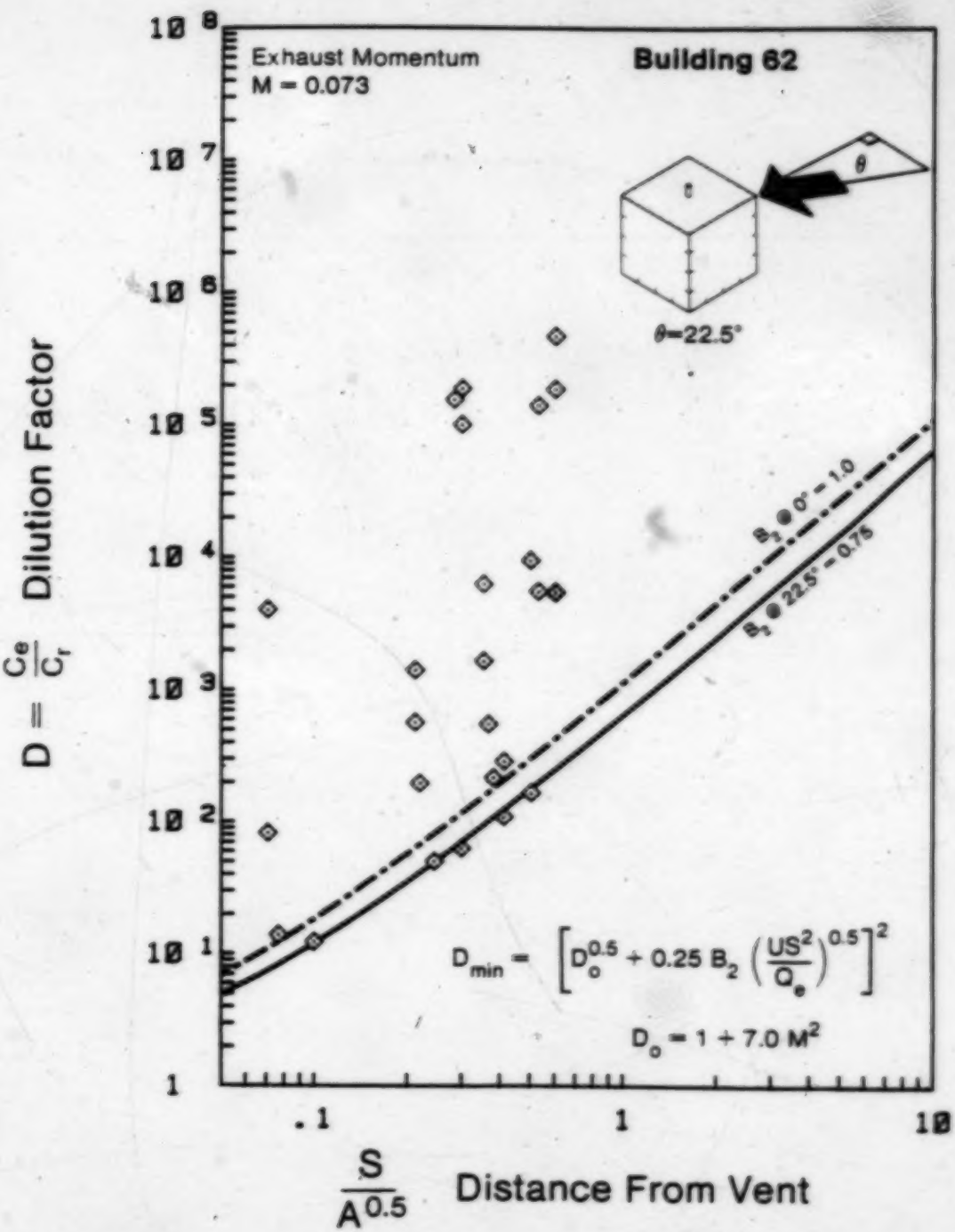

Figure A4-13 Effect of wind angle on minimum dilution for a cubical building with low exhaust momentum M = 0.073 and wind angle θ = 22.5°

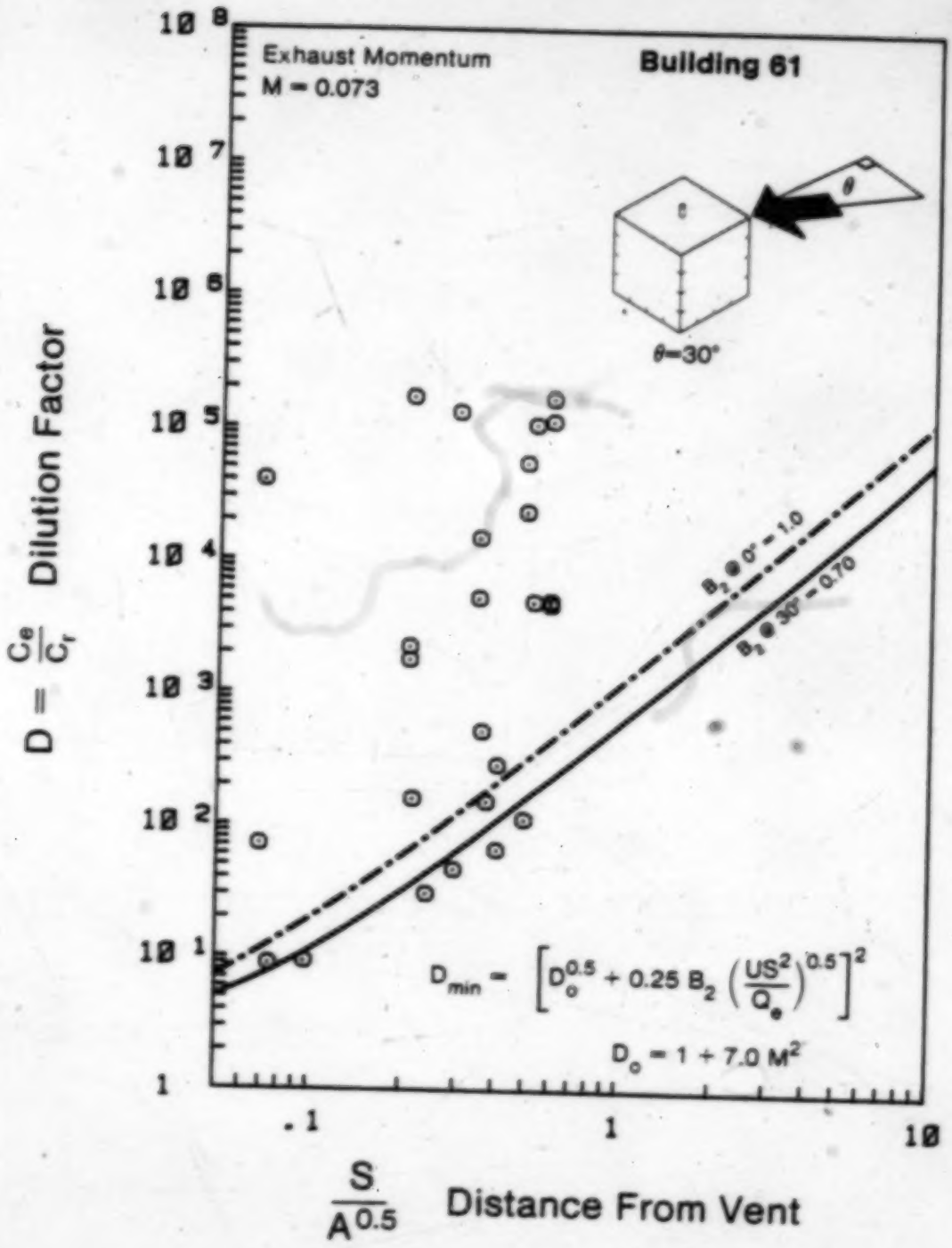

Figure A4-14 Effect of wind angle on minimum dilution for a cubical building with low exhaust momentum M = 0.073 and wind angle θ = 30°

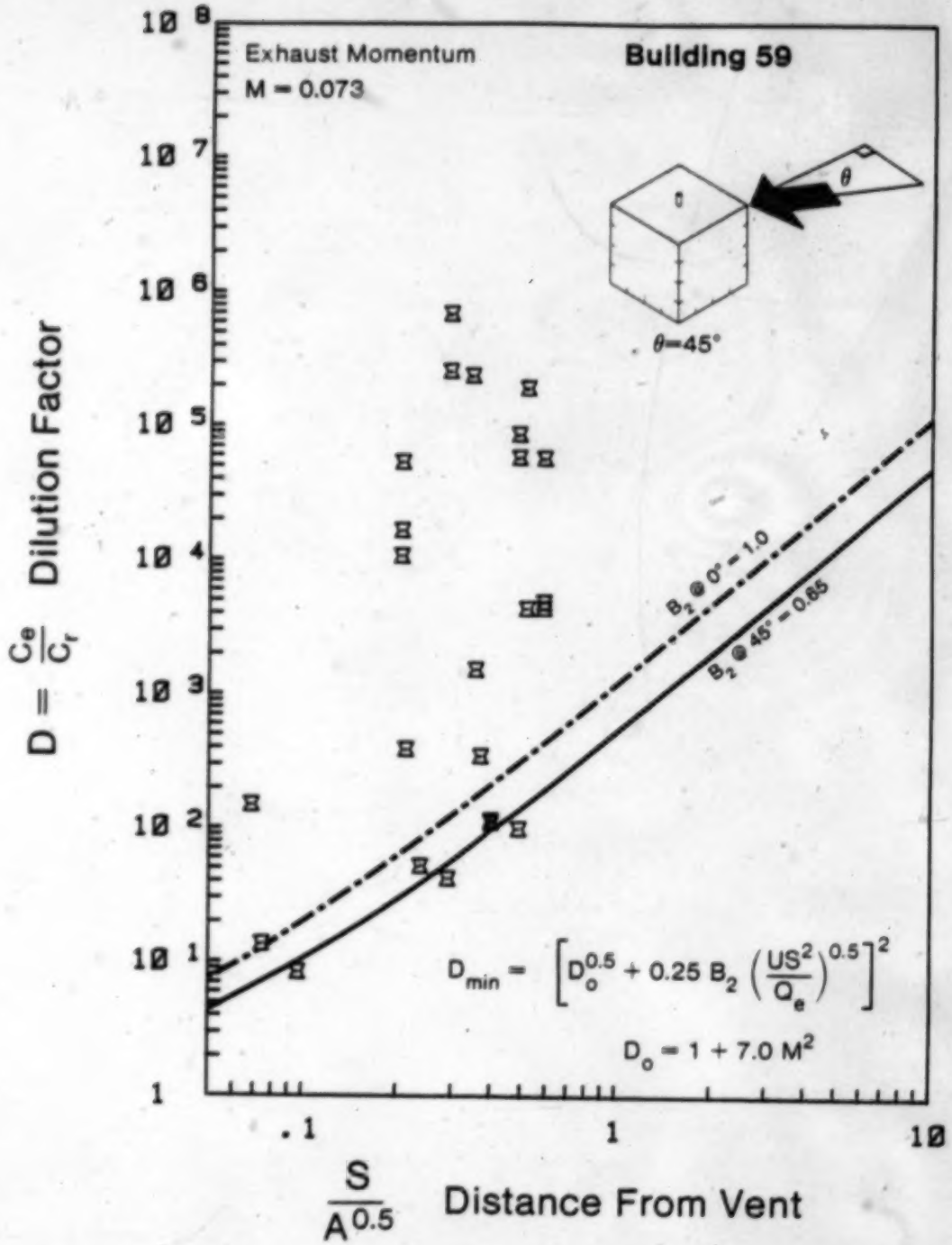

Figure A4-15 Effect of wind angle on minimum dilution for a cubical building with low exhaust momentum M = 0.073 and wind angle θ = 45°

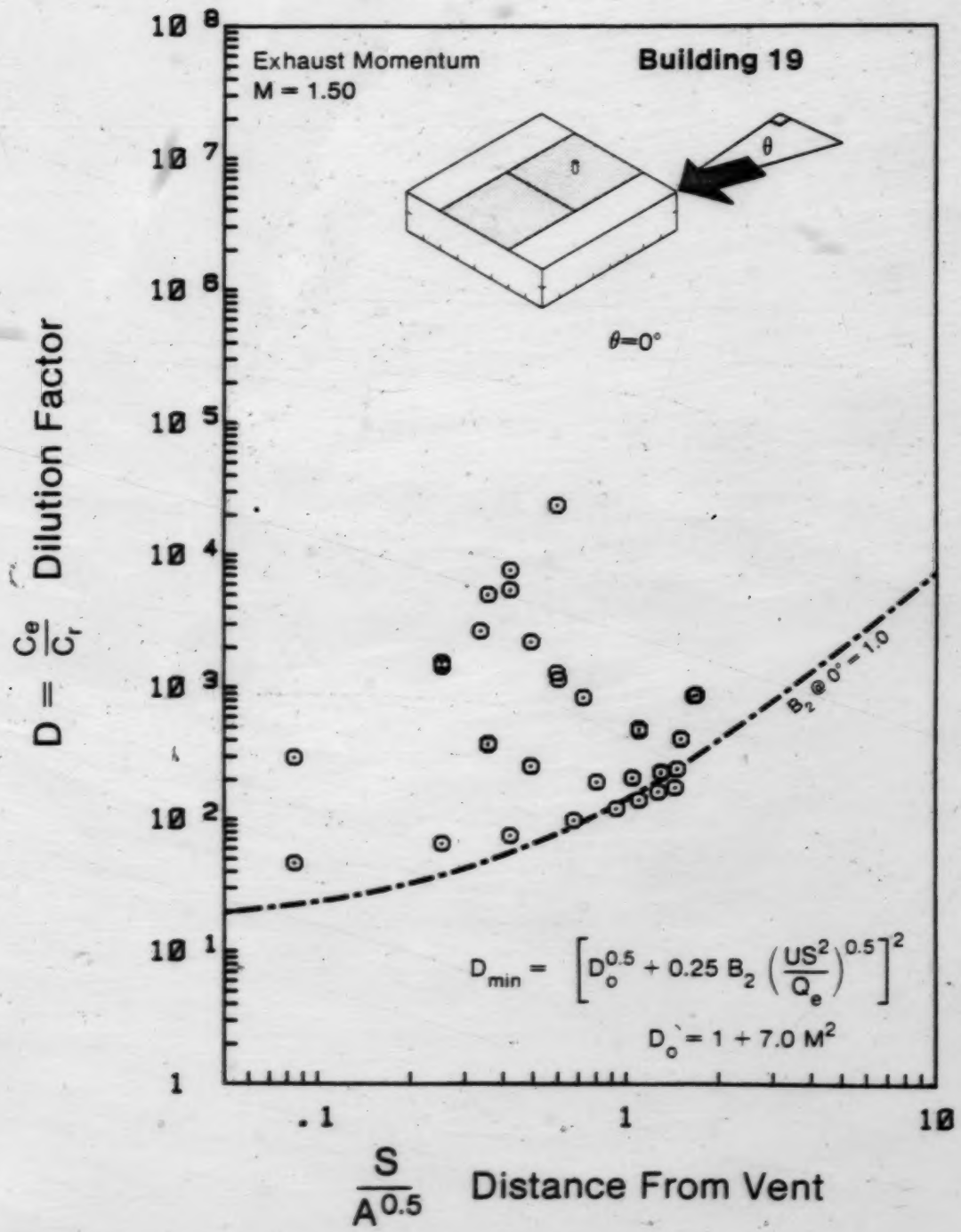

Figure A4-16 Effect of wind angle on minimum dilution for a medium rise building with high exhaust momentum M = 1.50 and wind angle θ = 0°.

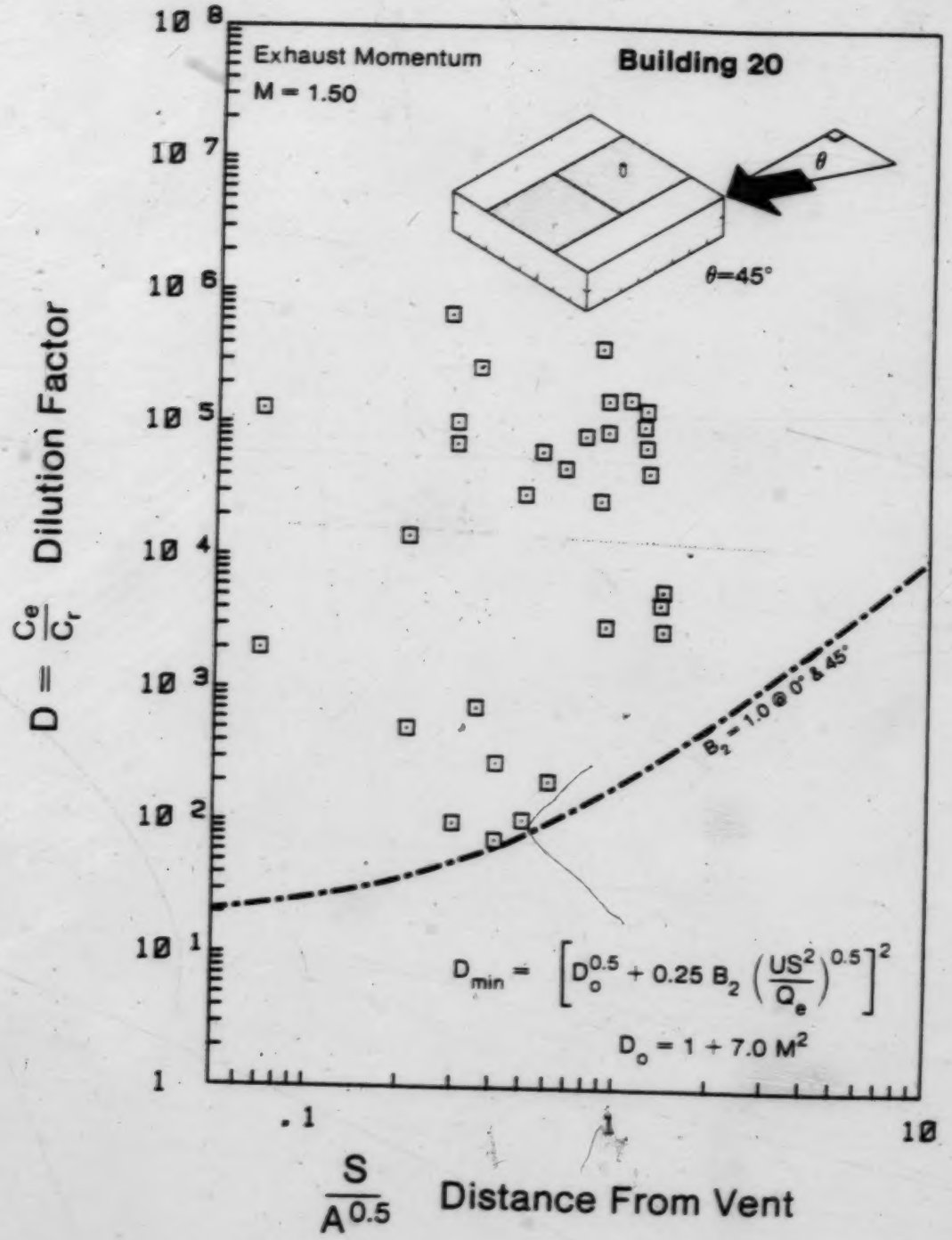

Figure A4-17 Effect of wind angle on minimum dilution for a medium rise building with high exhaust momentum M = 1.50 and wind angle θ = 45°

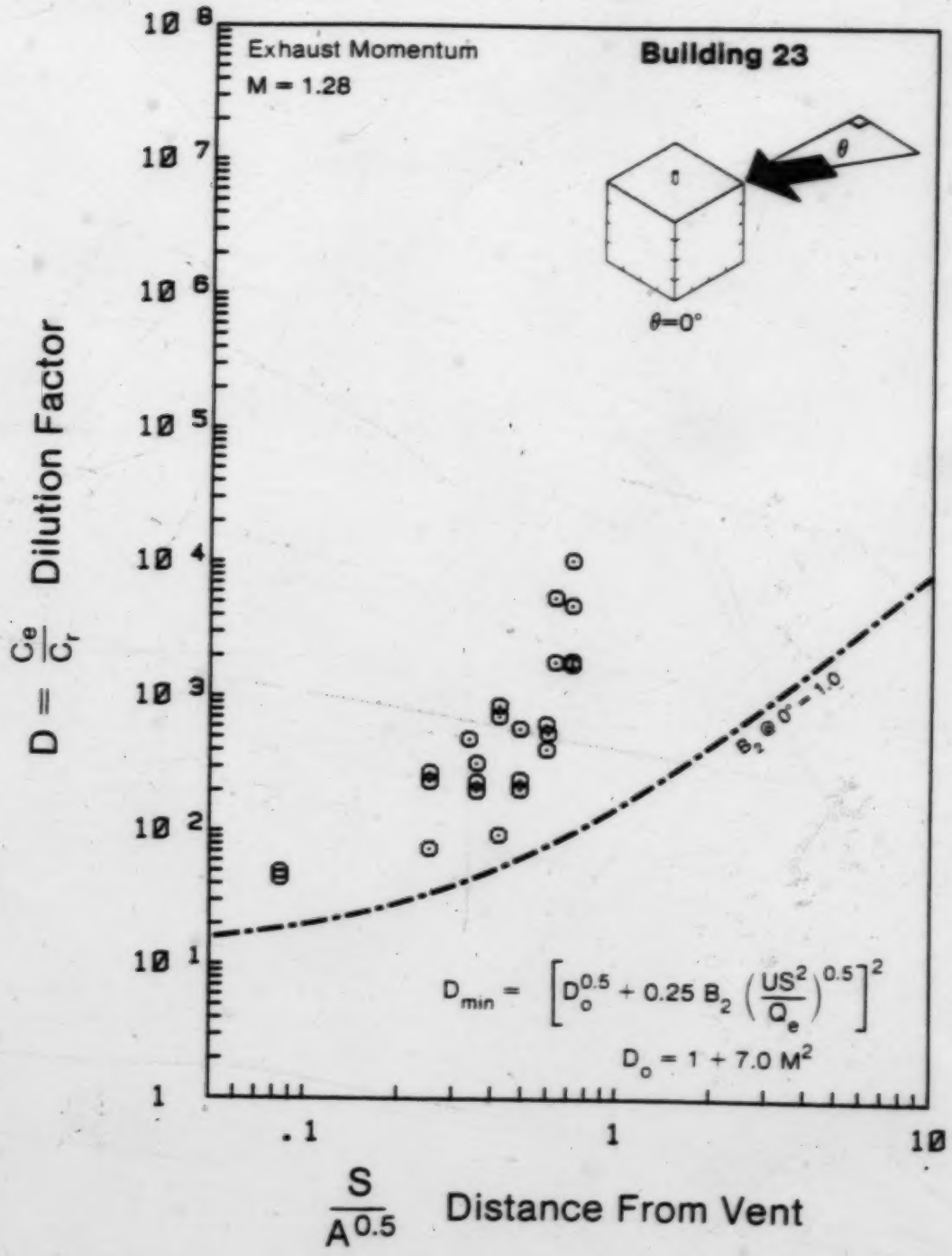

Figure A4-18 Effect of wind angle on minimum dilution for a medium rise building with high exhaust momentum M = 1.28 and wind angle θ = 0°

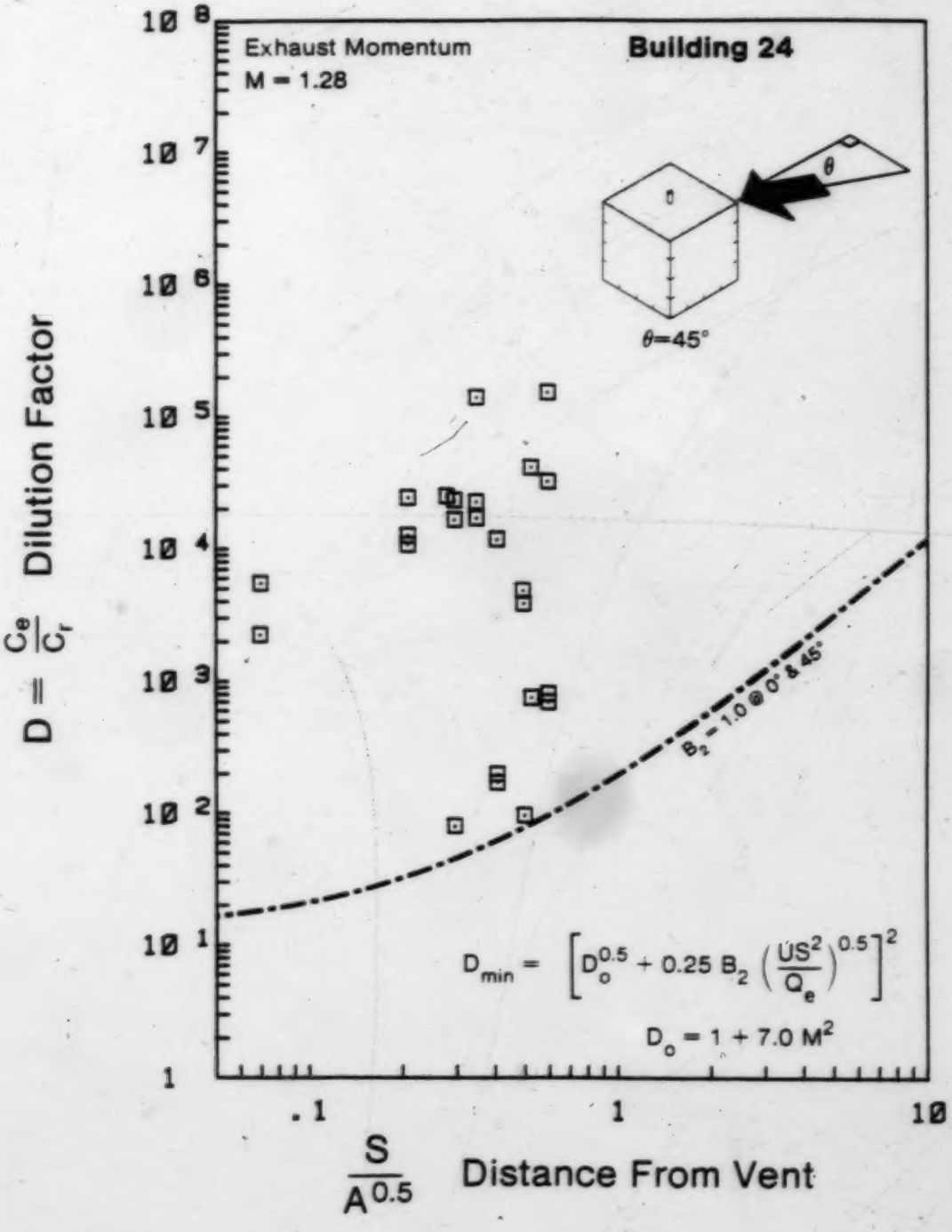

Figure A4-19 Effect of wind angle on minimum dilution for a medium rise building with high exhaust momentum M = 1.28 and wind angle θ = 45°

APPENDIX A5

Additional Experimental Data on the Effect of Building Shape on Dilution

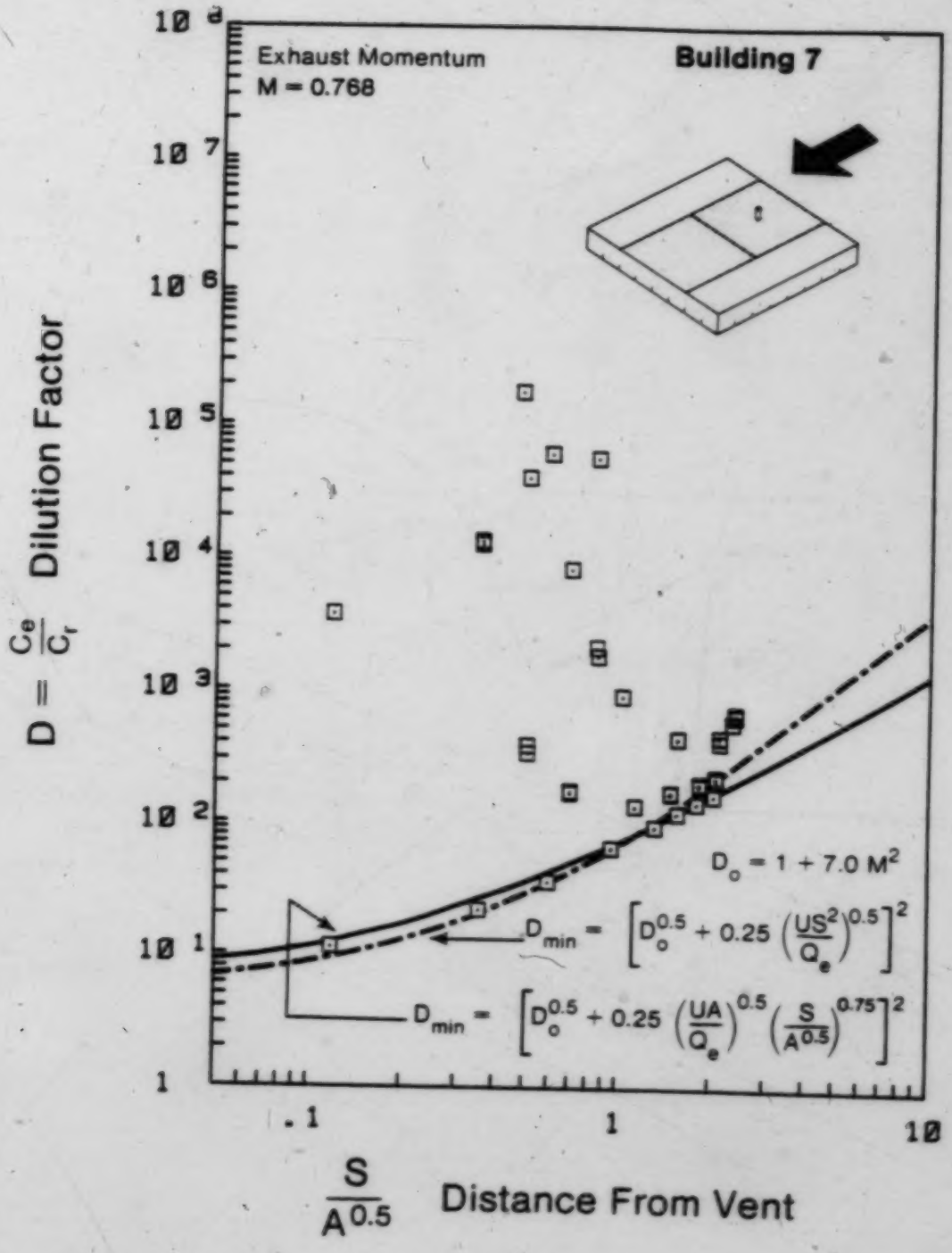
Exhaust Momentum
M = 0.768
Building 7
$D = \frac{C_e}{C_r}$ Dilution Factor
$D_o = 1 + 7.0\ M^2$
$D_{min} = \left[D_o^{0.5} + 0.25\left(\frac{US^2}{Q_e}\right)^{0.5}\right]^2$
$D_{min} = \left[D_o^{0.5} + 0.25\left(\frac{UA}{Q_e}\right)^{0.5}\left(\frac{S}{A^{0.5}}\right)^{0.75}\right]^2$
$\frac{S}{A^{0.5}}$ Distance From Vent

Figure A5-1 Effect of building shape on minimum dilution for a low rise building with medium exhaust momentum M = 0.768

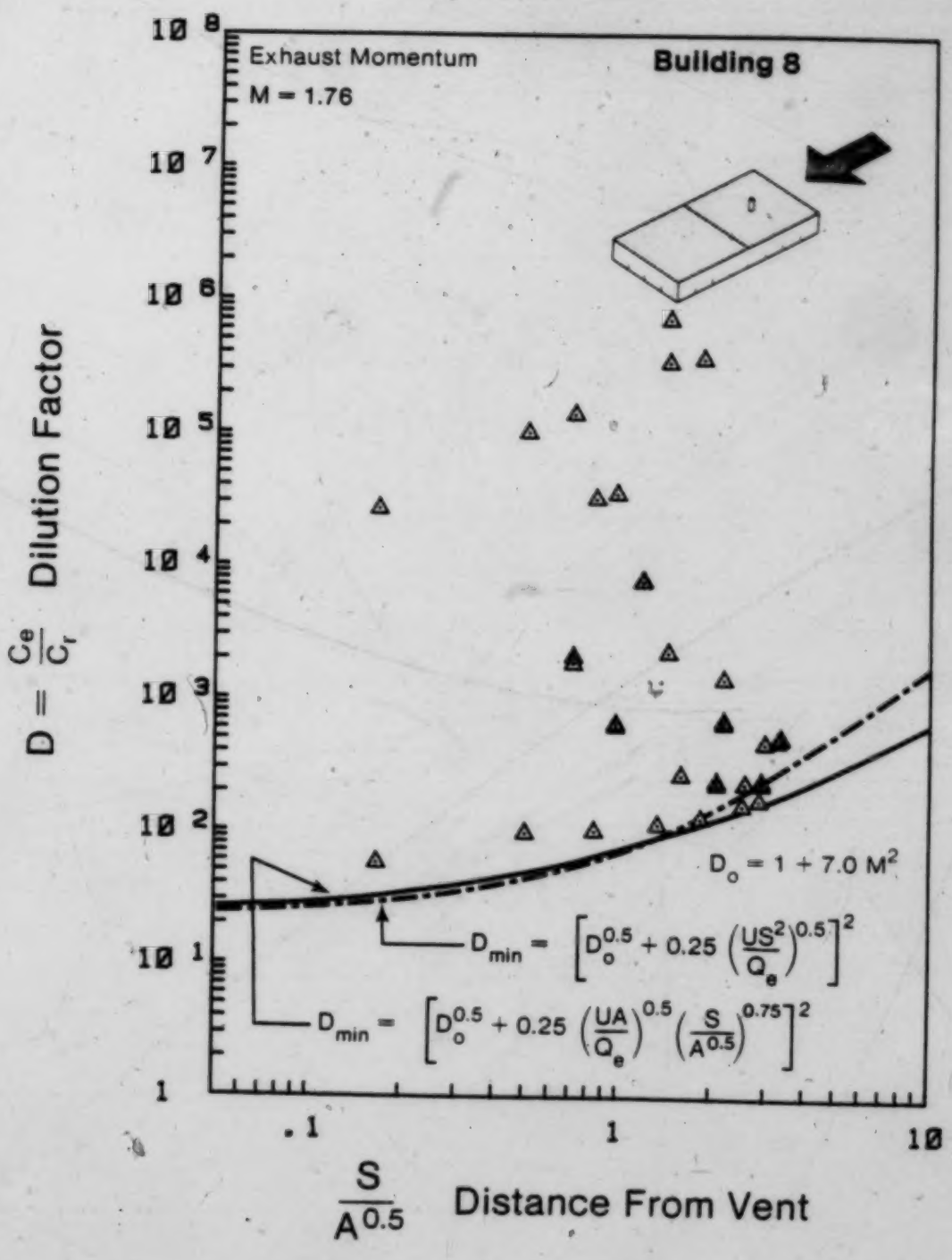
Exhaust Momentum
M = 1.76
Building 8
$D = \frac{C_e}{C_r}$ Dilution Factor
$D_o = 1 + 7.0\ M^2$
$D_{min} = \left[D_o^{0.5} + 0.25\left(\frac{US^2}{Q_e}\right)^{0.5}\right]^2$
$D_{min} = \left[D_o^{0.5} + 0.25\left(\frac{UA}{Q_e}\right)^{0.5}\left(\frac{S}{A^{0.5}}\right)^{0.75}\right]^2$
$\frac{S}{A^{0.5}}$ Distance From Vent

Figure A5-2 Effect of building shape on minimum dilution for a low rise building with high exhaust momentum M = 1.76

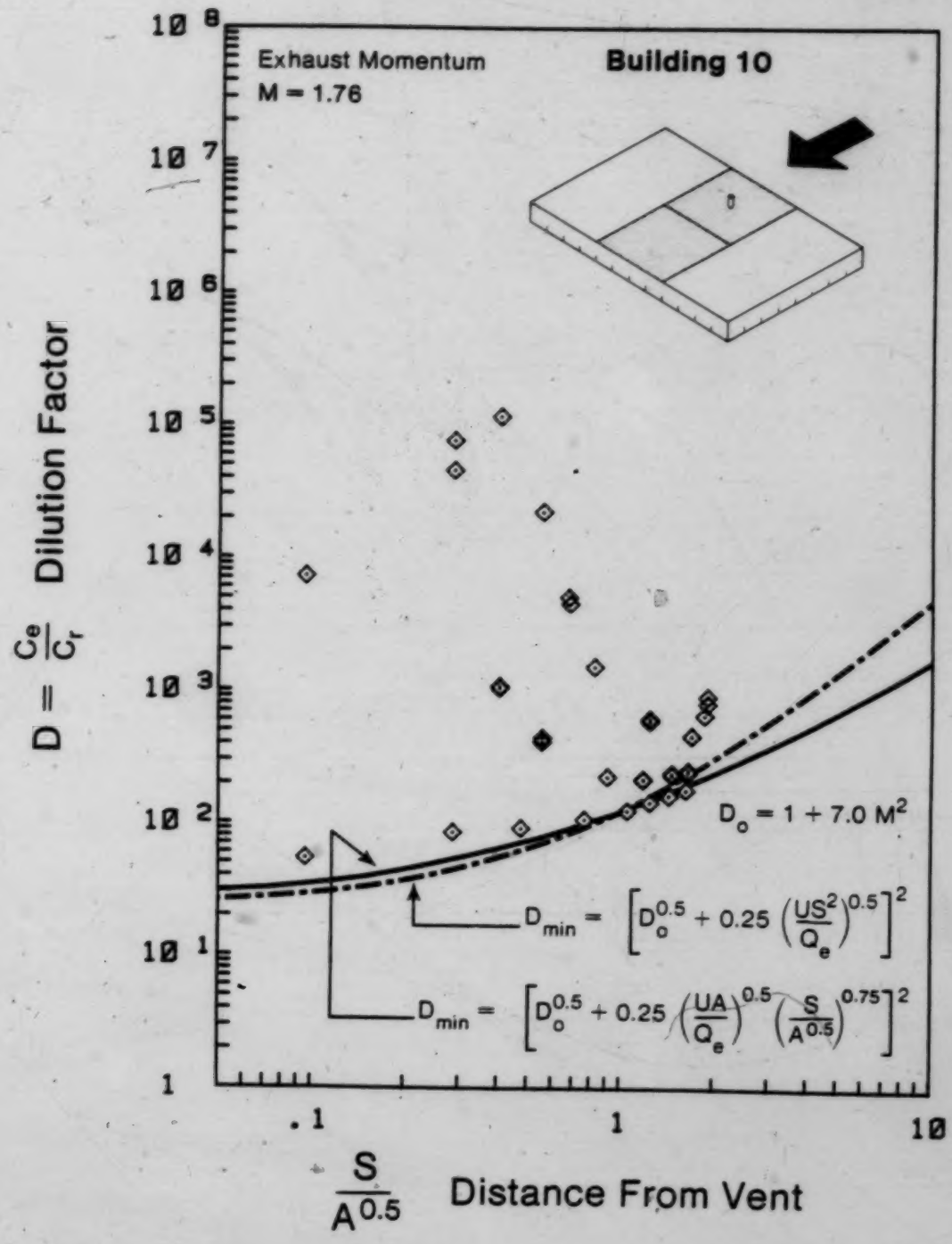

Figure A5-3 Effect of building shape on minimum dilution for a low rise building with high exhaust momentum M = 1.76

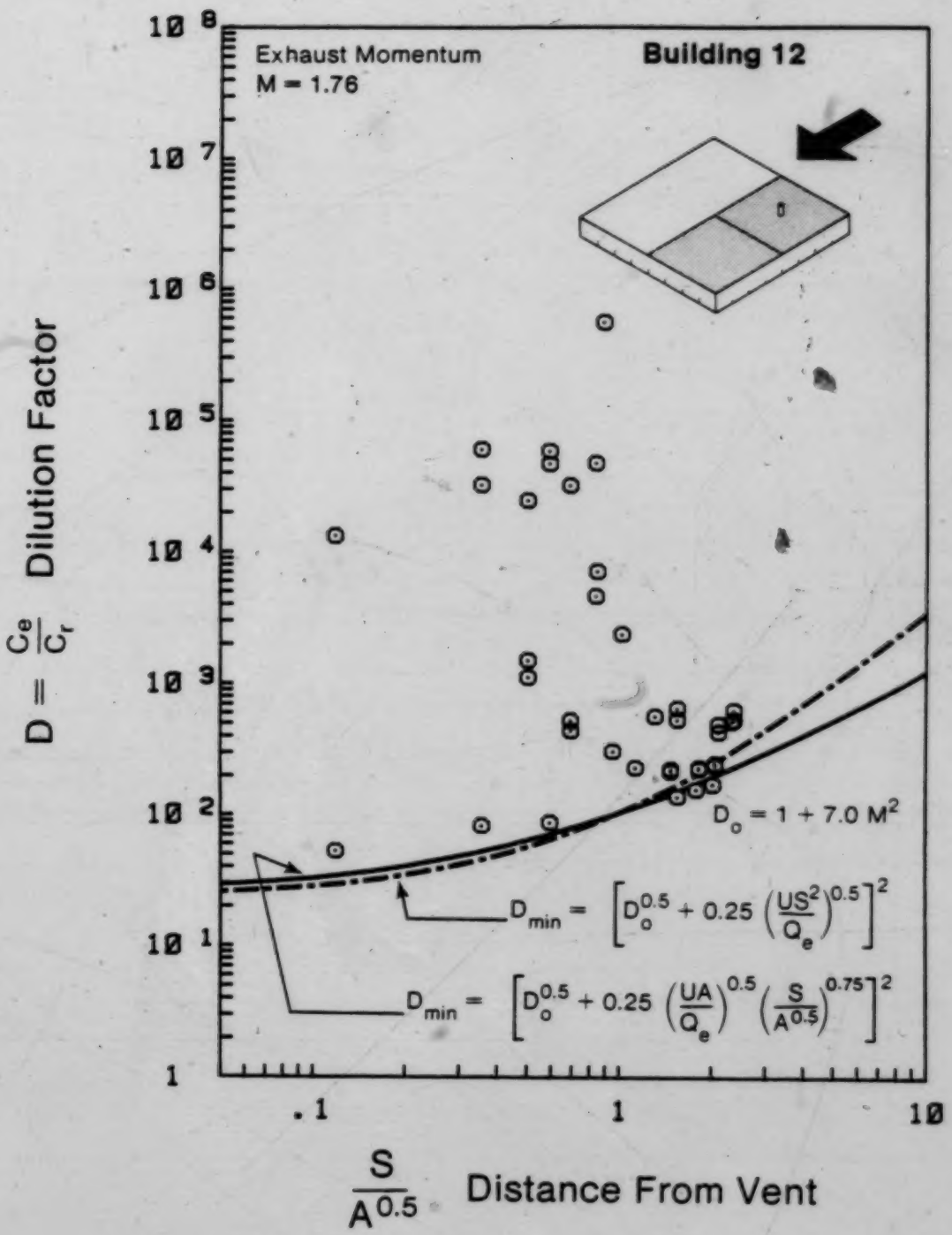

Figure A5-4 Effect of building shape on minimum dilution for a low rise building with high exhaust momentum M = 1.76

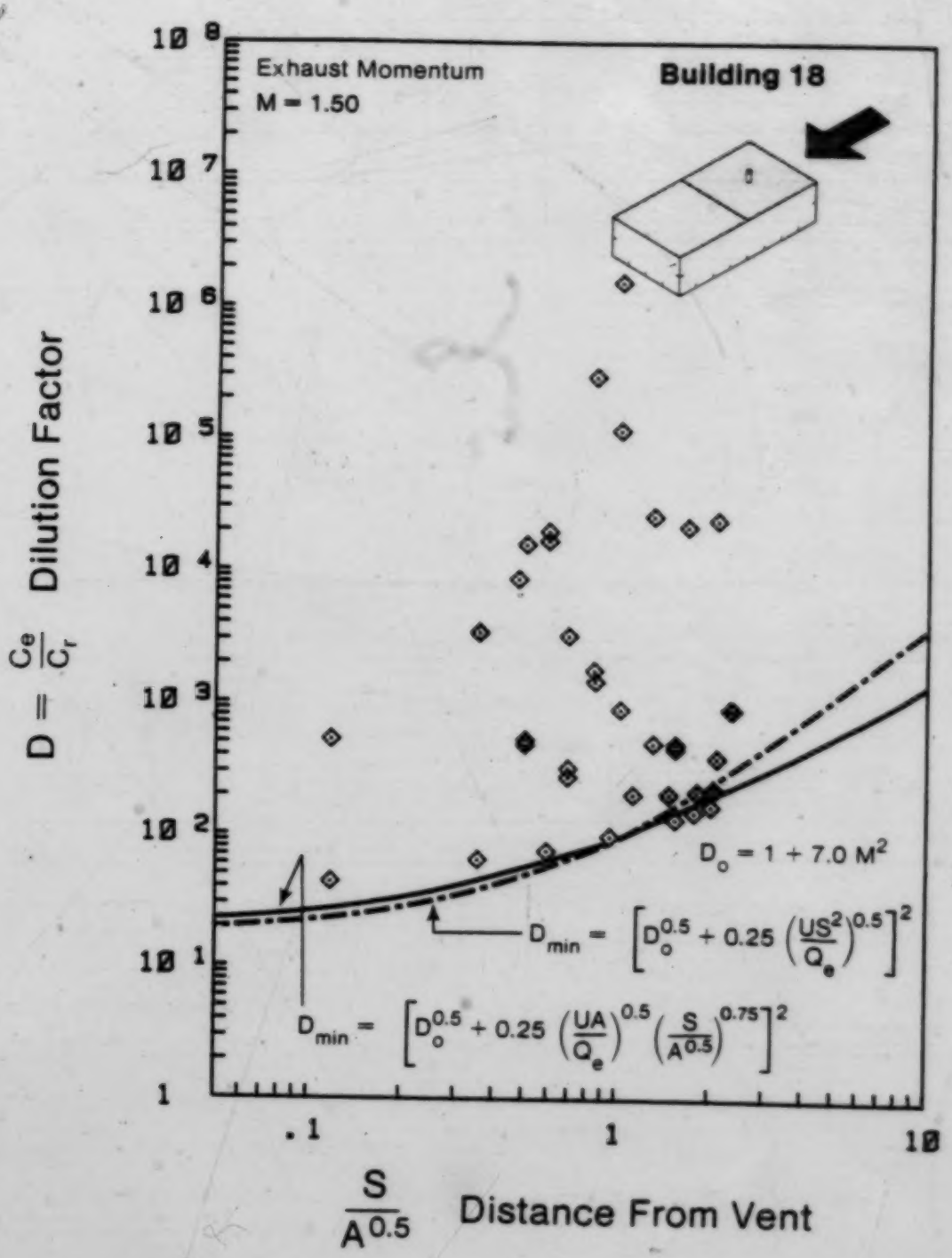

Figure A5-5 Effect of building shape on minimum dilution for a medium rise building with high exhaust momentum M = 1.50

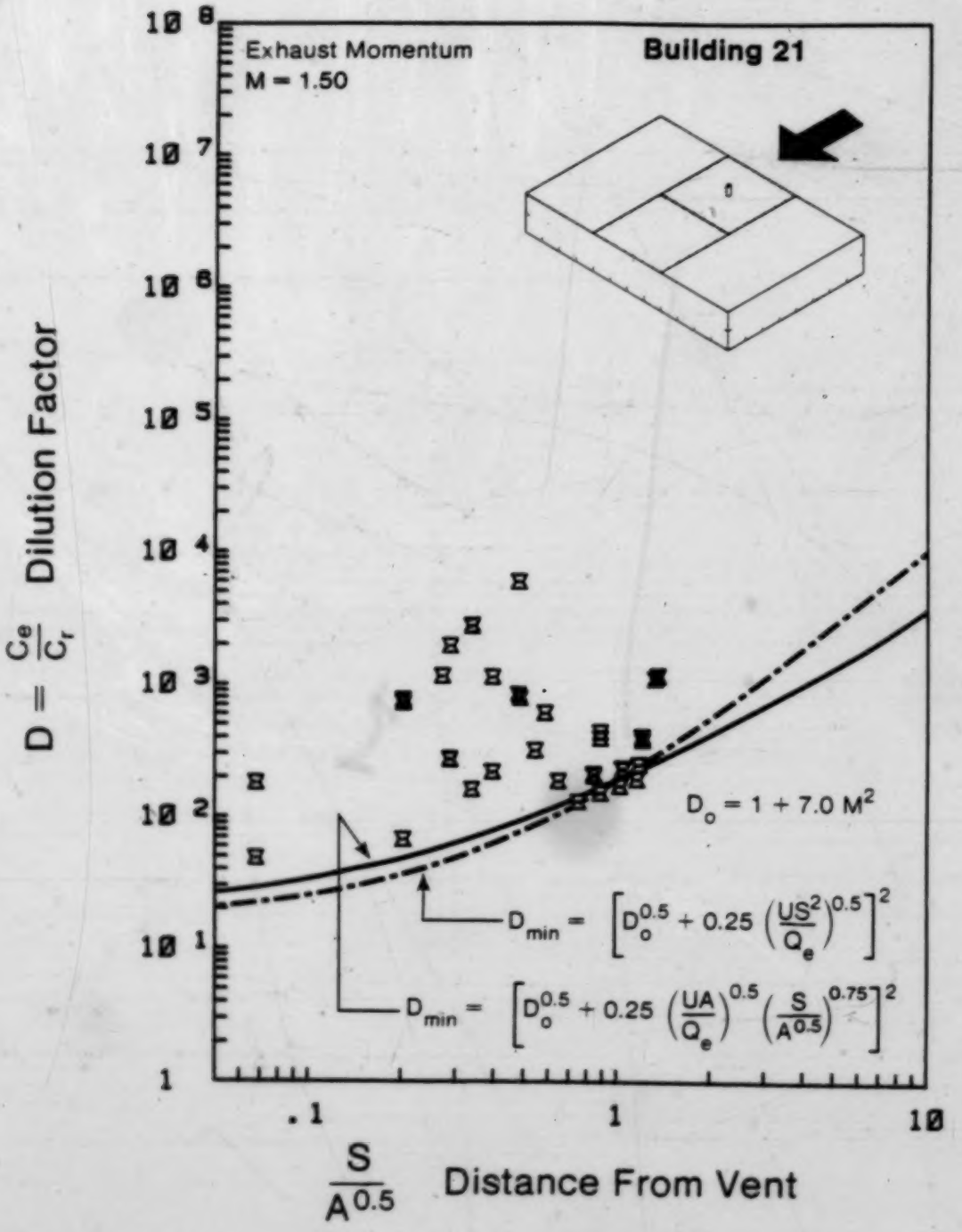

Figure A5-6 Effect of building shape on minimum dilution for a medium rise building with high exhaust momentum M = 1.50

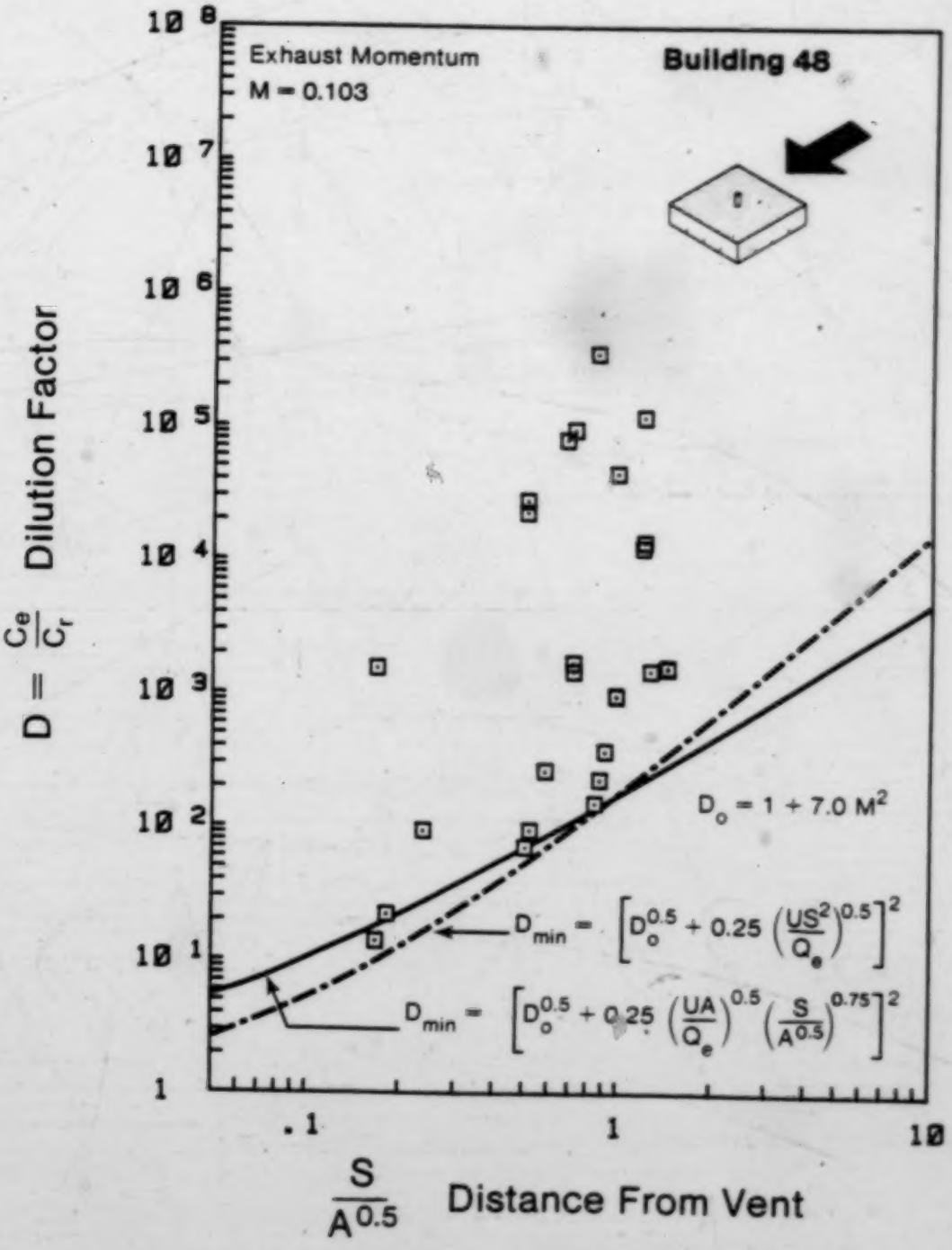

Figure A5-7 Effect of building shape on minimum dilution for a low rise building with low exhaust momentum M = 0.103

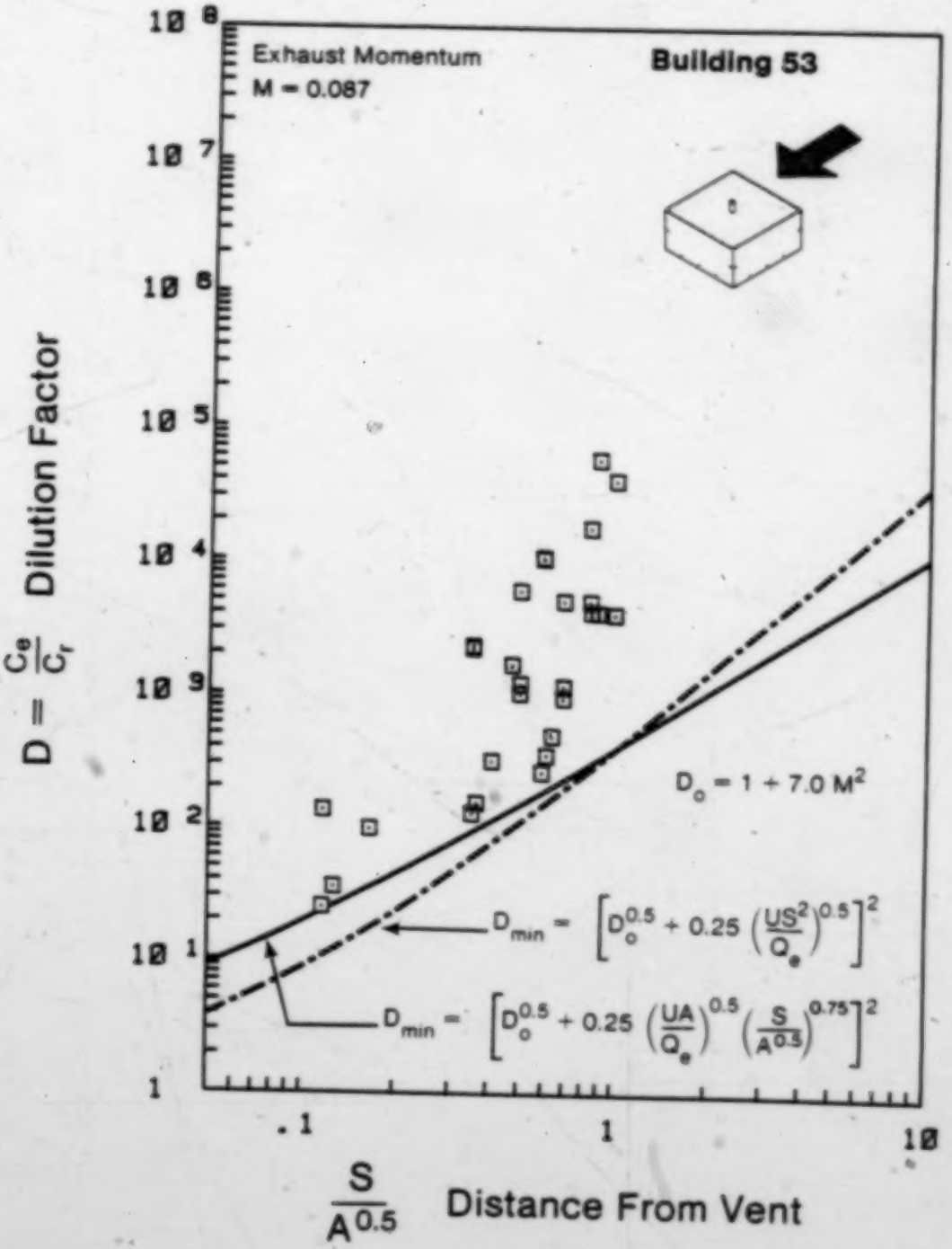

Figure A5-8 Effect of building shape on minimum dilution for a medium rise building with low exhaust momentum M = 0.087